

Meteotsunami Occurrence and Behavior in the Great Lakes

By

Adam J. Bechle

A dissertation submitted in partial fulfillment of
the requirements for the degree of

Doctor of Philosophy

(Civil and Environmental Engineering)

at the

UNIVERSITY OF WISCONSIN-MADISON

2015

Date of final oral examination: 12/15/2015

The dissertation is approved by the following members of the Final Oral Committee:

Chin H. Wu, Professor, Civil and Environmental Engineering

Kenneth W. Potter, Professor, Civil and Environmental Engineering

Samuel N. Stechmann, Associate Professor, Mathematics

Matthew H. Hitchman, Professor, Atmospheric and Oceanic Sciences

David A.R. Kristovich, Adjunct Associate Professor, Atmospheric Sciences

Eric J. Anderson, Physical Scientist, Great Lakes Environmental Research Laboratory

Abstract

Meteotsunamis, or meteorological tsunamis, are water waves generated by an atmospheric disturbance that behave similar to seismic tsunamis in both physical characteristics and disastrous potential. The Laurentian Great Lakes have a particularly impactful meteotsunami history, as many events have resulted in damage, injury, and even death. The objective of this dissertation is to characterize Great Lakes meteotsunamis in terms of both physical mechanisms and their occurrences and causes.

The behavior of meteotsunami waves in the Great Lakes is examined through simulation of two notable Lake Michigan meteotsunami events, on June 26, 1954 and July 6, 1954. For both events, atmospheric pressure and wind perturbations were found to be essential to explain the magnitude of the wave activity. In the June 26 meteotsunami, long wave resonance was the primary cause of the destructive wave, though the storm also generated edge waves which persisted for many hours, hindering rescue efforts. The maximum wave heights for the July 6 event were revealed to be the product of a superposition of edge waves and long waves. The results from these simulations demonstrate the enclosed Lake Michigan basin retained and focused wave energy, leading to their large magnitude, long duration, and destructive nature.

The occurrence of meteotsunamis in Lake Michigan is quantified at 10 locations from up to 20 years of water level records. Meteotsunami height data are fit with the Pareto Type 1 distribution to estimate exceedance probabilities. The largest annual return level (0.62 m) occurs at Calumet Harbor, IL. Analysis of radar imagery indicates that Lake Michigan meteotsunamis are associated primarily with convective storm structures, with a secondary contribution from frontal storms. Meteotsunami association with convective storm structures is more prevalent in southern Lake Michigan while frontal storm structures have a greater association with

meteotsunamis in northern Lake Michigan. Meteotsunamis occur primarily from late spring to early summer, which is before the peak convective season but after the peak cyclone season.

Expanding upon the Lake Michigan analysis, meteotsunami occurrence is quantified at water level stations across the Great Lakes. Consistent with the Lake Michigan analysis, Great Lakes meteotsunamis tend to occur in the late-spring to mid-summer and are primarily associated with convective storms. Meteotsunami characteristics are analyzed with respect to the physical and atmospheric setting of the Great Lakes to investigate regional patterns. Within a lake, meteotsunami size tends to increase along the major axis of the lake in the direction of storm propagation. The specific type of convective storm structures associated with meteotsunamis varies longitudinally across the region, consistent with the spatial distribution of mesoscale convective complexes. Relationships between meteotsunami seasonality and lake depth and shelf slope suggest that bathymetry may have a role in the timing of meteotsunami occurrences throughout the Great Lakes. Overall, the regional-scale analysis of meteotsunamis in the Great Lakes reveals valuable insight into the role of physical and atmospheric setting on meteotsunami occurrence.

Finally, a database of meteotsunamis reported worldwide is gathered and regions of high meteotsunami activity are identified. Reported meteotsunamis are located primarily in the northern hemisphere in temperate or continental climates and over wide shelves. Globally, reported meteotsunamis tend to occur during the warm season. Compared with the Great Lakes, meteotsunamis in Northern Europe and the Mediterranean tend to occur later in the warm season.

Acknowledgements

I would like to thank the many people who have supported me throughout my graduate studies at the University of Wisconsin-Madison. First of all, I must thank my advisor Dr. Chin Wu. His guidance has been critical to my development as a researcher and he has always given me opportunities to pursue interesting work. I would also like to thank my committee members, Dr. Ken Potter, Dr. Sam Stechmann, Dr. Matthew Hitchman, Dr. Eric Anderson, and Dr. David Kristovich. Specifically, Dr. Potter provided me solid foundation in statistical analysis, Dr. Anderson has continuously provided support to my meteotsunami studies in the Great Lakes, and Dr. Kristovich has taught me a great deal about storms over the Great Lakes. I would also like to thank Dr. David Schwab for encouraging me to study meteotsunamis and mentoring me along the way. A special thanks to the late Dr. John Hoopes for challenging me to think critically about research. His presence on my committee is truly missed.

This work was supported by the National Science Foundation's Graduate Research Fellowship Program, the Cooperative Institute for Limnology and Ecosystems Research Long-term Great Lakes Fellowship, and UW-Madison/UW-Milwaukee Intercampus Research Incentive Grants Program, the University of Wisconsin Sea Grant Institute, and the Becker Travel Grant.

The support I received from my colleagues in the Water Resources Engineering/Environmental Fluid Mechanics program was integral to my success, whether in the form of technical help, field assistance, research discussion, or simple camaraderie. In particular, I would like to thank Josh Anderson for being a great colleague and friend through my entire graduate career. From a technical standpoint, his tireless leadership in the development of Skynet made my numerical simulations possible. Madeline Magee has always been there when I needed

to talk things through. Working with Alex Campbell helped me find the joy of discovery and collaboration amid the struggle [of research].

I have had many great teachers throughout my life that nurtured my love of learning and I'd like to thank a few in particular. Ms. Margaret Van Deurzen instilled within me a sense of duty to go out and make the world a better place. I learned to write from a pair of social studies teacher, Mr. Jason Baudhuin and Mr. Mike Wittig, and I am grateful for your efforts to go above and beyond for your students. Mr. Jack Batten inspired in me a love of physics, discovery, and teaching. Coach Jack Drankoff pushed me, the slowest runner on his track team, to be better than I ever imagined I could have been and along the way taught me lifelong lessons about hard work, tenacity, and humility.

I would also like to thank my family and friends for their encouragement during my graduate studies. Thank you to my parents, Jon and Sharon, for their unwavering supportive every step of the way. I cannot begin to explain the advantages they gave me in life and I truly appreciate your love, support, and sacrifice. My sister Lauren has always been in my corner and her passion for teaching inspires me to keep working towards what I love. I have my grandfather, Warren, to thank for my smarts. Other significant contributions to my smarts include Pat, Jerome, and Lorraine. Dan has been a great friend to share the graduate experience with and I am indebted to you for keeping me sane along the way. Garrett, Zach, Corey, and Mike all made great efforts to keep me human when I thought I might be turning into a researching robot. Finally, I would like to express my gratitude to Colleen for her love and support. You always provided me with valuable perspective, kept me focused on the important things, and motivated me to power through and finish this thing up. I am excited to see where life will take us.

Table of Contents

1.	Introduction.....	1
1.1.	Meteotsunami Background	1
1.2.	Meteotsunamis in the Great Lakes	3
1.3	Research Objectives	5
1.4.	Introduction to the Dissertation.....	6
1.5	References.....	7
2.	The Lake Michigan Meteotsunamis of 1954 Revisited.....	12
2.1	Introduction.....	12
2.2.	Hydrodynamic modeling and data	18
2.3.	Results.....	23
2.3.1.	June 26, 1954 Meteotsunami.....	23
2.3.2.	July 6, 1954 Meteotsunami	34
2.4.	Discussion	45
2.4.1.	Role of edge waves and long waves	45
2.4.2.	Effects of an enclosed basin	46
2.4.3.	Wind Stress versus atmospheric pressure	47
2.5.	Summary	48
2.6.	Acknowledgements	50
2.7.	References.....	50
3.	Meteotsunami Occurrences and Causes in Lake Michigan.....	56
3.1.	Introduction.....	56
3.2.	Study Site	59
3.3.	Methods	61
3.3.1.	Data Sources.....	61
3.3.2.	Meteotsunami Identification	64
3.3.3.	Cumulative Frequency Analysis.....	65
3.3.4.	Conditional Occurrence Analysis	67
3.3.5.	Monthly Occurrence Statistics	68
3.3.6.	Storm Structure Classification.....	68

3.4. Results.....	71
3.4.1. Exceedance Probability.....	71
3.4.2. Conditional Meteotsunami Occurrence	76
3.4.3. Seasonal Occurrence.....	77
3.4.4. Storm Structures Associated with Meteotsunamis	79
3.5. Discussion.....	83
3.5.1. Meteotsunami Statistics versus Storm Structure Statistics	83
3.5.2. Size-Frequency Distribution Parameters	85
3.5.3. Role of Wave Reflection.....	87
3.5.4. Comparisons with Worldwide Meteotsunami Occurrence	88
3.6. Summary and Conclusions	90
3.7. Acknowledgements	91
3.8. References.....	92
4. Regional Characteristics of Meteotsunamis in the Laurentian Great Lakes.....	102
4.1. Introduction.....	102
4.2. Methods	106
4.3. Results.....	109
4.3.1. Great Lakes Basin-Wide Characteristics	109
4.3.2. Lake-by-Lake Comparisons	113
4.4. Discussion and Conclusions.....	118
4.6. References.....	119
5. Worldwide Meteotsunami Occurrence	127
5.1 Introduction.....	127
5.2. Methods	128
5.3. Results.....	129
5.4. Discussion and Conclusions.....	132
5.5. References.....	133
6. Conclusion	140
6.1 Summary.....	140
6.2 Conclusions.....	142
6.3 Recommendations for Future Work	145

6.4. References	148
Appendix A Supplemental Material for Chapter 4	153
Appendix B Supplemental Material for Chapter 5	159

List of Tables

Table 3-1: Summary of water level stations and probability distribution fits	72
Table 3-2: Conditional occurrence of meteotsunamis between station pairs represented by the percent of meteotsunamis at a reference station for which meteotsunamis also occur at a co-occurring stations within +/- 6 hours.	77
Table 4-1: Pearson correlation coefficients of the linear regressions between meteotsunami characteristics (columns) and parameters which describe of the physical and atmospheric settings of each station (rows). Linear trends that are significant at the 95% level are in bold.	110

List of Figures

Figure 1-1 Schematic of meteotsunami formation involving (i) <i>wave generation</i> by an atmospheric disturbance moving at a speed to (ii) excite a <i>propagation resonance</i> . As the wave moves to the coast, (iii) <i>local mechanisms</i> such as shoaling and harbor resonance transform the wave to dangerous heights.....	1
Figure 2-1: Unstructured model grid mesh overlaid on Lake Michigan bathymetry. Bottom slopes along the west and east coasts are shown at the bottom-left; and at the top-left is a zoomed view of the coast near the Chicago lakeshore.....	13
Figure 2-2: Observed June 26, 1954 atmospheric pressure and wind records (black lines) at Wilson Avenue Crib station (taken from (Platzman 1958)) and corresponding input meteorological forcing functions (blue lines) used for the hydrodynamic model.	21
Figure 2-3: Observed July 6, 1954 atmospheric pressure records at Wilson Avenue Crib station (taken from (Donn and Ewing 1956)) and hourly wind records available at the Glenview Naval Air Station, IL. The blue lines are the input meteorological forcing functions for hydrodynamic model.	22
Figure 2-4: Time series of modeled water levels (line) and observations (dot) at Wilson Avenue Crib in response to the meteorological forcings on June 26, 1954 from Figure 2-2.	24
Figure 2-5: Lake Michigan water level in response to meteorological forcings on June 26, 1954 from Figure 2-2 (times are in CST).	26
Figure 2-6: Time series of modeled water levels (line) and observations (dot) at shore-based locations throughout Lake Michigan in response to the meteorological forcings on June 26, 1954. For gauge locations, see Figure 2-1.	30
Figure 2-7: Time series of water levels at Wilson Avenue Crib in response to perturbation of meteorological disturbance direction for the June 26, 1954 meteotsunami.	33
Figure 2-8: Time series of modeled water levels (line) and observations (dot) at Wilson Avenue Crib in response to the meteorological forcings on July 6, 1954 from Figure 2-3.	36
Figure 2-9: Lake Michigan water level in response to meteorological forcings on July 6, 1954 from Figure 2-3 (times are in CST).	37
Figure 2-10: Time series of modeled water levels (line) and observations (dot) at shore-based locations throughout Lake Michigan in response to the meteorological forcings on July 6, 1954. For gauge locations, see Figure 2-1.	41

Figure 2-11: Time series of water levels at Wilson Avenue Crib in response to perturbation of meteorological disturbance direction for the July 6, 1954 meteotsunami.	44
Figure 2-12 Time series of water levels at Wilson Avenue Crib in response to perturbation of meteorological disturbance speed for the July 6, 1954 meteotsunami.	45
Figure 3-1: Lake Michigan bathymetry and locations of NOAA-NOS water level and NWS-ASOS surface meteorology stations.	60
Figure 3-2: Observations of a meteotsunami event at Calumet Harbor (CAL) on August 4, 2008. At the KORD ASOS station, sudden rises in (a) atmospheric pressure and (b) wind speed occur at 12:15. At 14:30, (c) a 0.91 meter meteotsunami is observed in the CAL water level record. Note that atmospheric pressure and water level data are high-pass filtered with a cutoff period of 6 hr. Radar imagery indicates this meteotsunami is associated with a linear convective system which (d) crossed the lake shoreline at 10:00 and (e) reached KORD (black square) at 12:15, consistent with rises in the atmospheric pressure and wind speeds measured at KORD.	63
Figure 3-3 Schematics of common storm structures associated with meteotsunamis: (a) cluster, (b) complex, (c) linear, (d) bow, (e) frontal, and (f) extratropical cyclone.	69
Figure 3-4: Histogram of events exceeding the absolute height threshold at Calumet Harbor, Menominee, and Green Bay. Note that the horizontal axis is scaled identically for each station with the y-intercept shifted to reflect differences in absolute thresholds.	73
Figure 3-5: Meteotsunami size observations (dots) fit with the Pareto Type 1 (solid line) and Generalized Pareto Distributions (dashed line).	75
Figure 3-6: Monthly distributions of meteotsunamis at each station, with bars subdivided into height quantiles (i.e. 75% to 100% are the largest 25% of events at a given station).	79
Figure 3-7: Distribution of storm structures associated with meteotsunamis at each station.	81
Figure 3-8: Monthly distribution of storm structures associated with meteotsunamis aggregated across all stations.	82
Figure 4-1: Map of Great Lakes meteotsunamis. Historic meteotsunami events from the literature and news reports are classified by impact. Meteotsunami 10-year return levels are calculated from fitting the Pareto Type 1 distribution to waves observed in NOAA/NOS water level records and plotted as scaled circles at the each station location. Also depicted are lake bathymetry contours and county-level population density.	105
Figure 4-2: Scatterplots of (a) lake axis location vs 10 year return level, (b) bottom slope vs mean month of occurrence, (c) longitude vs the fraction of events associated with linear storms, and (d)	

longitude vs the fraction of events associated with complex convective storms. The observed data from each station are plotted as dots (●), the regression line as a dashed line (---). Identified outliers are denoted with a cross (x) but remain included in the regressions. 111

Figure 4-3: Lake-wide meteotsunami height observations (dots) fit with the Pareto Type 1 distribution (solid line). 114

Figure 4-4: (a)-(f) Monthly distributions of meteotsunamis observed in each lake. (g)-(l) Annual distribution of meteotsunamis observed in each lake, normalized for the number of stations operational in each year. A five year moving average in annual meteotsunami occurrences is also plotted. 115

Figure 4-5: Distribution of storm structures associated with meteotsunamis which exceed the 1-year return level, with warm colors (red, orange, and yellow) representing convective structures, cool colors (blues) representing frontal-type structures, and green representing atmospheric gravity waves. 117

Figure 5-1: Occurrence and impact of meteotsunamis worldwide 130

Figure 5-2: Monthly distribution of meteotsunami events reported in the literature, databases, and news reports. 131

1. Introduction

1.1. Meteotsunami Background

Meteotsunamis (or meteorological tsunamis), are propagating water waves generated by a moving atmospheric disturbance. Meteotsunamis exhibit many similarities with seismic tsunamis, as both have wave periods of 2 minutes to 2 hours and undergo resonant amplification that transforms relatively small waves in the open water into destructive forces at the coast [Monserat *et al.* 2006]. As atmospherically forced shallow water waves, meteotsunamis can be considered a specialized type of storm surge [Rao 1967], with the term meteotsunami used to describe waves that behave more like seismic tsunamis than hurricane surges [Monserat *et al.* 2006]. Meteotsunamis are also distinct from seiche, which is a standing wave that occurs at a free gravitational oscillation mode of an enclosed or semi-enclosed basin [Rabinovich, 2009] whereas meteotsunamis occur at the sub-basin scale.

The formation of destructive meteotsunamis requires three processes: (i) wave generation, (ii) propagation resonance, and (iii) local amplification, as shown in Figure 1-1.

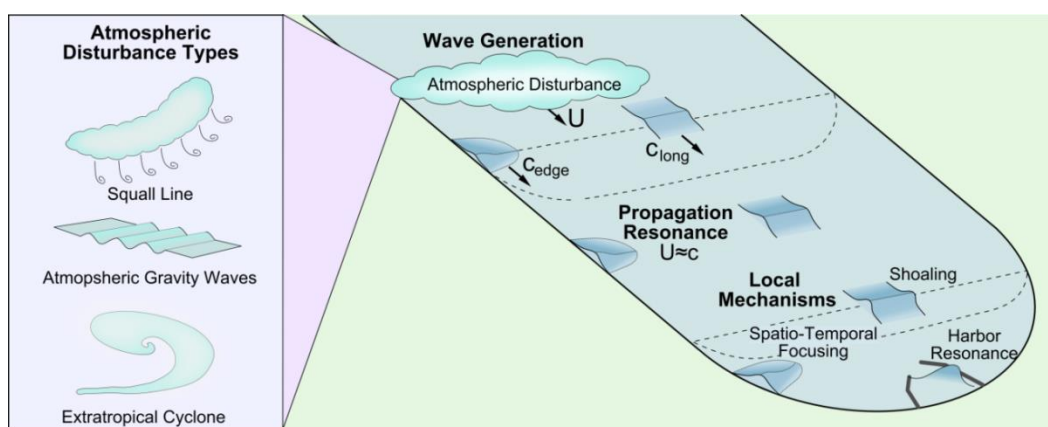


Figure 1-1 Schematic of meteotsunami formation involving (i) *wave generation* by an atmospheric disturbance moving at a speed to (ii) excite a *propagation resonance*. As the wave moves to the coast, (iii) *local mechanisms* such as shoaling and harbor resonance transform the wave to dangerous heights.

First, the pressure and wind perturbations of an atmospheric disturbance, such as a frontal passage, gravity wave, or cyclone, generates an initial water level oscillation in the open water, termed a meteorological wave [Rabinovich 2009]. These meteorological waves are either long waves, which travel in open water and are governed by shallow water wave speed, or edge waves, which are coastally trapped by topographic refraction and are governed by an edge wave dispersion relation [Ursell 1952]. Second, propagation resonance occurs when the atmospheric disturbance and the meteorological wave travel at a similar speed, e.g. $U \approx c_{long}$ or $U \approx c_{edge}$, which allows atmospheric energy to be constantly fed into the meteorological wave and can increase wave amplitude by up to an order of magnitude [Donn and Balachandran, 1969]. Long waves are amplified under the condition of Proudman resonance, in which the generating atmospheric disturbance propagates with a speed U approximately equal to the long wave phase speed [Proudman, 1929]. Edge waves are amplified under the condition of Greenspan resonance, when the atmospheric disturbance and the generated edge wave mode have similar speeds and wavelengths [Greenspan, 1956]. Finally, local mechanisms enhance meteotsunamis as the waves approach the shore and coastal features. Wave height can be amplified by up to two orders through a combination of shoaling, shelf resonance, reflection, refraction, and harbor resonance [Vilibić, 2008]. A strong atmospheric disturbance that propagates over a water body with the characteristics to produce a combination of wave generation, propagation resonance, and local amplification can lead to a meteotsunami with destructive potential [Hibiya and Kajiura, 1982].

Meteotsunamis of up to 6 meters have occurred worldwide [Montserrat et al., 2006; Rabinovich et al., 2009, Vilibić et al., 2014c]. Single events have caused tens of millions of dollars in economic loss by inundating coastal towns [Vilibić et al., 2004; Orlić et al., 2010], sinking boats [Vilibić et al., 2008; Asano et al., 2012], and damaging coastal structures [Mercer,

2002; Tanaka, 2010; Whitmore and Knight, 2014]. The human impact of meteotsunamis can be devastating, with meteotsunamis having resulted in numerous injuries [Churchill *et al.*, 1995; Vučetić *et al.*, 2009; Šepić *et al.*, 2009a] and deaths [Hibiya and Kajiura, 1982; Haslet and Bryant, 2009; Cho *et al.*, 2013] throughout the world.

1.2. Meteotsunamis in the Great Lakes

The Laurentian Great Lakes are a region with an active and impactful meteotsunami history, illustrated by many events which have resulted in destruction and multiple deaths [Ewing *et al.*, 1954; Donn, 1959; Irish 1965; Murty and Freeman, 1973; As-Salak and Schwab, 2004]. While meteotsunamis have been reported in all Great Lakes, they are particularly destructive in Lakes Michigan and Erie. In Lake Michigan, a retreating 6 meter wave pulled ten people to their deaths at Grand Haven, MI on July 4, 1929 [Grand Haven Tribune, 1929] and three people drowned at Holland, MI on July 13, 1938 when a series of long waves swept many people off of piers [Joint Archives of Holland, 2001]. The most notorious Great Lakes meteotsunami occurred on June 26, 1954, when a large wave reported to be 3 meters impacted the coast of Lake Michigan near Chicago and swept many fishermen off of piers at Montrose Harbor, with a total of seven people drowning [Ewing *et al.*, 1954]. More recently, a strong meteotsunami capsized a tug boat at the White Lake, MI harbor in 1998 [NOAA, 1998] and seven people drowned on July 4, 2003 at Sawyer, MI in an incident initially attributed to rip currents [Daniels, 2004] though the water level records indicates a moderate meteotsunami occurred around the time of the drownings. In Lake Erie, a 4 meter wave struck Cleveland on the morning of June 23, 1882. One person drowned, barges were grounded, and fires were extinguished at a steel rolling mill, with estimated damages totaling \$30,000 (\$700,000 in current dollars) [Cleveland Plain Dealer

1882]. On the evening of April 12, 1912, a large wave at Ashtabula, OH broke a steamship loose from her moorings, sending the vessel into a collision with a freighter [*New York Times* 1912]. The most tragic Lake Erie meteotsunami occurred on May 31, 1942, when a 4 meter wave struck the coast surrounding Cleveland [*Toledo Blade* 1942]. The wave pulled many fishermen into the lake and capsized small boats, with seven drowning. Recently on May 27, 2012 in Madison, OH a 2 meter meteotsunami swept three swimmers a half-mile offshore where they were fortunately rescued by a jet skier [*Anderson et al.*, 2015]. Clearly, meteotsunamis pose a threat to Great Lakes coastlines and understanding meteotsunami behavior and occurrence in the Great Lakes is vital to mitigate the impacts of these coastal hazards.

Many key knowledge gaps remain in the understanding of meteotsunami behavior in the Great Lakes. First, historical records of Great Lakes meteotsunamis indicate that significant wind stress has been present in many of these events [*Ewing et al.*, 1954; *Donn and Ewing*, 1956; *As-Salak and Schwab*, 2004], a unique feature compared with many meteotsunamis across the globe that are primarily attributed only to pressure perturbations [*Orlić et al.*, 2010; *Renault et al.*, 2011]. Nevertheless, the question remains: *What is the relative importance of wind stress compared with atmospheric pressure perturbations on these events?* Second, though Great Lakes meteotsunami events have been classified generally as either long wave [*Ewing et al.*, 1954; *Irish*, 1965] or edge wave [*Donn and Ewing*, 1956; *Donn*, 1959], these two types of wave likely do not occur in isolation. This leads to the question: *Do long waves and edge waves interact to create meteotsunamis.* Third, because destructive meteotsunamis are likely the combination of the “perfect” combination of atmospheric disturbance propagation speeds and directions over the right bathymetry and coastlines [*Harris*, 1958], the following question arises: *How sensitive are*

Great Lakes meteotsunamis to the propagation speed and direction of the causative atmospheric disturbance?

Beyond the known historic events, the overall meteotsunami climate of the Great Lakes is poorly understood, which leaves many key knowledge gaps in the understanding of Great Lakes meteotsunami occurrence. First, as the number of known Great Lakes meteotsunamis is limited only to a handful of reported large events, challenges remain in quantifying meteotsunami occurrence frequency, leaving the question: *How often do meteotsunamis occur in the Great Lakes?* Second, as a local phenomenon, the meteotsunami occurrence is expected to vary spatially, leading to the question: *Where do meteotsunamis occur in the Great Lakes?* Third, while the reported meteotsunami events generally happened in the warm season, little information is available to answer the question: *When do meteotsunamis occur in the Great Lakes?* Fourth, the specific types of atmospheric disturbances associated with historic meteotsunamis in the Great Lakes are poorly documented, leading to the question: *What types of storms are associated with meteotsunamis on the Great Lakes?* Finally, as meteotsunami formation is dependent upon the interaction between an atmospheric disturbance and the water body, meteotsunamis can be influenced by variations in storm climate and bathymetry. Thus, to understand the similarities and differences in meteotsunami occurrence across the Great Lakes, the following question is posed: *How do patterns in meteotsunami characteristics in the Great Lakes region correspond to the physical and atmospheric setting of the region?*

1.3 Research Objectives

The aim of this dissertation is to characterize meteotsunamis in terms of both physical mechanisms and historical meteotsunami occurrences. To address this goal, the research is

focused initially on the behavior of meteotsunamis in Lake Michigan, followed by an examination of meteotsunami occurrences throughout the Great Lakes region and worldwide. Guided by key knowledge gaps in the understanding of meteotsunamis in the Great Lakes, specific objectives of the dissertation are as follows:

- 1) Investigate the detailed physical behavior of historic meteotsunamis in Lake Michigan to reveal interaction between edge waves and long waves, the relative contribution of pressure and wind perturbations, and the sensitivity to storm speed and direction.
- 2) Characterize the occurrence of meteotsunamis in Lake Michigan in terms of size-frequency, seasonal distribution, and associated storm structures
- 4) Identify patterns in meteotsunami occurrence in view of the physical and atmospheric features of the Great Lakes region; and
- 4) Quantify worldwide meteotsunami occurrence characteristics from reported events.

1.4. Introduction to the Dissertation

Chapter 2 examines the behavior of two historically significant Lake Michigan meteotsunamis which occurred in 1954 with numerical simulation to reveal the role of long and edge waves in these events, quantify the relative contribution of wind and pressure forcings to the meteotsunami waves, and examine the sensitivity of the waves to the causative atmospheric disturbance speed and orientation. In Chapter 3, water level and radar records are analyzed to characterize the meteotsunami occurrences in Lake Michigan in terms of meteotsunami magnitude, seasonal occurrence, and corresponding atmospheric forcing. Chapter 4 extends this analysis to the entire Great Lakes basin to characterize meteotsunamis throughout the region and investigate patterns in the context of the physical and atmospheric features of the region. A

database of meteotsunamis across the globe is compiled in Chapter 5 to understand global patterns in meteotsunami occurrence. Finally, conclusions and recommendations for future work are offered in Chapter 6.

1.5 References

- Anderson, E.J., Bechle, A.J., Wu, C.H., Schwab, D.J., Mann, G.E., and Lombardy, K.A. (2015a), Reconstruction of a meteotsunami in Lake Erie on 27 May 2012: Roles of atmospheric conditions on hydrodynamic response in enclosed basins. *J. Geophys. Res. Oceans*. Accepted Author Manuscript, doi: 10.1002/2015JC010883.
- Asano, T., T. Yamashiro, and N. Nishimura (2012), Field observations of meteotsunami locally called “abiki” in Urauchi Bay, Kami-Koshiki Island, Japan, *Nat. Hazards*, 64, 1685–1706, doi:10.1007/s11069-012-0330-2.
- As-Salek, J.A., and D.J. Schwab (2004), High-frequency water level fluctuations in Lake Michigan, *Journal of Waterway, Port, Coastal and Ocean Engineering*, 130(1), 45-53. doi: 10.1061/(ASCE)0733-950X.
- Cho, K.-H., J.-Y. Choi, K.-S. Park, S.-K. Hyun, Y. Oh, and J.-Y. Park (2013), A synoptic study on tsunami-like sea level oscillations along the west coast of Korea using an unstructured-grid ocean model, *J. Coastal Res.*, 65, 678–683.
- Churchill, D.D., S.H. Houston, and N.A. Bond (1995), The Daytona Beach wave of 3-4 July 1992 – A shallow-water gravity-wave forced by a propagating squall line, *Bull. Amer. Meteor. Soc.*, 76(1), 21-32, doi: 10.1175/1520-0477(1995)076<0021:TDBWOJ>2.0.CO;2.
- Cleveland Plain Dealer (1882), A tidal wave. June 24, 1882.

- Daniels, Joyce, ed. (2004) "Rip Currents: Be Aware, Swim with Care." *Upwellings* 27 (June 2004): 4-7.
- Donn, W. L. (1959), The Great Lakes storm surge of May 5, 1952, *J. Geophys. Res.*, 64(2), 191–198, doi:10.1029/JZ064i002p00191.
- Donn, W. L. and Balachandran, N. K. (1969) Coupling between a moving air-pressure disturbance and the sea surface, *Tellus*, 21(5), 701–706.
- Donn, W.L., and M. Ewing (1956), Stokes' edge waves in Lake Michigan, *Science*, 124, 1238–1242, doi: 10.1126/science.124.3234.1238.
- Ewing, M., F. Press, and W. J. Donn (1954), An explanation of the Lake Michigan wave of 26 June 1954, *Science*, 120, 684–686, doi:10.1126/science.120.3122.684.
- Grand Haven Daily Tribune (1929), Fifth body recovered from lake today. 1929, July 5
- Greenspan, H. P. (1956), The generation of edge waves by moving pressure disturbances, *J. Fluid Mech.*, 1, 574–592.
- Haslett, S.K., H.E. Mellor, and E.A. Bryant (2009), Meteo-tsunami hazard associated with summer thunderstorms in the United Kingdom, *Phys. Chem. Earth*, 34, 1016-1022, doi: 10.1016/j.pce.2009.10.005.
- Hibiya, T., and K. Kajiura (1982), Origin of the Abiki phenomenon (a kind of seiche) in Nagasaki Bay, *J. Oceanogr. Soc. Jpn.*, 38, 172–182, doi:10.1007/BF02110288.
- Irish, S.M. (1965), The prediction of surges in the southern basin of Lake Michigan: part II. A cases study of the surge of August 3, 1960, *Mon. Weather Rev.*, 93(5), 275–281, doi: doi: 10.1175/1520-0493(1965)093<0282:TPOSIT>2.3.CO;2.

- Mercer, D., J. Sheng, R. J. Greatbatch, and J. Bobanović (2002), Barotropic waves generated by storms moving rapidly over shallow water, *J. Geophys. Res.*, *107*(C10), 3152, doi:10.1029/2001JC001140.
- Monserrat, S., I. Vilibić, and A. B. Rabinovich (2006), Meteotsunamis: Atmospherically induced destructive ocean waves in the tsunami frequency band, *Nat. Hazards Earth Syst. Sci.*, *6*, 1035–1051, doi:10.5194/nhess-6-1035-2006.
- Murty, T. S., and N.G. Freeman (1973), Applications of the concepts of edge waves and numerical modelling to storm surge studies on Lake Huron, in Proc., 16th Conf. Great Lakes Research, pp. 533-548, Intl. Association of Great Lakes Research, Ann Arbor, Michigan.
- New York Times. (1912) Tidal wave sweeps Erie. April 14, 1912.
- NOAA (1998) Storm Data: May 1998, Vol. 40(5), pp. 177.
- Orlić, M., D. Belušić, I. Janeković, and M. Pasarić (2010), Fresh evidence relating the great Adriatic surge of 21 June 1978 to mesoscale atmospheric forcing, *J. Geophys. Res.*, *115*, C06011, doi:10.1029/2009JC005777.
- Platzman G.W (1958), A numerical computation of the surge of 26 June 1954 on Lake Michigan, *Geophysica*, *6*(1), 407–438.
- Platzman G.W. (1965), The prediction of surges in the southern basin of Lake Michigan: Part I. The dynamical basis for prediction, *Monthly Weather Review* *93*(5), 275-281.
- Proudman, J. (1929), The effects on the sea of changes in atmospheric pressure, *Mon. Not. R. Astron. Soc.*, *2*, 197–209.
- Rabinovich, A.B. (2009), Seiches and harbor oscillations, in Handbook of Coastal and Ocean Engineering, edited by Kim, Y.C., 193-236, World Scientific Publishing Company, Toh Tuck Link, Singapore.

- Rao, D.B. (1967), Response of a lake to a time-dependent wind stress, *J. Geophys. Res.*, 72(6), 1697–1708, doi:10.1029/JZ072i006p01697.
- Renault L, Vizoso G, Jansá A, Wilkin J, Tintoré J (2011) Toward the predictability of meteotsunamis in the Balearic Sea using regional nested atmosphere and ocean models. *Geophysical Research Letters* 38. doi:10.1029/2011GL047361
- Šepić, J., I. Vilibić, and D. Belušić (2009), The source of the 2007 Ist meteotsunami (Adriatic Sea), *J. Geophys. Res.*, 114, C03016, doi:10.1029/2008JC005092.
- Tanaka, K. (2010), Atmospheric pressure-wave bands around a cold front resulted in a meteotsunami in the East China Sea in February 2009, *Nat. Hazards Earth Syst. Sci.*, 10, 2599–2610, doi:10.5194/nhess-10-2599-2010.
- Toledo Blade (1942) Killer wave slams Cleveland. May 31, 1942.
- Ursell F (1952) Edge waves on a sloping beach. *Proceedings of the Royal Society Series A* 214(1116):79-98
- Vilibić, I. (2005) Numerical study of the Middle Adriatic Coastal waters' sensitivity to the various air pressure travelling disturbances. *Annales Geophysicae*, 23(12), 3569-3578.
- Vilibić I (2008) Numerical simulations of the Proudman resonance. *Continental Shelf Research* 28:574– 581. doi:10.1016/j.csr.2007.11.005
- Vilibić, I., N. Domijan, M. Orlić, N. Leder, and M. Pasarić (2004), Resonant coupling of a traveling air-pressure disturbance with the east Adriatic coastal waters, *J. Geophys. Res.*, 109, C10001, doi:10.1029/2004JC002279.
- Vilibić I, Domijan N, Cupic S (2005) Wind versus air pressure seiche triggering in the Middle Adriatic Coastal waters. *Journal of Marine Sciences* 57(1-2):189-200

- Vilibić, I., S. Monserrat, A. B. Rabinovich, and H. Mihanović (2008), Numerical modelling of the destructive meteotsunami of 15 June, 2006 on the coast of the Balearic Islands, *Pure Appl. Geophys.*, *165*, 2169–2195, doi:10.1007/s00024-008-0426-5.
- Vilibić, I., S. Monserrat, and A.R. Rabinovich (2014), Meteorological tsunamis on the US East Coast and in other regions of the World Ocean, *Nat. Hazards*, *74*, 1-9, doi:10.1007/s11069-014-1350-x.
- Vučetić, T., I. Vilibić, S. Tinti, and A. Maramai (2009), The Great Adriatic flood of 21 June 1978 revisited: An overview of the reports, *Phys. Chem. Earth*, *34*, 894-903, doi:10.1016/j.pce.2009.08.005.
- Whitmore, P., and B. Knight (2014), Meteotsunami forecasting: Sensitivities demonstrated by the 2008 Boothbay, Maine, event, *Nat. Hazards*, *74*, 11–23, doi:10.1007/s11069-014-1056-0.

2. The Lake Michigan Meteotsunamis of 1954 Revisited

The following is re-produced with permission from Springer. The final publication is available at <http://link.springer.com/article/10.1007%2Fs11069-014-1193-5>

Bechle, A. J., and C. H. Wu (2014), The Lake Michigan meteotsunamis of 1954 revisited, *Nat. Hazards*, 74, 155–177, doi:10.1007/s11069-014-1193-5.

2.1 Introduction

In the summer of 1954, the Chicago coastline was impacted by two large tsunami-like wave incidents just 10 days apart. On June 26, 1954, a large wave occurred at the coast of Lake Michigan near Chicago, with heights of up to 3 meters reported in some locations (Ewing et al. 1954). The wave initially struck the North Shore of Chicago and swept many fishermen off of piers at Montrose Harbor, with a total of seven people drowning. News of the wave spread quickly along the lakefront and police and lifeguards cleared people from the waterfront, where many beaches were inundated up to 50 meters inland. Strong oscillations persisted in the lake long after the disaster, with the Chicago Daily News reporting that rescue and recovery efforts were hindered by strong currents for up to 34 hours after the initial wave arrival. Just 10 days later, on July 6, another series of large waves impacted the Chicago shoreline, with a maximum recorded wave height exceeding 1.25 meters, followed by 0.3 m waves which persisted for over 24 hours (Donn and Ewing 1956). In fact, the harbormaster at Belmont Harbor reported to the Chicago Tribune that lake conditions on July 6th meteotsunami were much more severe than on June 26th. Fortunately, owing to the heightened awareness from the fatal event 10 days prior, sufficient warnings were issued and no loss of life occurred (Hughes 1965). Both events exhibited tsunami-like behavior and were revealed to be meteorologically induced. For that

reason, they are called meteorological tsunamis, or meteotsunamis (Monserrat et al. 2006). Nevertheless, major disparities in the metrological forcings of these two events caused the subsequent meteotsunami waves to have quite different behaviors.

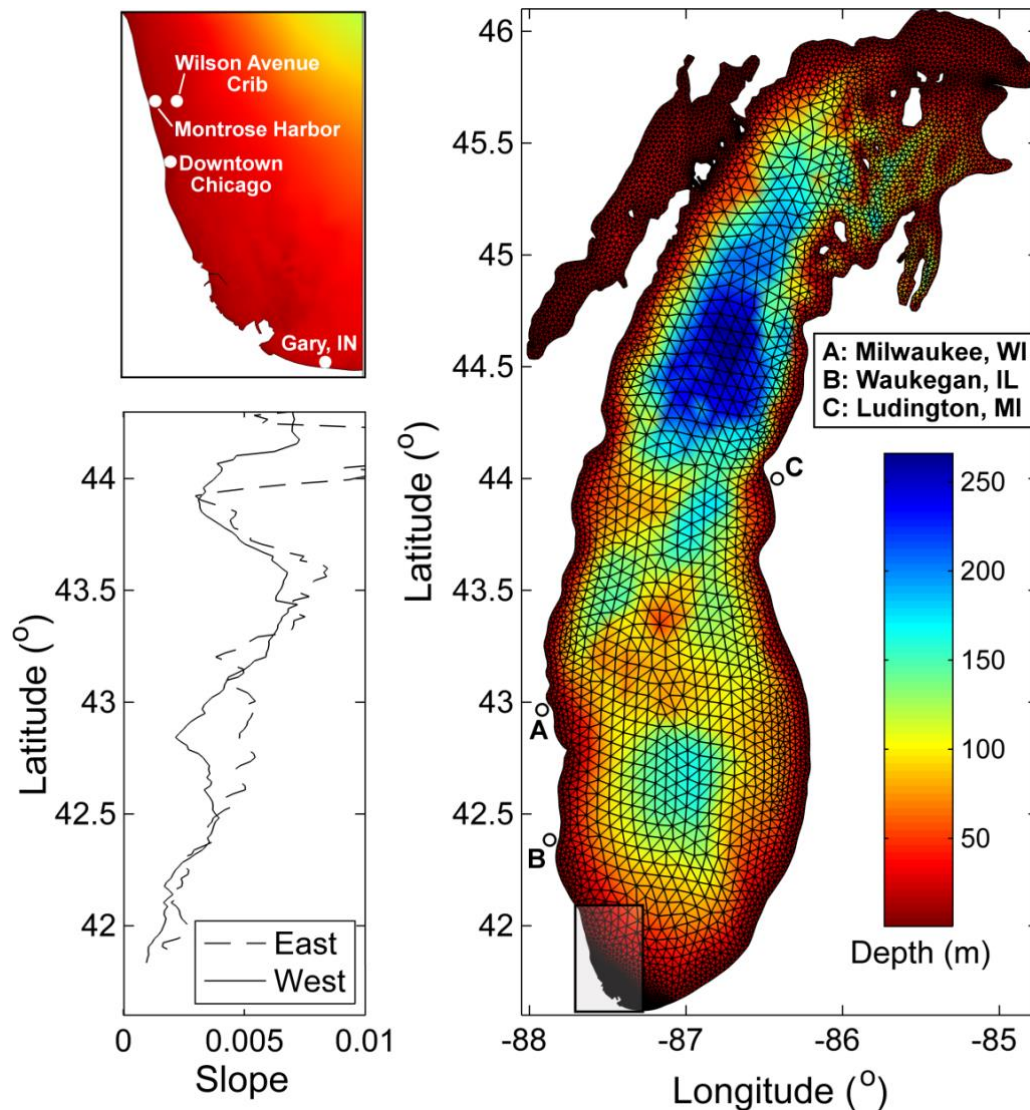


Figure 2-1: Unstructured model grid mesh overlaid on Lake Michigan bathymetry. Bottom slopes along the west and east coasts are shown at the bottom-left; and at the top-left is a zoomed view of the coast near the Chicago lakeshore.

The June 26, 1954 meteotsunami was associated with a squall line storm with wind of approximately 25 m/s and a rapid jump in atmospheric pressure of approximately 300 Pa over 4

minutes. From the arrival times of the pressure disturbance at meteorological stations around the lake, the squall line was determined to move across the lake at 29 m/s with a direction of 135° from north (Ewing et al. 1954). The propagation pathway coincided with a long stretch of water depths between 75 to 90 meters (Figure 2-1), corresponding to an estimated long wave speed of 27 to 30 m/s. Ewing et al. (1954) deduced that the large wave event was caused by Proudman resonance (Proudman 1929), which occurs when the atmospheric disturbance speed matches that of the long wave speed such that atmospheric energy is constantly fed into the water wave, growing amplitude by up to an order of magnitude. The amplified wave first impacted the southeast coast of the lake, where wave heights of 1.5 to 2 meters were reported. The wave then reflected off of the coast, returned westward across the lake, and finally struck the Chicago lakefront with a destructive 3 meter magnitude. The assertion of Proudman resonance by Ewing et al. (1954) was supported by numerical modeling of the event by Platzman (1958). Specifically, the moving speed of the squall line was perturbed in multiple simulations, with the maximum amount of energy transmitted to the lake by a squall line moving at 29 m/s, suggesting that the June 26, 1954 meteotsunami event may have been a worst-case scenario of Proudman resonance. Nevertheless, this early modeling study was limited in resolution, as the 4km grid did not resolve significant higher frequency wave content ($T \sim 10$ minutes) that appeared in the observations. In addition, the model atmospheric disturbance only considered atmospheric pressure fluctuations while excluding the wind forcing, yielding wave heights that underpredicted the observations by a factor of two. Platzman (1965) used this model to conduct a sensitivity study of the response of Lake Michigan to a generic pressure and wind forcing, producing nomograms of maximum wave height and wave arrival time with respect to various disturbance speeds and directions. These nomograms suggest that wind stress, which was

neglected in the model of Platzman (1958), was responsible for over half of the wave energy of the destructive June 26 meteotsunami. While these results provide insight into the general behavior of meteotsunamis in Lake Michigan, Platzman (1965) recognized the limitations of the “rudimentary” representation of pressure and wind forcings. Furthermore, Platzman (1965) suggested constructing meteorological forcings from observations combined with a higher resolution computational grid to reveal the true character of these waves. Overall, the findings in Ewing et al. (1954), Platzman (1958), and Platzman (1965) lay out a basic understanding of the devastating June 26, 1954 Lake Michigan meteotsunami. Nevertheless, important aspects of the wave behavior have remained unresolved, including the final wave magnitude, observed high frequency waves, and long-lasting oscillations.

The July 6, 1954 meteotsunami was associated with a large pressure jump propagating over the lake, though with a much different character than the squall line which occurred 10 days prior (Donn and Ewing 1956). The atmospheric pressure raised 350 Pa over a period of 30 minutes and then decreased by 500 Pa over the next 4 hours. The pressure fluctuation was accompanied by strong northern winds of 30 m/s over a similar time scale. Isochrones for this event indicate that the pressure fluctuation propagated at 22 m/s in a direction of 155° from north. Compared to the June 26th event, this atmospheric disturbance propagated slower and in a more meridional direction with a much more gradual pressure fluctuation. The passage of the pressure fluctuations coincided with large waves along the west coast of the lake, with the wave height in excess of 1.25 meters observed near Chicago. Donn and Ewing (1956) concluded that these oscillations were edge waves, which are waves trapped to the coast by topographic refraction. The speed of edge waves, c_{edge} , is governed by the dispersion relationship

$$c_{edge} = gT \tan[\beta(2n + 1)] / 2\pi \quad (2-1)$$

where β is the lake bottom slope, T is the edge wave period, and g is the acceleration due to gravity (Ursell 1952). Based on the average bottom slope of $\beta = 0.0022$ along the southwest coast of Lake Michigan calculated at the 50 m contour (Figure 2-1) and an observed wave period of 110 minutes, the estimated edge wave speed is 23 m/s, nearly identical to the atmospheric disturbance speed. Thus, the large magnitude of the waves was attributed to a match between the speed of the atmospheric disturbance and the edge waves; this process is known as Greenspan resonance (Greenspan 1956). The modeling results of Platzman (1965) indicate that a storm of this speed and direction would generate edge waves of approximately 1 meter in magnitude, with wind stress as the dominant forcing. Nevertheless, the arrival time of the waves after the passing of the storm predicted by Platzman (1965) (120 minutes) is much greater than was observed (34 minutes), likely owing to the generic pressure and wind forcings used to drive the model which deviate greatly from the recorded meteorology. In addition, maximum wave heights in the observations were not achieved in the first wave arrival, as would be expected from pure Greenspan edge wave resonance (Greenspan 1956). Instead, the maximum wave height occurred with the second wave, suggesting that interaction between multiple waves may have occurred in this event. Donn and Ewing (1956) also observed small shorter period waves ($H \sim 0.15\text{m}$, $T \sim 20$ minutes) superposed on top of the larger edge waves, but no resolute explanation for these oscillations was made. Despite producing large waves, the July 6th wave did not garner as much attention compared with the fatal June 26th meteotsunami. As a result, the understanding of this edge wave resonance has been limited to the data analysis of Donn and Ewing (1956) and generic modeling of Platzman (1965). Many features of the July 6 meteotsunami remain unknown, including the nature of the resonant wave growth, the occurrence of the maximum waves later in the wave train, and the source of the high frequency waves.

The overall objective of this paper is to address the uncertainties which remain in the explanations of these two historic Lake Michigan meteotsunami events regarding the atmospheric forcing, wave growth, high frequency fluctuations, and the long duration of the oscillations. First, we address the relative weighting between atmospheric pressure and wind stress on the meteotsunami generation. Whereas for most observed meteotsunamis, the wind speeds have not been great enough to dominate the wave behavior (Vilibić et al. 2005; Orlić et al. 2010; Renault et al. 2011), the modeling sensitivity study by Platzman (1965) in Lake Michigan suggests that the wind speeds in these events did contribute a significant portion of the meteotsunami energy. Nevertheless, as the “rudimentary” implementations of pressure and wind speed recognized by Platzman (1965) do not faithfully represent the meteorology of these events, we examine the response of the lake to the observed meteorological forcings. Second, we aim to explain the character of the wave growth, specifically the largest wave in the July 6th event which occurred in the middle of the wave train. Furthermore, the sensitivity of the wave growth mechanisms to atmospheric disturbance orientation and speed is explored. Third, we investigate the significant higher frequency content of these meteotsunami events ($T < 20$ min) that were not explained by the effects of Proudman and Greenspan resonances (Ewing et al. 1954; Donn and Ewing 1956). Finally, we aim to explain the long duration of the water level oscillations in these meteotsunamis, specifically the unexpectedly long lasting waves present in the June 26th event.

The paper is structured as follows. Section 2.2 details the hydrodynamic modeling and atmospheric data. In Section 2.3, the results are presented for the two meteotsunami events, June 26 and July 6, 1954. In Section 2.4, salient features of these meteotsunamis are discussed to address the aforementioned uncertainties that remain for these events. Finally, conclusions are drawn in Section 2.5.

2.2. Hydrodynamic modeling and data

The hydrodynamic model Semi-Implicit Eulerian-Lagrangian Finite Element (SELFE) (Zhang and Baptista 2008a; Zhang et al. 2011) is employed in this paper. SELFE is a well validated model and has been used to study hurricane response (Cho et al. 2012), tsunami propagation (Zhang and Baptista 2008b; Zhang et al. 2011), and inundation (Witter 2011; Fortunato et al. 2013). SELFE solves the three dimensional Reynolds-averaged Navier Stokes Equations

$$\frac{\partial u}{\partial x} + \frac{\partial v}{\partial y} + \frac{\partial w}{\partial z} = 0 \quad (2-2)$$

$$\frac{Du}{Dt} = fv + \frac{\partial}{\partial x}(g\eta) + \frac{\partial}{\partial x}\left(\frac{P_a}{\rho_o}\right) + \frac{\partial}{\partial z}\left(K_m \frac{\partial u}{\partial z}\right) + \frac{\partial}{\partial x}\left(F_x \frac{\partial u}{\partial x}\right) + \frac{\partial}{\partial y}\left(F_y \frac{\partial v}{\partial y}\right) \quad (2-3)$$

$$\frac{Dv}{Dt} = -fu + \frac{\partial}{\partial y}(g\eta) + \frac{\partial}{\partial y}\left(\frac{P_a}{\rho_o}\right) + \frac{\partial}{\partial z}\left(K_m \frac{\partial v}{\partial z}\right) + \frac{\partial}{\partial x}\left(F_x \frac{\partial u}{\partial x}\right) + \frac{\partial}{\partial y}\left(F_y \frac{\partial v}{\partial y}\right) \quad (2-4)$$

$$\frac{\partial \eta}{\partial t} + \frac{\partial}{\partial x} \int_{-h}^{\eta} u \, dz + \frac{\partial}{\partial y} \int_{-h}^{\eta} v \, dz = 0 \quad (2-5)$$

where x , y , and z are Cartesian coordinates; u , v , and w are velocity components; ρ_o is density; η is free surface elevation; h is the bathymetric depth; P_a is surface atmospheric pressure; g is gravitational acceleration; f is Coriolis factor; K_m is vertical eddy viscosity; and F_x and F_y are horizontal eddy viscosity. Wind stress is applied at the surface boundary and is calculated from a quadratic drag formulation:

$$K_m \left(\frac{\partial u}{\partial z}, \frac{\partial v}{\partial z} \right) = \frac{\rho_a}{\rho_o} C_D |W| (W_x, W_y) \text{ at } z = \eta \quad (2-6)$$

where $|W|$ is the magnitude of the wind speed, (W_x, W_y) are the wind speed components, ρ_a is the density of air, ρ_o is the density of water at the surface, and C_D is the drag coefficient. A linear relationship between drag coefficient and wind speed is assumed (Sheppard 1958), as the winds used in this study approach but do not exceed observed drag coefficient saturation thresholds, above which linearity breaks down (Powel et al. 2003; Donelan et al. 2004); specifically, the

empirical linear relationship used is that of Smith (1980). Bottom friction is applied at the bottom boundary and is calculated from the quadratic drag law:

$$K_m \left(\frac{\partial u}{\partial z}, \frac{\partial v}{\partial z} \right) = C_f \sqrt{u^2 + v^2} (u, v) \text{ at } z = -h \quad (2-7)$$

where C_f is the bottom drag coefficient. The governing equations are solved on an unstructured horizontal grid with a hybrid S-Z vertical coordinate system. A Galerkin finite element scheme is used to solve the pressure gradient while advection terms are treated with a higher-order Eulerian-Lagrangian scheme. Semi-implicit time-stepping is used to avoid mode splitting and allow for large time steps.

The model domain encompasses the entire Lake Michigan basin. The horizontal grid is a triangular unstructured mesh with a resolution ranging from 1000 meters in the open water down to 30 meters along some sections of the coast, yielding 109892 computational elements. The vertical grid is composed of 10 layers (Song and Haidvogel 1994). A time step of $\Delta t = 25$ s is chosen based on the semi-implicit scheme. A bottom drag coefficient of $C_f=0.0025$ is used based on calibration against water level results from the Great Lake Coastal Forecasting Model (Kelly et al. 1998; O'Connor et al. 1999) (not be shown here for brevity). The model is forced with moving disturbances of atmospheric pressure and wind stress constructed to emulate historical observations of the two meteotsunami events. The atmospheric pressure gradients characteristic of meteotsunami-causing disturbances are calculated based upon an integral approach in which the line integral of pressure around the perimeter of each computational element is used to calculate the pressure gradient of the element. As the atmospheric disturbances in this study are approximated by analytical definitions, these line integrals can be calculated numerically with high precision to give a better representation of the rapidly varying pressure disturbance than the original vertex-based gradient calculation in SELFE.

The first event is the June 26, 1954 meteotsunami, caused by a squall line thunderstorm propagating across the lake. Atmospheric pressure and wind speed observations of this event from the Wilson Avenue Crib meteorological station (see Figure 2-1 for location) were originally published by Platzman (1958), shown as black lines in Figure 2-2. Atmospheric pressure experienced a rapid increase of 300 Pa over a period of 4 minutes starting at 6:25 Central Standard Time (all subsequent times are in CST), maintained a constant pressure over 90 minutes, and ended with a slow 200 Pa decrease over an additional 90 minutes. Wind speed sharply increased to 25 m/s over the course of a minute with the arrival of the squall line at 6:21 and subsequently decreased to zero over a period of 30 minutes. In the model, we approximated the atmospheric pressure disturbance spatially as a trapezoidal pressure perturbation (blue lines in Figure 2-2), with an initial 300 Pa increase over 7 km, 160 km of constant pressure, and a 200 Pa decline over a subsequent 160 km. Similarly the wind stress of the squall line was represented using a triangular wind speed perturbation, with an initial 25 m/s increase over 2 km and a 25 m/s decline over a subsequent 54 km. Due to limited available spatial information, both the atmospheric pressure and wind speed perturbations were assumed to be a straight linear front constant over the lake and propagated at 29 m/s at a direction 135° from north (Ewing et al. 1954).

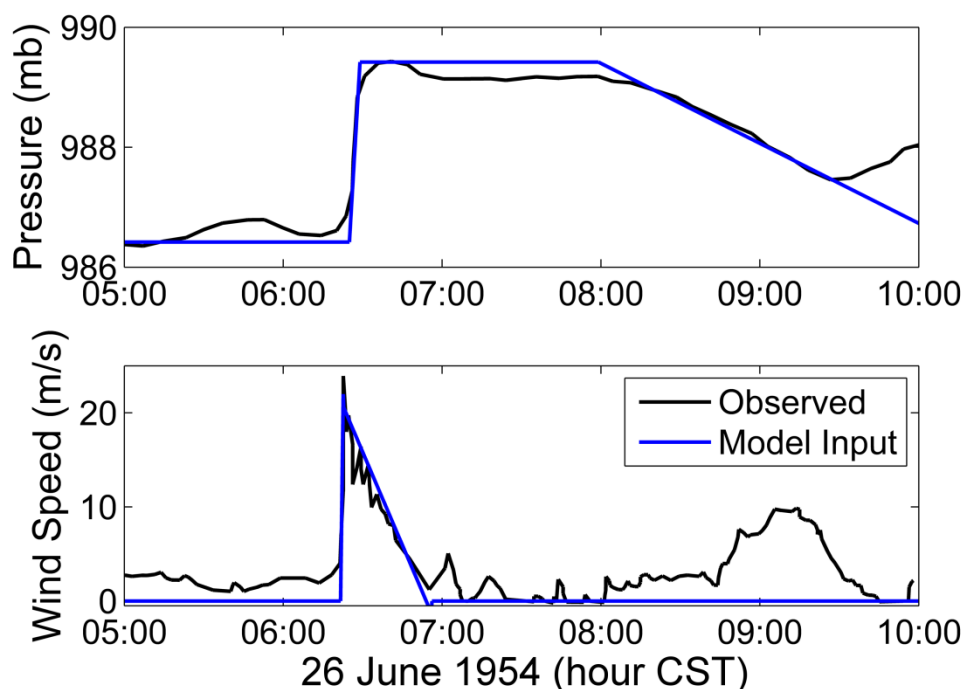


Figure 2-2: Observed June 26, 1954 atmospheric pressure and wind records (black lines) at Wilson Avenue Crib station (taken from (Platzman 1958)) and corresponding input meteorological forcing functions (blue lines) used for the hydrodynamic model.

The second meteotsunami occurred on July 6, 1954 and was associated with a pressure disturbance, though strong winds were also noted. Pressure observations of this event from the Wilson Avenue Crib meteorological station were originally published by Donn and Ewing (1956), shown as a black line in Figure 2-3. An increase in atmospheric pressure of 350 Pa occurred over a period of 30 minutes starting at 15:02, followed by a much slower 500 Pa decrease in pressure over an additional 4 hours. The atmospheric pressure disturbance was spatially approximated as a triangular pressure perturbation (blue line in Figure 2-3), with an initial 350 Pa pressure increase over 40 km and a 500 Pa decline in pressure over a subsequent 315 km. Donn and Ewing (1956) did not report wind anemometer data though wind speed was noted to have sharply increased from 10 m/s to 32 m/s over the 30 minute period of pressure rise. The best available data for this event are from the hourly wind record at the Glenview Naval Air

Station (shown as dots in Figure 2-3), which confirm this wind speed but are temporally too coarse to infer more detail about the wind field. Based on the descriptions of the wind behavior by Donn and Ewing (1956), a triangular wind speed perturbation is assumed here with an increase in wind to 32 m/s over 40 km and a subsequent decrease back to 10 m/s over an additional 80 km, shown as a blue line in Figure 2-3. Both the atmospheric pressure and wind speed perturbations are assumed to be a straight linear front constant over the lake and are propagated across the model domain at 22 m/s at a direction 155° from north, in accordance with the observations by Donn and Ewing (1956).

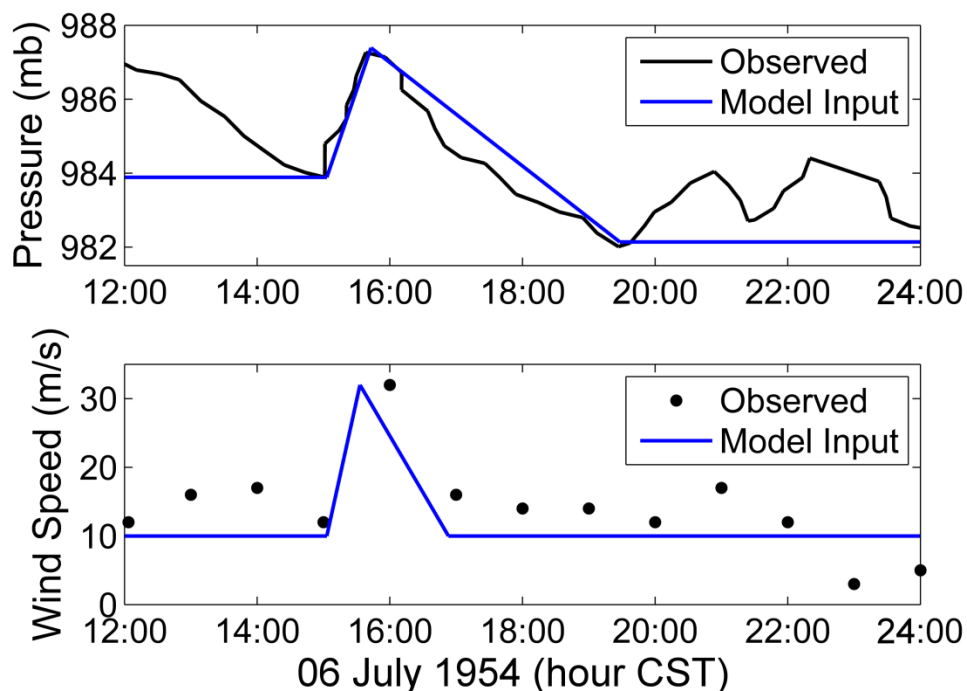


Figure 2-3: Observed July 6, 1954 atmospheric pressure records at Wilson Avenue Crib station (taken from (Donn and Ewing 1956)) and hourly wind records available at the Glenview Naval Air Station, IL. The blue lines are the input meteorological forcing functions for hydrodynamic model.

2.3. Results

2.3.1. June 26, 1954 Meteotsunami

Model results are first compared with the water level observations at Wilson Avenue Crib (Figure 2-4), located at (41.97°N, 87.59°W), 4 km east of Montrose Harbor where the main disaster occurred (Platzman 1958). Since Wilson Avenue Crib was the only open-water water level station to record the June 26, 1954 meteotsunami, these observations provide insight into the nature of the propagating meteotsunami wave, unlike shore-based gauges which can be adulterated by local mechanisms such as harbor oscillations (Rabinovich 2009). To elucidate the importance of pressure and wind on the meteotsunami formation, we run the model for three separate forcing scenarios: i) pressure only, ii) wind only, and iii) pressure and wind. Figure 2-4 shows that neither the pressure nor wind forcing alone is sufficient to reach the magnitude of the water level oscillations but the wave height resulting from the combination of both pressure and wind forcing closely matches the observed wave time series. Interestingly, the time series resulting from a superposition of the “pressure only” and “wind only” records is nearly identical to the time series of the simultaneous pressure and wind forcing scenario, suggesting that the wave behaves in a linear manner. Pressure accounted for approximately 60% of the wave height and wind stress contributed the remaining 40% of the event.

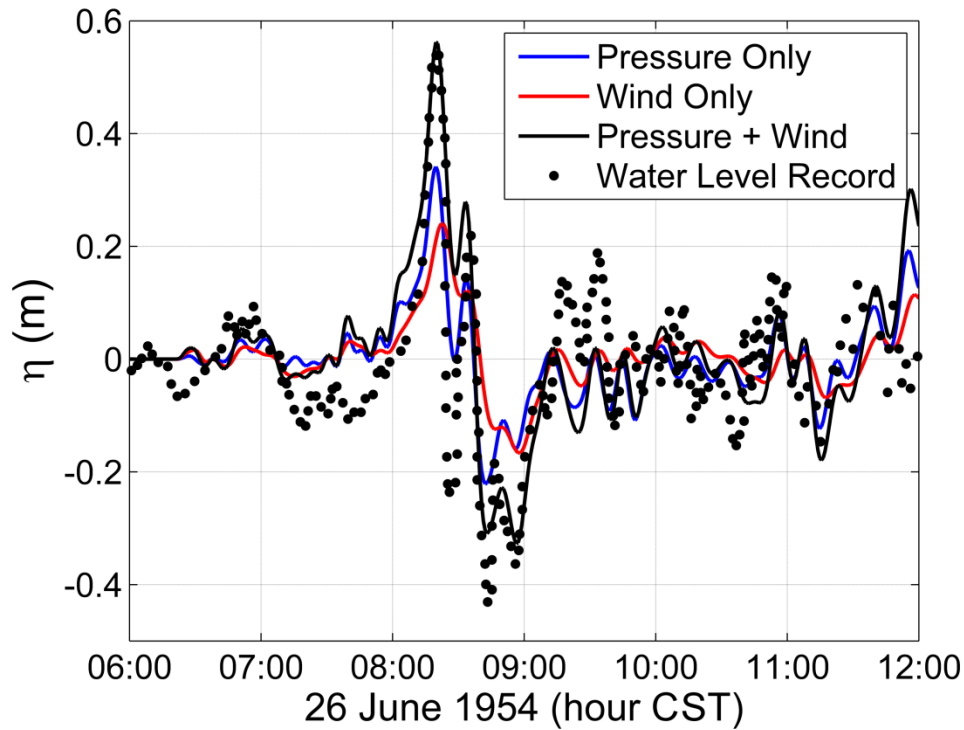


Figure 2-4: Time series of modeled water levels (line) and observations (dot) at Wilson Avenue Crib in response to the meteorological forcings on June 26, 1954 from Figure 2-2.

This finding agrees with an analytical comparison of the pressure and wind terms of Equation 2-2 and 2-3; the atmospheric pressure term is calculated as $\partial(P_a/\rho)/\partial x$, the fourth term of Equation 2-2, whereas the wind term is $\tau/\rho H$, derived from fifth term of Equation 2-2 where wind stress, τ , is calculated from the formulation of Equation 2-6 and the vertical derivative is taken as a linear gradient over depth, H (Orlić et al. 2010). From the pressure rise of 300 Pa over 7 km, the pressure term is $4.3 \times 10^{-5} \text{ m/s}^2$ and from a maximum wind speed of 25 m/s over a resonant depth of 80 meters, the wind term is $2.1 \times 10^{-5} \text{ m/s}^2$. This analytical analysis attributes 67% of the wave height to pressure and 32% to wind, which is a greater imbalance than depicted in the model. Nevertheless, as shown in Figure 2-2, the pressure gradient rise acted over 4 minutes, while the wind speed varied linearly over 30 minutes. To account for the effects of the different pressure and wind disturbance forms, these two terms are integrated over the pressure and wind

perturbations of Figure 2-2. When averaged over the duration of the perturbations, the pressure term is $7.2 \times 10^{-6} \text{ m/s}^2$ and wind is $5.7 \times 10^{-6} \text{ m/s}^2$. This yields a pressure and wind partitioning of 56% and 44%, respectively, closer to the model result of 60%/40% split between pressure and wind. As the wind term is dependent upon depth, wind is expected to have a greater influence than pressure over depths shallower than 60 m (see Figure 2-1) (Orlić et al. 2010), though the subsequently slower shallow water speeds ($c < 24 \text{ m/s}$) would not promote significant Proudman resonance (Platzman 1958). The model of Platzman (1965), which forced the lake with generic pressure and wind disturbances, suggested that pressure accounted for 43% of the wave height and wind for 57%; the majority of the wave height is incorrectly attributed to wind stress because the Platzman (1965) model was forced with a both lower pressure gradient and a longer duration wind stress field than was observed in the actual disturbance. Thus, while generic atmospheric disturbances provide an approximate indication of meteotsunami behavior, properly represented meteorological conditions are crucial to capture detailed meteotsunami wave mechanisms.

With both pressure and wind forcing included, the model represents the magnitude and arrival time (8:20) of the devastating initial wave and the subsequent oscillations ($t > 8:25$) which the simulations of Platzman (1958) could not replicate. This result illustrates the importance of the higher resolution grid used in this study ($\sim 1 \text{ km}$) compared to the coarse resolution grid employed in Platzman (1958) ($\sim 4 \text{ km}$). The source of the first of these subsequent oscillations ($T = 15 \text{ min}$) was initially thought to be a “second surge” indicative of a high frequency wave front with the remaining oscillations ($T = 9 \text{ min}$) attributed to background lake level fluctuations (Platzman 1958). The simulations in this study reveal the first subsequent oscillation (8:33) to instead be the long wave reflected off of the west coast of Lake Michigan and propagating eastward towards open water while the successive oscillations that persisted for the duration of

the reported water level record ($t > 9:15$) were a train of anticyclonic propagating edge waves. Details of these oscillations will be analyzed through the spatial wave propagation through the entire lake.

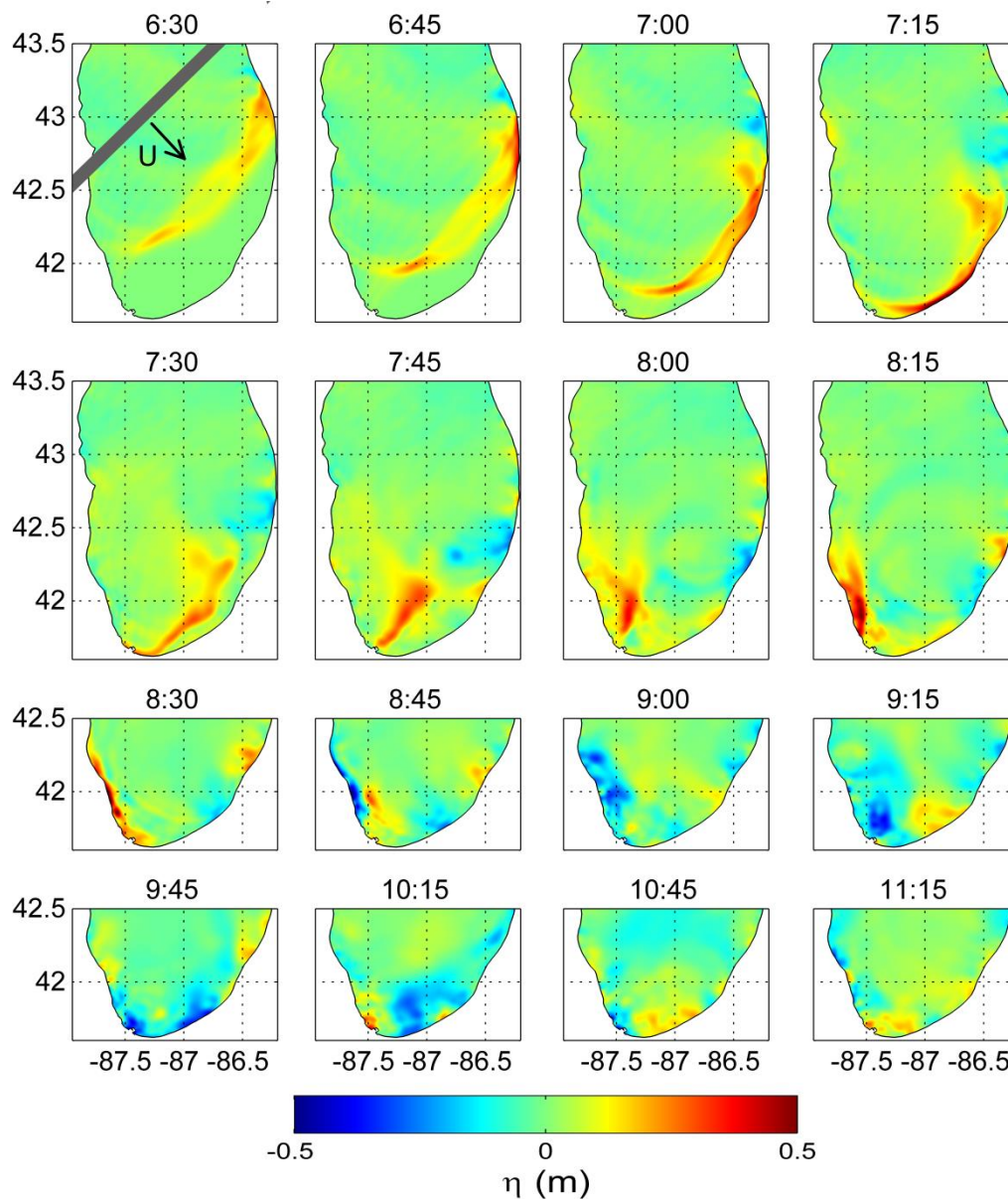


Figure 2-5: Lake Michigan water level in response to meteorological forcings on June 26, 1954 from Figure 2-2 (times are in CST).

The spatial propagation of the meteotsunami wave in response to the combined pressure and wind forcing is given in series of snapshots in Figure 2-5. The first snapshot at 6:30 depicts the long wave that has propagated with the squall line for nearly 100 minutes, resulting in a resonant growth in the open water to a 0.2 m crest height. The location of the largest crest height corresponds to the Proudman resonance depths of 75 to 90 meters, where the shallow water wave speed closely matched the squall line speed. The lowest heights of this wave front occurred in the middle of the lake, i.e., between longitudes of 87.0°W and 86.5°W , corresponding to the deepest point in southern Lake Michigan with the water depth of 160 meters (see Figure 2-1). As a result, the disturbance did not meet the Proudman resonance condition at this location and wave growth was limited. Fifteen minutes later at 6:45, two distinct waves existed between longitudes of 87.0°W to 86.5°W , where the leading wave traveled at the faster free wave speed of the 150 meter deep water and the trailing wave was the forced wave aligned with the squall line. Meanwhile, the northern edge of the wave front first impacted the east coast of the lake at (42.6°N , 86.4°W). By 7:00 much of the long wave impacted the east coast of the lake while the northern extent of the wave (42.7°N , 86.4°W) already began to reflect back westward. At 7:15, the long wave hit the southeast shore of the lake, reaching crest heights of 0.65 m, while north of 42.2°N , the wave reflected off the coast and travelled westward. By 7:30, the incident long wave fully reflected off the east coast. As the reflected wave approached the Chicago lakeshore at 7:45, the large horizontal extent of the original long wave (~150 km) that spanned diagonally across the lake converged to approximately 50 km. This was caused by the concave shape of the east coast of Lake Michigan, which acted to focus the reflected wave and direct the propagation towards Chicago. Between 8:00 and 8:15, the reflected wave crest was refracted by the bathymetry to align with the coastline (Hibiya and Kajiura 1982), reaching a maximum offshore

wave crest height of 0.43 m. Finally, the reflected wave struck the Chicago lakefront at 8:30, with maximum wave heights in the model occurring less than 2 km south of Montrose Harbor where the seven fatalities occurred. As seen at 8:45, the long wave reflected off of the Chicago lakeshore and propagated back eastward. This phenomenon explains the high frequency “second surge” observed by Platzman (1958) at 8:35 in the Wilson Avenue Crib water level record (Figure 2-4). Indeed, this wave should be considered neither a second surge nor a high frequency component of the meteotsunami but instead a reflected wave propagating in the offshore direction. The reflected wave gave the appearance of a high frequency wave when described by Platzman (1958) because the water level record was taken from Wilson Avenue Crib, located 4 km offshore such that a reflected wave would appear rather quickly after the incident wave in the water level measurements. The 4 km grid of the model by Platzman (1958) was too coarse to resolve a reflected wave at this location, as the simulated Wilson Avenue Crib record was derived from a node adjacent to the model boundary. Thus, the cause of this apparent high frequency fluctuation was mistaken as a “second surge” when in reality, the source of this oscillation was a reflected wave which was propagating offshore and did not contribute to the disaster at the coast.

A series of 0.5 m high waves occurred along the coast for many hours after the initial meteotsunami wave struck Chicago, starting at approximately 9:15 (Harris 1957). While these waves were not responsible for the drownings that occurred, the waves were still troublesome, as the Chicago Daily News reported that rescue and recovery efforts were hindered by strong currents and turbid waters that persisted for over a day. As seen in Figure 2-5 between 8:45 and 9:15, a large portion of the wave energy caused by the Produman resonance dissipated as the reflected long wave propagated back towards the eastern shore of Lake Michigan, likely owing

to the convex shape of western coastline near Chicago where the wave reflected. Thus, the persistent oscillations were likely not due to a continual reflection of the destructive wave. The results of this simulation reveal that the strong waves that long-lasting oscillations were instead an edge wave train generated by the squall line simultaneous to the long wave meteotsunami. Figure 2-5 at 6:30 shows that edge waves were generated by the squall line along the east coast at (43.1°N, 86.4°W). This edge wave structure has two alongshore antinodes, characteristic of the first harmonic edge wave mode (Ursell 1952). The existence of first harmonic edge waves is verified by calculating the expected wave speed based upon the edge wave dispersion relation given by Equation 3-1, with the wave period of 12 minutes observed in the model, the bottom slope $\beta = 0.008$ from Figure 2-1, and a mode number $n = 1$. The calculated speed of 29 m/s matches the disturbance propagation speed of 29 m/s, confirming the existence of first harmonic mode edge waves. As these harmonic edge waves traveled with the squall line, Greenspan resonance grew the waves to a relatively large 0.2 m crest height. A train of edge waves developed by 6:45, evident by the trough following the forced edge wave at (43.2°N, 86.6°W). By 7:00, the squall line crossed the shoreline and no longer travelled in resonance with the edge waves, resulting in a freely propagating edge wave train led by the 0.2 m trough at (43.1°N, 86.3°W). Between 7:00 and 7:45, the edge wave train encountered a slope change from $\beta = 0.006$ to $\beta = 0.002$. Free edge waves propagating over gradually shallowing slopes slow in celerity and increase height in an effect similar to shoaling (Kurkin and Pelinovsky 2003). Indeed, at 7:45, the edge wave velocity slowed to 15 m/s and the trough reached a height of 0.38 m at (42.3°N, 86.3°W), exceeding the maximum height of the Proudman resonant long wave which struck this location at 7:08. This evidence indicates the importance of the harmonic edge wave in this event, which was never reported before. As seen at 8:15, the edge wave reduced to a

trough height of 0.25 m as the waves propagated around the convex shoreline near (42.1°N, 86.5°W). As the long wave meteotsunami wave struck the Chicago lakefront and reflected back into the open water, the edge wave train continued to propagate anticyclonically around the lake shore, eventually impacting the Chicago lakefront from 9:15 onward. This can also be seen in the Wilson Avenue Crib water level record (Figure 2-4), in which oscillations persisted at this station for the extent of the record. The edge wave train revealed here likely explains the strong currents and turbid waters reported by the Chicago Daily News which impeded rescue and recovery efforts for over a day after the initial wave struck.

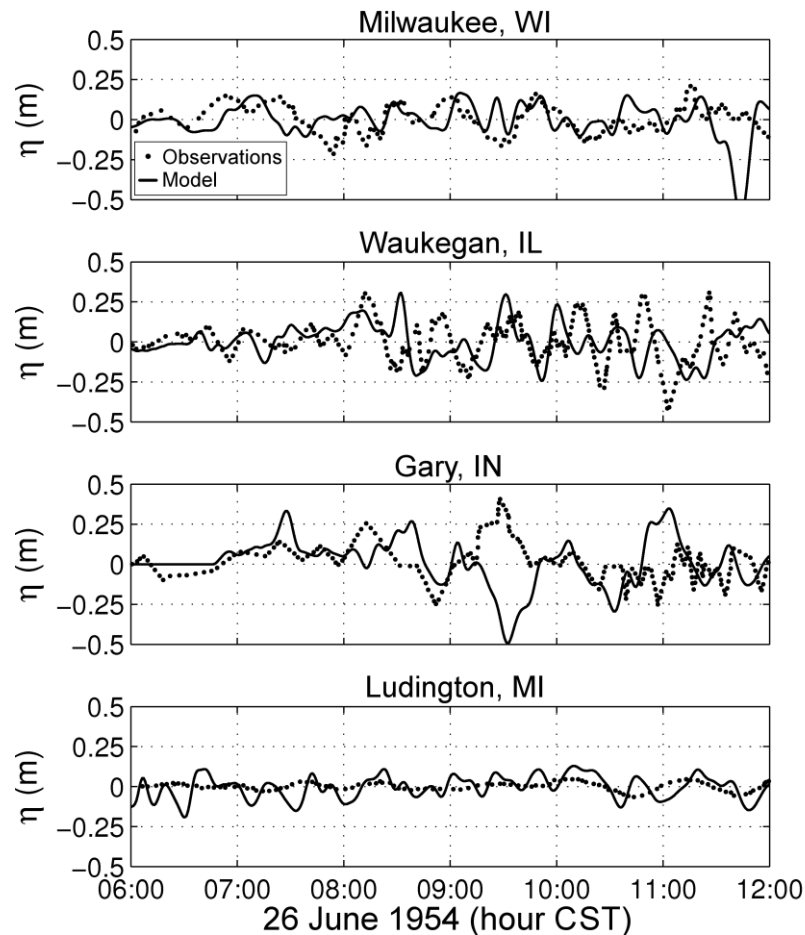


Figure 2-6: Time series of modeled water levels (line) and observations (dot) at shore-based locations throughout Lake Michigan in response to the meteorological forcings on June 26, 1954. For gauge locations, see Figure 2-1.

To verify the spatial patterns observed in the model snapshots, in Figure 2-6 model results are compared with water level observations reported by Harris (1957) at shore-based gauges located at Milwaukee, WI; Waukegan, IL; Gary, IN; and Ludington, MI (see Figure 2-1 for map of locations). Note that as the shore-based gauges are within harbors, the observed wave signal is likely masked by harbor oscillation modes (Rabinovich 2009). In this paper the model grid does not resolve the scale of harbors at these locations, as simulating the interactions was not the intent. Nevertheless, a comparison of the observations with nearby model results provides an indication of wave magnitude and arrival time at the harbor. At Milwaukee (43.0°N , 87.9°W), which is 140 km north of Chicago, the model predicts an initial 0.25 m high wave arrival at 7:08, 15 minutes after the observed wave actually arrived with similar magnitude. This oscillation is associated with a small edge wave train propagating along the west coast of the lake, visible in Figure 2-6 at 7:15. While the main destructive wave did not extend north to Milwaukee, a 0.3 m wave appears in both the observation and model time series at approximately 9:00; this wave was a weak long wave reflection off the east coast of the lake and can be seen in Figure 2-6 at 8:15 propagating to the northwest at (42.7°N , 87.8°W). Subsequent oscillations occurred at Milwaukee from 11:00 onward in both the observations and model results, attributed to the anticyclonic edge waves which were generated on the east coast of the lake. At Waukegan (42.4°N , 87.8°W), which is 70 km north of Chicago, the model predicts an initial wave arrival at 8:09 with crest height of 0.18 m followed by a second wave at 8:31 of 0.5 m height. Both waves can be seen in Figure 2-6 at 8:15, with the first wave already at Waukegan and the second wave approaching the coast. The modeled waves arrived at Waukegan slightly ahead of the observed waves, which appeared in the record at 8:12 and 8:41 with similar magnitude. Subsequently, both the model and observations depict reasonably large ($H \sim 0.5$ m) oscillations for the remainder

of the wave record ($t > 9:30$) at Waukegan which are the anticyclonic edge waves. At Gary (41.6°N , 87.3°W) near the southern extent of the lake, the model predicts a wave arrival at 8:38, which is well after the observed arrival at 8:12. Overall, the character of the observed water level time series is replicated by the model, specifically between 8:00 and 10:00 (corresponding to $\sim 8:30$ to 10:30 in model results), and this temporal discrepancy exists throughout the record. At Ludington (43.9°N , 86.5°W), which is located on the east side of the lake, waves of moderate height ($H \sim 0.2$ m) appear early in the model time series, associated with the passing of the simulated disturbance over Ludington at 5:40. Water level oscillations were not noticeable in the observations until 10:00. This discrepancy may be explained by the location of the water level gauge, which is separated from Lake Michigan by a harbor and a narrow channel, an arrangement which likely damped the small open lake oscillations. The oscillations that appear in the water level observations after 10:00 are revealed by the model to be a train of cyclonic edge waves. Overall, the model time series capture the nature of the water level observations well. The slight deviations in wave arrival times between the model and observations are likely due to the assumption of a straight linear disturbance front used in the model whereas isochronal analysis of the event indicate that the front may have been slightly curved (Harris 1957). Nevertheless, over-lake surface meteorology observations are not available to accurately depict the actual shape of the disturbance. Discrepancies in oscillation frequency and magnitude are likely due to the harbors within which the observations were made, which were not resolved in the computational grid but modify the open water wave signal with local oscillation periods.

Finally, the sensitivity of the June 26th meteotsunami event to atmospheric disturbance velocity is examined by perturbing the simulated disturbance propagation direction. Platzman (1958) determined that meteotsunami wave energy wave for this event is maximized for a squall

line moving at 29 m/s, concluding that this speed most effectively matches the long wave speed for optimum Proudman resonance. The nomograms of Platzman (1965) provided further insight into the response of Lake Michigan to a combination of disturbance speeds and directions. In this paper we aim to examine the detailed behavior of the June 26th event. Thus the focus of this sensitivity is on the time series at Wilson Avenue Crib; for more general discussion of lake-wide response, readers are referred to Platzman (1965). The propagation direction of the disturbance is perturbed in 10° increments, with the resulting water level time series at Wilson Avenue Crib plotted in Figure 2-7.

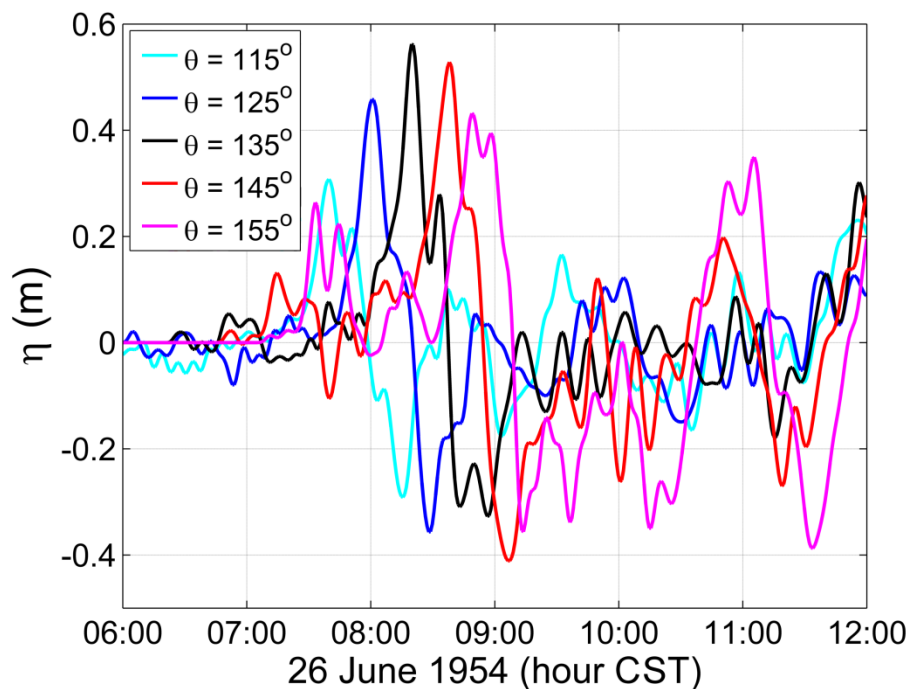


Figure 2-7: Time series of water levels at Wilson Avenue Crib in response to perturbation of meteorological disturbance direction for the June 26, 1954 meteotsunami.

Compared to the actual event ($\theta = 135^\circ$), a more zonal propagation pathway ($\theta = 125^\circ$) results in an 8% reduction in maximum wave height and an earlier wave arrival by 19 minutes. Subsequent

oscillations are on the same order of magnitude as the original event. An even more zonal propagation ($\theta = 115^\circ$) results in a 33% reduction in the maximum wave height with a 40 minute earlier arrival. A more meridonal propagating storm ($\theta = 145^\circ$) results in a 6% increase in maximum wave height and an 18 minute later arrival; this is consistent with the nomograms of Platzman (1965) which indicated the largest possible wave height would occur at this orientation. Spatial snapshots similar to Figure 2-5 at 8:30 (not shown for brevity) reveal the extent of the Chicago coastline impacted by the destructive wave is minimized for $\theta = 145^\circ$, suggesting that this disturbance orientation leads to the most optimal reflected wave focusing off of the concave east coast. This may explain why the 145° orientation of the event results in the largest wave magnitude. In addition, a pronounced 0.1 m wave crest appeared ahead of the destructive wave at 7:15, which is attributed to a forced edge wave caused by a disturbance orientation that is more perpendicular to the coast than the actual event. Large oscillations ($H \sim 0.4\text{m}$) occurred after the destructive wave (10:00 and 11:00), which are anticyclonic edge waves generated on the east coast. An even more meridonal propagation ($\theta = 155^\circ$) yields a 12% reduction in wave height and a later arrival time (8:50), but larger edge waves before (7:40, $H \sim 0.3\text{m}$) and after (11:00, $H \sim 0.7\text{m}$) the destructive long wave. Overall, the perturbations reveal that a slightly more meridonal propagating storm (i.e., $\theta = 145$) on June 26th may have resulted in not only a larger long wave, but also much larger edge waves preceding and proceeding the disastrous event.

2.3.2. July 6, 1954 Meteotsunami

Model results for the July 6, 1954 meteotsunami are compared with the water level observations at Wilson Avenue Crib (see Figure 2-8), originally reported by Donn and Ewing (1956). The relative role of pressure and wind in this event is assessed by forcing the model with

pressure only, wind only, and combined pressure and wind scenarios. Figure 2-8 illustrates that the model with combined pressure and wind forcings matches the overall magnitude and phase of the water level fluctuations but underpredicts the maximum water level rise at 16:30. In addition, the model exhibits the high frequency oscillations ($T \sim 20$ min) observed by Donn and Ewing (1956); these oscillations are due to a first harmonic edge wave mode, with more details provided later. In comparison with “pressure only” and “wind only” scenarios, the model with the combined forcings yields the better agreement with observations, in particular for the time between 15:30 and 19:00. Much like the June 26th event, the sum of the “pressure only” and “wind only” time series is almost equal to that of the simultaneously forced case, suggesting that nonlinear effects are negligible to the open water shallow water meteotsunami waves considered in this study. Nonlinear effects are expected to be more important in nearshore harbors where the waves would become steeper and more asymmetric (Vilibić et al. 2008), though these features were not resolved by the computational grid in this study. The result suggests that both pressure and wind forcings were essential to cause the water level oscillations, with wind stress as the dominant source of wave energy, accounting for 68% of the wave height and pressure responsible for approximately 32% of the wave height.

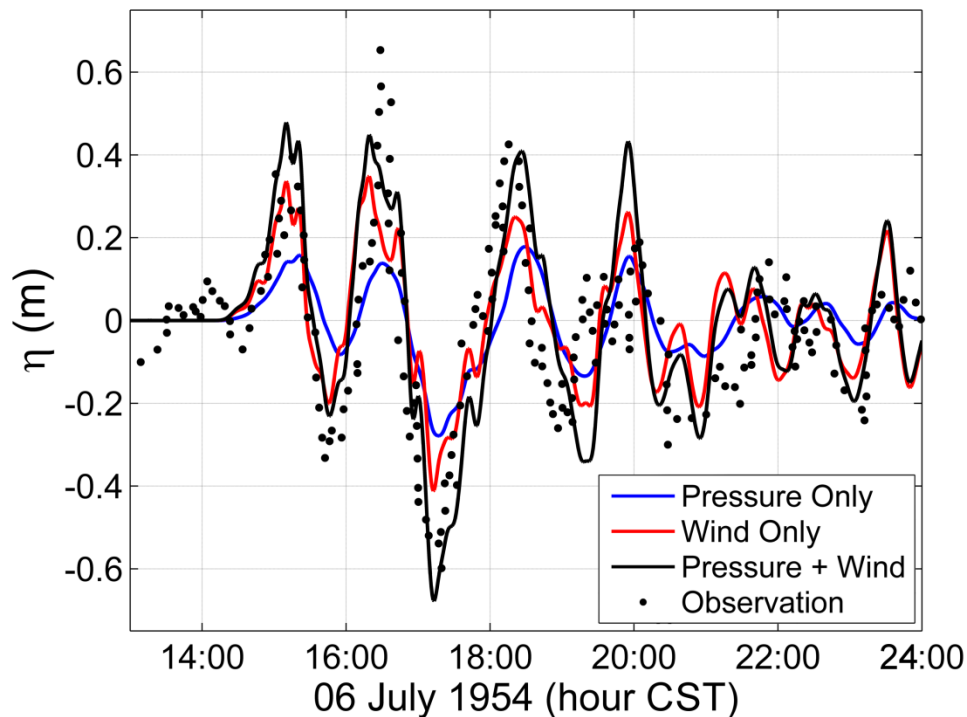


Figure 2-8: Time series of modeled water levels (line) and observations (dot) at Wilson Avenue Crib in response to the meteorological forcings on July 6, 1954 from Figure 2-3.

The dominance of wind in this event is to be expected based on an analytical comparison of pressure and wind terms, owing to the shallower depths over which the edge waves propagate. From the pressure rise of 350 mb over 40 km, the pressure term of Equation 2-2 is $8.8 \times 10^{-6} \text{ m/s}^2$. As the main waves in this case were edge waves generated over coastal slopes, a maximum wind speed of 32 m/s is applied over the mean shelf depth of 25 meters to give a wind term from Equation 2-2 of $1.1 \times 10^{-4} \text{ m/s}^2$. This partitioning would attribute only 7% of the wave height to pressure and 93% to wind, which is a greater imbalance than depicted in the model. As in Section 3.1, this estimate is revised by integrating and averaging the pressure and wind terms over the temporal perturbation forms in Figure 2-3. This procedure yields a pressure term of $8.9 \times 10^{-6} \text{ m/s}^2$ and wind term of $3.2 \times 10^{-5} \text{ m/s}^2$, a pressure and wind partitioning of 22% and 78%, respectively. This partitioning of wave energy source is similar to that found by Platzman (1965)

for a disturbance of the same propagation speed and direction but narrower, generic pressure and wind forms, with 76% of the wave height attributed to wind stress and 24% to pressure. The major difference with the Platzman (1965) results, however, is the wave arrival times; whereas the nomogram of Platzman (1965) indicated that the wave train would arrive at Wilson Avenue Crib approximately 120 minutes after the disturbance passes, the model in this study simulates a 37 minute lag in wave arrival, much closer to the observed 34 minutes and a critical improvement if such model results were to be used in a predictive capacity.

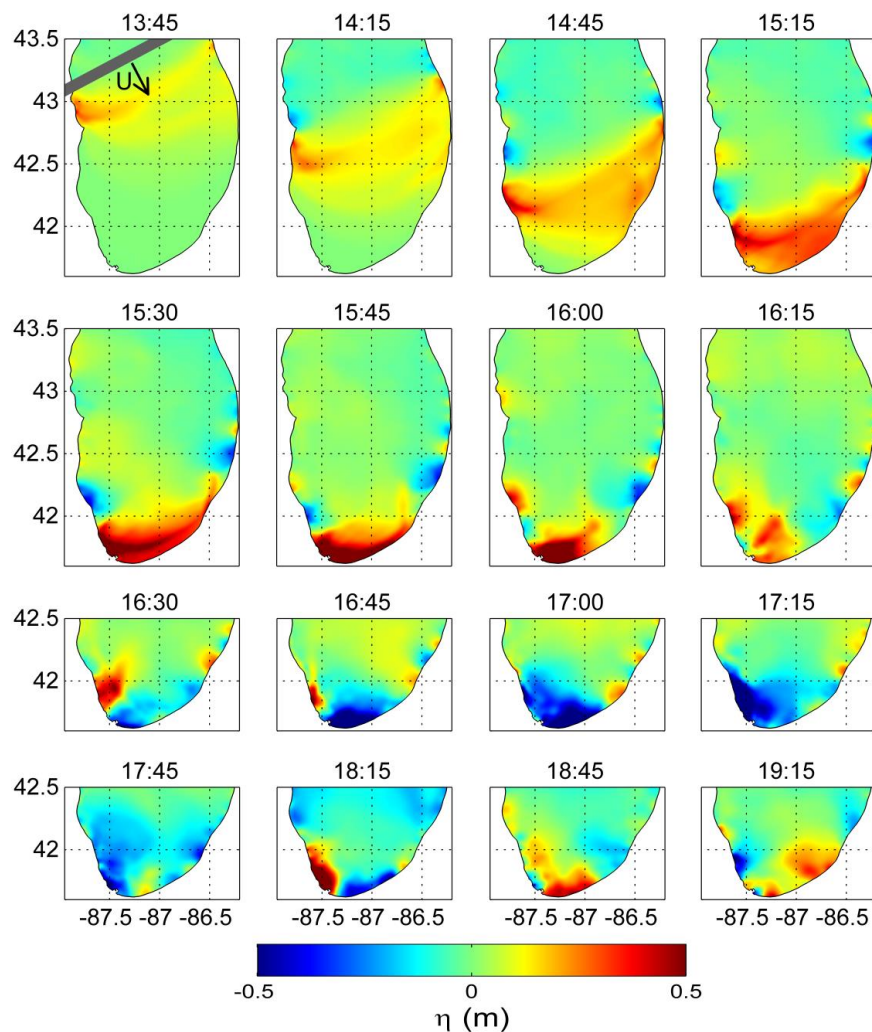


Figure 2-9: Lake Michigan water level in response to meteorological forcings on July 6, 1954 from Figure 2-3 (times are in CST).

The spatial propagation of the July 6th meteotsunami is examined in detail in a series of snapshots in Figure 2-9. By 13:45, the atmospheric disturbance generated edge waves on both the west and east coasts of the lake. At 43°N on the west coast, the slope is $\beta=0.004$ (see Figure 2-1) and the edge waves had a period of $T=60$ min, yielding an edge wave speed of 23 m/s from Equation 2-1, which is a near Greenspan resonant match with the atmospheric disturbance speed of 22 m/s. Along the east coast, slopes are too steep, i.e. $\beta=0.007$ at 43.5°N, to experience Greenspan resonance, yielding a much small edge wave compared with the west coast. At 14:15, the leading edge wave along the west coast grew to a crest height of 0.34 m over constant slopes and the edge wave train increased in duration. The length of an edge wave train continuously increases because edge wave group velocity is half the phase velocity, giving an edge wave train a duration that is equal to the length of time the edge waves have been propagating (Munk et al. 1956). Along the east coast, the edge waves grow over the shallower slope of $\beta=0.005$ at 43.1°N, a more optimal condition for Greenspan resonance than to the north. At 14:45, the edge waves on the west coast grew to 0.6 m and a significant first harmonic component developed, evident by the offshore antinode. At this location along the west coast (42.1°N), the slope decreases to $\beta=0.0035$ and the oscillations had a period of 20 minutes. These properties yield a first harmonic edge wave speed of 20 m/s from Equation 2-1, a near Greenspan resonant match with the 22 m/s disturbance speed. Edge wave growth along the east coast became steady at this time with a 0.25 m crest height. In addition, a long wave with a 0.2m crest height formed across the lake and moving with the atmospheric disturbance. The lake depth in this area is 50~60 meters, corresponding to a long wave speed of 22~24 m/s which matched the disturbance speed to induce Proudman resonant wave growth. By 15:15, the west coast edge wave propagated to the Chicago lakefront with a crest height of 0.4 m, corresponding to the first wave arrival at the

Wilson Avenue Crib gauge (see Figure 2-8). The first harmonic edge wave mode was responsible for the high frequency component ($T \sim 20$ min) of this first arrival wave in Figure 2-8. Meanwhile at the offshore, the long wave grew to a crest height of 0.4 m as it propagated into shallower (~ 40 meters) water depths. This long wave growth is in agreement with the findings of Vilibić (2008) for a Proudman resonant wave which propagates over upward sloping bathymetry. Specifically, wave heights increase owing to shoaling, as well as the superposition of the forced wave, which maintains the disturbance speed, and a free wave which now travels slower over the shallower bathymetry. At 15:45, the leading west coast edge wave propagated south of Chicago with the trough of the edge wave train corresponding to the Wilson Avenue Crib low water level at 15:40 (Figure 2-8). The long wave also impacted the southern coast of the lake, yielding water level fluctuations in which the long wave was indistinguishable from the cyclonic west coast edge waves. At 16:00, the long wave reflected off the southern coast of the lake and, as seen at 16:15, propagated northwest towards Chicago. Coincidentally, an edge wave crest (42°N , 87.6°W) from the west coast edge wave train was also propagating towards Chicago at this time. This edge wave and the reflected long wave met at 16:30, leading to a superposed wave that was responsible for the largest peak (0.65 m) recorded at the Wilson Avenue Crib gauge, though the model results do not fully resolve this peak wave at Wilson Avenue Crib (see Figure 2-8). This may be attributed to the use of a spatially homogenous atmospheric disturbance to force the model; in reality, the actual disturbance was undoubtedly spatially heterogeneous, though could not be characterized due on the limited available atmospheric data. Nevertheless the model faithfully depicts the interactions of edge and long waves just 5 km south of the Wilson Avenue Crib gauge location with a resulting wave crest height of 0.7 m. Also at 16:30, the leading trough of the cyclonic edge wave train generated along the west coast propagated to (41.6°N , 87.2°W)

while the leading trough of the anticyclonic edge wave train generated along the east coast propagated to (41.9°N, 86.7°W), with the two edge wave trains propagating towards each other. At 16:45 the edge wave trains generated on the east and west coasts met at (41.6°N, 87.3°W) and superposed to a 0.7 m trough. By 17:00, the long wave trough began to reflect off the southern coast of the lake and was responsible for the 0.6 m trough in the Wilson Avenue Crib water level record (Figure 2-8). The cyclonic and anticyclonic edge wave trains further interacted to create a 1.1 m wave trough at (41.6°N, 87.4°W). The subsequent water level fluctuations in the lake were primarily due to the edge waves generated from both the east and west coasts, as the long wave reflected to the north of Lake Michigan. Of note is an additional superposition of the oppositely propagating edge wave trains which occurred at 18:45 (41.6°N, 87.2°W), where the two distinct edge waves can be seen just after the cyclonic and anticyclonic edge waves met 7 minutes previous with a resulting crest height of 1.2 m; these edge waves can further be seen propagating away from each other at 19:15, with the cyclonic edge wave at (41.8°N, 86.7°W) and the anticyclonic edge wave at (41.6°N, 87.3°W). The edge wave energy persisted in the lake for the duration of the 24 hour model run, consistent with the observations of Donn and Ewing (1956).

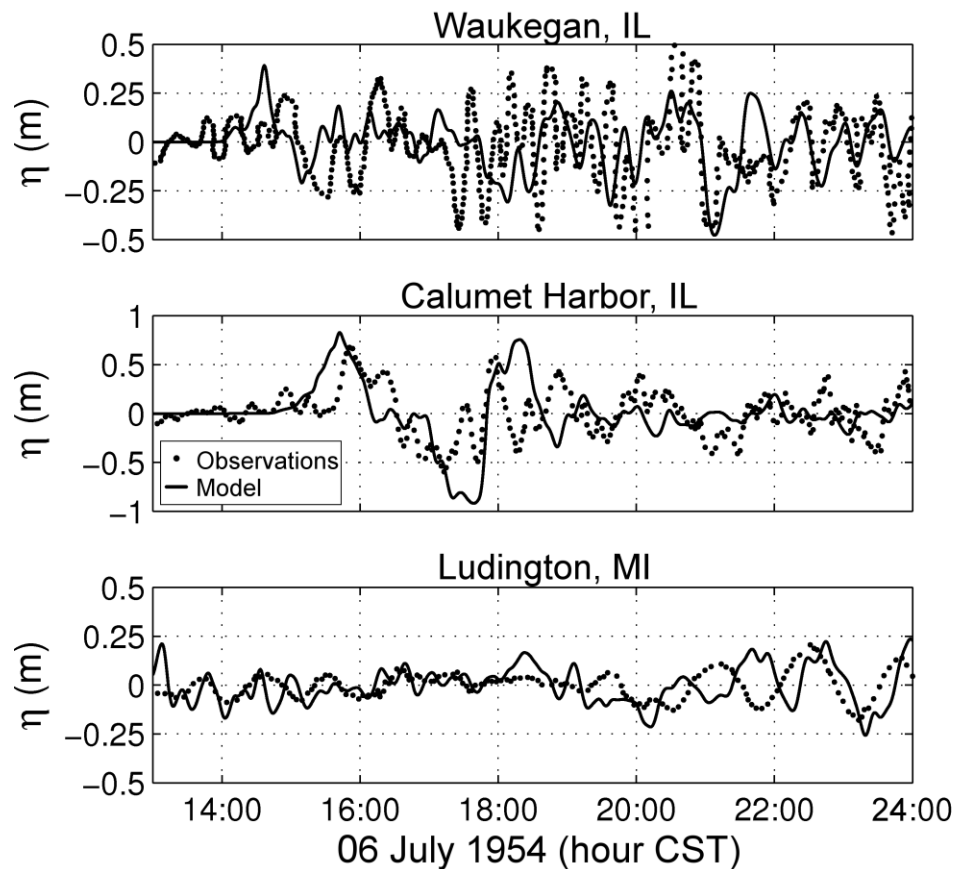


Figure 2-10: Time series of modeled water levels (line) and observations (dot) at shore-based locations throughout Lake Michigan in response to the meteorological forcings on July 6, 1954. For gauge locations, see Figure 2-1.

To verify the spatial patterns observed in the model snapshots, Figure 2-10 compares model results with water level observations reported by Donn and Ewing (1956) at shore-based gauges located at Waukegan, IL; Calumet Harbor, IL; and Ludington, MI (see Figure 2-1 for map of locations). Similar to Figure 2-6, the shore-based gauges are all located within harbors which are not resolved in the model. As a result the observed wave signal is likely contaminated by harbor oscillation modes whereas the model results could not exhibit these effects. At Waukegan, the first wave arrived in the observations at 14:55 with crest height of 0.25 m, consistent with the leading cyclonic edge wave generated on the west coast (Figure 2-9, 14:45).

The model predicts the edge waves to arrive 15 minutes earlier at 14:40 with a larger height of 0.4 m. The anticyclonic edge wave train generated on the east coast arrived at Waukegan at 17:14 in the observations with initial wave heights of approximately 0.8 m which diminished to 0.25 m by 22:00. The model depicts this edge wave train arrival 26 minutes later at 17:40 with smaller heights of 0.5 m persisting for the duration of the model run. The oscillations in the observations occurred at a slightly higher frequency ($T \sim 17$ minutes) and magnitude ($H \sim 0.8$ m) compared with the model ($T \sim 22$ minutes, $H \sim 0.5$ m), though the effects of the harbor may be the source of these discrepancies. At Calumet Harbor (41.7°N , 87.5°W), the leading edge wave arrivals in the observations (18:51) and the model (18:42) were within 10 minutes, with the observed wave crest height ($H \sim 0.7$ m) slightly smaller than the model ($H \sim 0.8$ m). Subsequent oscillations at Calumet Harbor exhibited similar character in the observations and the model, with the modeled waves slightly larger than in observations. Interestingly, while both Calumet Harbor and Waukegan are near Chicago, the impact of the reflected long wave which struck Wilson Avenue Crib at 16:45 was not apparent in either record, illustrating the focused and episodic nature of the edge wave/long wave superposition. At Ludington, early oscillations were small ($H \sim 0.2\text{m}$) in both the observations and the model since the edge waves along the east coast were fairly early in development at this location and had not yet achieved large Greenspan resonant growth. A relatively large wave ($H \sim 0.4\text{m}$) appeared at 18:25 in the model results, associated with the long wave reflection propagating back northward. The cyclonic edge waves generated on the west coast propagated around the lake and reached Ludington at 21:15 in the observations and 20:40 in the model, with heights eventually reaching 0.4 m in the observations and 0.5 m in the model. These oscillations persisted at Ludington for the duration of both the observation and model records. Overall, the model time series reasonably match the

observations, with some slight discrepancies in arrival time likely due to the assumed linear atmospheric disturbance front whereas isochrones suggest that the actual disturbance front may have been slightly curved (Donn and Ewing 1956).

The sensitivity of the July 6th meteotsunami event to atmospheric disturbance velocity is examined by perturbing both propagation direction and speed. While the nomograms of Platzman (1965) provide the maximum wave height in response to a wide range of disturbance velocities, in this paper we aim to examine the detailed wave behavior specific to the July 6th event. First, disturbance direction is perturbed $\pm 10^\circ$ from the original 155° , with the resulting time series at Wilson Avenue Crib plotted in Figure 2-11. The more meridonal propagation pathway ($\theta=165^\circ$) results in a later arriving yet a slightly larger initial edge wave at 15:30, owing to the fact that the disturbance propagates closer to direction of edge wave propagation along the coast. Nevertheless, the angle of long wave reflection changes, which alters the superposition of long wave and edge wave and results in a 25% smaller trough height at 17:10. For the more zonal propagation ($\theta=145^\circ$), the initial edge wave arrives earlier (14:45) but with 75% of the height of the base case, the result of the disturbance pathway being less aligned with the alongshore edge wave propagation direction. In comparison with the original base case ($\theta=155^\circ$), the wave heights in this case are lower (i.e. at 16:55) due to a combination of the reduced edge wave heights and the change in long wave reflection angle. Overall, the perturbations reveal that edge wave height in this event could have been greater with a more meridonal disturbance propagation but the edge wave/long wave superposition was maximized at Wilson Avenue Crib for the actual disturbance orientation ($\theta=145^\circ$).

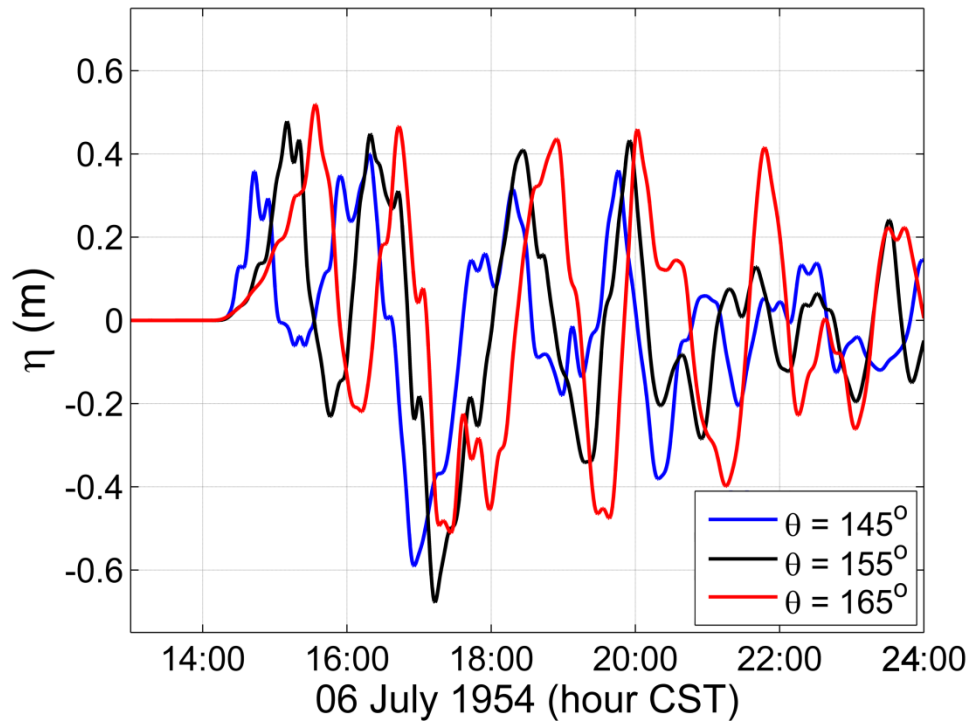


Figure 2-11: Time series of water levels at Wilson Avenue Crib in response to perturbation of meteorological disturbance direction for the July 6, 1954 meteotsunami.

The atmospheric disturbance speed is perturbed from the original 22 m/s in 2 m/s increments, yielding 20, 24, and 26 m/s disturbances, with a comparison of the resulting water levels at Wilson Avenue Crib plotted in Figure 2-12. The slower disturbance ($U=20$ m/s) results in later arriving (15:29) and slightly smaller water level fluctuations, with mechanisms similar to the base case. The slightly faster disturbance ($U=24$ m/s) leads to an earlier arriving wave train (14:53) with a 10% smaller height, likely owing to a deviation from the ideal Greenspan resonant speed. An appreciable change in behavior is observed for $U=26$ m/s, in which a 66% smaller initial edge wave occurs at 14:18, as this disturbance speed further departs from the Greenspan resonant edge wave speed. Nevertheless, the faster disturbance speed approaches the Proudman resonant speed for the open water of Lake Michigan ($c = 29$ m/s), so a much larger long wave is generated, reflecting back to the gauge at 15:38 with a 0.6 m crest height. At this disturbance

speed, the hypothetical meteotsunami event would be attributed primarily to the long wave instead of edge waves, drawing more similarities to the June 26th wave than the July 6th event under consideration. Overall, the sensitivity study of the July 6th event conducted here reveals that changes in disturbance speed and direction can dramatically affect the character of meteotsunami wave produced, including changing the dominant wave type.

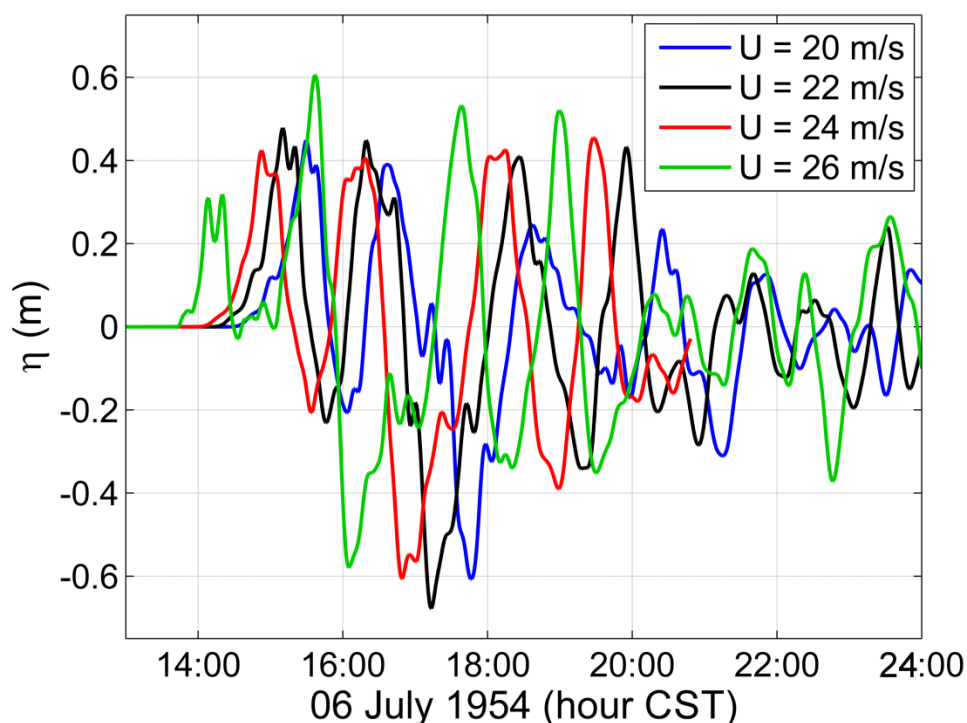


Figure 2-12 Time series of water levels at Wilson Avenue Crib in response to perturbation of meteorological disturbance speed for the July 6, 1954 meteotsunami.

2.4. Discussion

2.4.1. Role of edge waves and long waves

The modeling results, in particular the snapshots in Figure 2-5 and Figure 2-9, uncover that both events generated long waves and edge waves simultaneously in Lake Michigan. Previously, Donn (1959) described an atmospheric disturbance on the Great Lakes which

generated edge waves on Lake Huron and long waves in Lake Erie, owing to the disturbance orientation relative to the shorelines of each lake. Nevertheless, simultaneous generation of edge waves and long waves on the same lake has yet to be documented as far as the authors are aware. While edge waves did not play a major role in the destructive wave that struck Chicago in the June 26th event, significant oscillations ($H > 0.5$ m) due to edge waves occurred hours after the initial wave. These persistent large waves were noted in witness accounts to hinder rescue and recovery efforts for hours after the deadly wave. The late arrival of these waves would have had no apparent connection to the squall line storm that had passed hours earlier and may have posed a threat to public safety had beaches not been cleared due to the fatal long wave. In the July 6th event, the largest wave observed was the result of edge wave and long wave superposition. The superimposed edge wave and long wave resulted in a peak water level 60% larger than the other waves in the edge wave train. Nevertheless, the presence of the long wave was not considered in the original analysis of Donn and Ewing (1956) because large Proudman resonance was ruled out as a source, owing to the slower disturbance speed. The hydrodynamic model results presented in this paper indicate that edge waves and long waves can be generated simultaneously by the same disturbance despite the fact that these waves may not achieve an optimal resonant condition. Indeed, interaction between long and edge waves can create a destructive event, as occurred on July 6, 1954. Therefore, study of future events in Lake Michigan and other enclosed basins is highly recommended to take both long and edge waves into consideration.

2.4.2. Effects of an enclosed basin

The simultaneous appearance of both edge waves and long waves in the two events can be attributed in part to the enclosed basin of Lake Michigan. For long waves, the enclosed basin allows for reflection and subsequent retention of wave energy in the southern basin of the lake.

In addition, the concave shape of the east coast of Lake Michigan acts to focus the reflected long waves propagating westward, as illustrated in Figure 2-5. This spatial focusing can result in a reflected wave on the west coast of the lake which exceed the wave incident at the east coast, as occurred on June 26, 1954. This type of directional spatial focusing is one of the mechanisms identified to cause freak waves (Nepf et al. 1998; Wu and Nepf 2002; Kharif and Pelinovsky 2003). Edge waves can persist for long durations as they travel around an enclosed coast, evident in the late wave arrivals on the west coast by anticyclonic edge waves generated on the east coast for the June 26 event. If edge waves are generated on both coasts, the two edge wave trains may meet and interact, as seen in Figure 2-9 for July 6, 1954 at 16:45 (41.6°N, 87.3°W) and 18:45 (41.6°N, 87.2°W). The resulting waves in this case were rather large, with the superposition leading to waves in excess of one meter crest height in some cases. The enclosed nature of the Lake Michigan basin makes these meteotsunamis unique and potentially more dangerous compared to meteotsunamis along an ocean or sea coast where wave reflection and propagation leads to energy leaving the area of concern.

2.4.3. Wind Stress versus atmospheric pressure

While the potential of wind stress to significantly contribute to meteotsunami height has been recognized (Vilibić et al. 2005; Orlić et al. 2010), in events studied to date wind stress has been viewed as a secondary forcing compared to atmospheric pressure (Šepić et al. 2008; Orlić et al. 2010; Renault et al. 2011). Coincidentally, the previous studies of these Lake Michigan meteotsunamis did not consider wind stress to be significant. The description of the July 6 event by Donn and Ewing (1956) merely mentioned that wind speeds exceeded 30 m/s whereas the modeling exercise by Platzman (1958) on the June 26 meteotsunami event only considered atmospheric pressure and neglected to account for wind stress. The generic modeling results of

Platzman (1965) indicated the potential for wind stress to dominate meteotsunami wave behavior, though not for a specific event. The model results in our study indicate that wind stress was responsible for 40% and 68% of the wave heights in the June 26 and July 6 events, respectively. Clearly, wind disturbance can play a significant role in generating meteotsunamis in Lake Michigan. It is also important to note that the observed wind speeds of 25 and 32 m/s for June 26 and July 6, respectively, are much greater than that of any other meteotsunami discussed in the literature. This may be an indication that squall line storms, which are characterized by strong winds (Rotunno et al. 1988; Wakimoto et al. 2006), may be a meteotsunami source unique to the Great Lakes. Furthermore, the occurrence of derechos, which are strong squall lines, have risen recently in the United States from approximately 10 events per year in 1986 to about 30 events per year by 2003 (Ashley *et al.* 2005), with the lower Great Lakes region emerging as a dominant corridor of derecho activity at the end of the 20th century (Bentley and Sparks, 2003). An increase in the number and severity of high-speed squall line events suggest the potential for more frequent and intense Great Lakes meteotsunamis in the near future.

2.5. Summary

In this paper, two distinct meteotsunami events that occurred on Lake Michigan in 1954 were revisited using a hydrodynamic modeling approach. Data analysis immediately following the events concluded that first event (June 26) was caused by Proudman resonance between a long wave and a squall line (Ewing et al. 1954), whereas the second event (July 6th) was attributed to a Greenspan resonance between a propagating pressure jump and an edge wave train (Donn and Ewing 1956). Nevertheless, the high resolution hydrodynamic modeling results in this paper reveal details on these events that the data analysis and early modeling could not resolve,

including the role of pressure and wind stress on meteotsunami formation, the character of the wave growth, significant higher frequency content present in the waves, and the long duration of the water level oscillations.

On June 26, 1954, a squall line with a rapid pressure jump and strong winds propagated southeast across the lake. The squall line propagation speed, approximately equal to the long wave speed in southern Lake Michigan, led to Proudman resonance that amplified a long wave. When this long wave struck the east and south coasts of the lake, the wave reflected back west and owing to the curvature of the shore, focused the wave front at the Chicago lakeshore. While the main wave front had a period of 90 minutes, observations revealed what appeared to be high frequency component ($T=15$ min) to this wave, termed a “second surge” by Ewing et al. (1954); the model results indicate that this apparent high frequency content was actually the reflection of the destructive wave off of the west coast and not a complex high frequency wave front as originally conjectured. Furthermore, model results reveal waves that arrived hours after the first wave struck Chicago were associated with a harmonic edge wave generated on the east coast of the lake by the squall line. The edge waves then propagated anticyclonically around the lake to impact the Chicago lakefront hours after the long wave energy had dissipated. Though the long wave was the cause of the fatal meteotsunami that struck Chicago, the significant edge wave energy persisted in the lake for a long duration, proving a hindrance to rescue missions and a potential danger owing to the arrival long after the squall line and long wave had passed.

Ten days later on July 6, another series of large waves struck the Chicago coast. Initially attributed to edge wave resonance by Donn and Ewing (1956), model simulations reveal that the largest of these waves was the product of a resonant edge wave superposed with a reflected long wave. This outcome stresses the role that the enclosed basin of Lake Michigan played in creating

a complex wave environment, as a significant portion of the wave energy was retained through reflection compared to the open sea condition. In addition, high frequency oscillations observed with the large waves were attributed to first harmonic edge wave modes. Another major finding was that the main source of energy for this event was wind stress, which is contrary both to the initial hypothesis of Donn and Ewing (1956) and the conventional conclusion in the meteotsunami literature that pressure gradient is the main driver of these large waves. Indeed, the importance of wind stress in both of the events examined in this study may indicate that the squall line storms which generate Great Lakes meteotsunamis may be fundamentally different from meteotsunami-causing storms elsewhere in the world.

2.6. Acknowledgements

This work was supported by the National Science Foundation's Graduate Research Fellowship Program, the Cooperative Institute for Limnology and Ecosystems Research Long-term Great Lakes Fellowship, and UW-Madison/UW-Milwaukee Intercampus Research Incentive Grants Program. The authors would like to thank Dr. David Schwab at the University of Michigan-Ann Arbor and Dr. Eric Anderson at NOAA-Great Lakes Environmental Research Laboratory for the advice and discussion on meteotsunamis in the Great Lakes. The authors would also like to thank the two anonymous reviewers whose comments greatly improved the manuscript.

2.7. References

Ashley WS, Mote TL, Bentley ML, (2005) On the episodic nature of derecho-producing convective systems in the United States. *International Journal of Climatology* 25:1915-1932

- Bently ML, Sparks JA (2003) A 15 year climatology of derecho-producing mesoscale convective systems over the central and eastern United States. *Climate Research* 24:129-139
- Cho KH, Wang HV, Shen J, Valle-Levinson A, Teng YC (2012) A modeling study on the response of the Chesapeake Bay to Hurricane Events of Floyd and Isabel. *Ocean Modeling* 49-50:22-46
- Donelan MA, Haus BK, Reul N, Plant WJ, Stiassnie M, Graber HC, Brown OB, Saltzman ES (2004) On the limiting aero-dynamic roughness of the ocean in very strong winds. *Geophysical Research Letters* 31: L18306, doi:10.1029/2004GL019460.
- Donn WL (1959) The Great Lakes storm surge of May 5, 1952. *Journal of Geophysical Research* 64(2):191-198
- Donn WL, Ewing M (1956) Stokes' edge waves in Lake Michigan. *Science* 124(3234):1238–1242
- Ewing M, Press F, Donn WJ (1954) An explanation of the Lake Michigan wave of 26 June 1954. *Science* 120(3122):684–686
- Fortunato AB, Rodrigues M, Dias JM, Lopes C, Oliveira A (2013) Generating inundation maps for a coastal lagoon: A case study in the Ria de Aveiro (Portugal). *Ocean Engineering* 64:60-71
- Greenspan HP (1956) The generation of edge waves by moving pressure disturbances. *Journal of Fluid Mechanics* 1:574–592
- Harris DL (1957) The effect of a moving pressure disturbance on the water level in a lake. *Meteorological Monographs* 2(10):46-57
- Hibiya T, Kajiura K (1982) Origin of “abiki” phenomenon (kind of seiches) in Ngasaki Bay. *Journal of Oceanographical Society of Japan* 38:172-182

- Hughes LA (1965) The prediction of surges in the southern basin of Lake Michigan: Part III. The operational basis for prediction. *Monthly Weather Review* 93(5):292-296
- Kelley JGW, Hobgood JS, Bedford KW, Schwab DJ (1998) Generation of three-dimensional lake model forecasts for Lake Erie. *Weather and Forecasting* 13(3):659-687
- Kharif C , Pelinovsky E (2003) Physical mechanisms of the rouge wave phenomenon. *European Journal of Mechanics B-Fluids* 22(6):603-634
- Kurkin A, Pelinovsky E (2003) Shallow-water edge waves above an inclined bottom slowly varied in along-shore direction. *European Journal of Mechanics B-Fluids* 22(4):305-316
- Monserrat S, Vilibić I, Rabinovich AB (2006) Meteotsunamis: atmospherically induced destructive ocean waves in the tsunami frequency band. *Natural Hazards and Earth System Sciences* 6(6): 1035-1051
- Munk W, Snodgrass F, Carrier G (1956) Edge waves on the continental shelf. *Science* 123(3187):127-132
- Nepf, H.M., Wu, C.H., Chan, E.S., (1998). A comparison of two- and three-dimensional wave breaking, *J. Physical Oceanography*, 28, N7, 1496-1510.
- O'Connor WP, Schwab DJ, Lang GA (1999) Forecast verification for eta model winds using Lake Erie storm surge water levels. *Weather and Forecasting* 14(1):119-133
- Orlić M, Belušić D, Janekovic I, Pasaric M, (2010) Fresh evidence relating the great Adriatic surge of 21 June 1978 to mesoscale atmospheric forcing. *Journal of Geophysical Research* 115. doi:10.1029/2009JC005777
- Platzman GW (1958) A numerical computation of the surge of 26 June 1954 on Lake Michigan. *Geophysica* 6(1):407-438

- Platzman GW (1965) The prediction of surges in the southern basin of Lake Michigan: Part I. The dynamical basis for prediction. *Monthly Weather Review* 93(5):275-281
- Powell MD, Vickery PJ, Reinhold TA (2003) Reduced drag coefficient for high wind speeds in tropical cyclones. *Nature* 422: 279–283
- Proudman J (1929) The effects on the sea of changes in atmospheric pressure. *Geophysical Supplement: Monthly Notices of the Royal Astronomical Society* 2(4):197–209
- Rabinovich AB (2009) Seiches and harbor oscillations, in: *Handbook of Coastal and Ocean Engineering*, edited by Kim, Y.C. World Scientific Publishing Company, Toh Tuck Link, Singapore, 193-236.
- Renault L, Vizoso G, Jansá A, Wilkin J, Tintoré J (2011) Toward the predictability of meteotsunamis in the Balearic Sea using regional nested atmosphere and ocean models. *Geophysical Research Letters* 38. doi:10.1029/2011GL047361
- Rotunno R, Klemp JB, Weisman ML (1988) A theory for strong, long-lived squall lines. *Journal of the Atmospheric Sciences* 45(3): 463-485
- Šepić J, Orlić M, Vilibić I (2008) The Bakar Bay seiches and their relationship with atmospheric processes. *Acta Adriatica* 49(2):107-123
- Sheppard PA (1958) Transfer across the earth's surface and through the air above. *Quarterly Journal of the Royal Meteorological Society* 84: 205–224
- Smith SD (1980) Wind stress and heat flux over the ocean in gale force winds. *Journal of Physical Oceanography* 10: 709–726.
- Song Y, Haidvogel D (1994) A semi-implicit ocean circulation model using a generalized topography-following coordinate system. *Journal of Computational Physics* 115(1):228–244

- Ursell F (1952) Edge waves on a sloping beach. *Proceedings of the Royal Society Series A* 214(1116):79-98
- Vilibić I (2008) Numerical simulations of the Proudman resonance. *Continental Shelf Research* 28:574– 581. doi:10.1016/j.csr.2007.11.005
- Vilibić I, Domijan N, Cupic S (2005) Wind versus air pressure seiche triggering in the Middle Adriatic Coastal waters. *Journal of Marine Sciences* 57(1-2):189-200
- Vilibić I, Monserrat S, Rabinovich A, Mihanovic H (2008) Numerical modeling of the destructive meteotsunami of 15 June, 2006 on the coast of the Baleric Islands. *Pure and Applied Geophysics* 165:2169-2195. DOI 10.1007/s00024-008-0426-5
- Wakimoto RM, Murphey HV, Nester A, Jorgensen DP, Atkins NT (2006) High winds generated by bow echoes. part I: overview of the Omaha bow echo 5 July 2003 storm during BAMEX. *Monthly Weather Review* 134(10): 2793–2812. doi: <http://dx.doi.org/10.1175/MWR3215.1>
- Witter RC, Jaffe B, Zhang Y, Priest GR (2011) Reconstructing hydrodynamic flow parameters of the 1700 tsunami at Cannon Beach, Oregon, USA. *Natural Hazards*. doi:10.1007/s11069-011-9912-7
- Wu CH, Nepf HM (2002) Breaking wave criteria and energy losses for three-dimensional breaking waves. *Journal of Geophysical Research-Oceans* 107(C10):41-1—41-18. DOI: 10.1029/2001JC001077
- Zhang Y, Baptista AM (2008a) SELFE: A semi-implicit Eulerian-Lagrangian finite-element model for cross-scale ocean circulation. *Ocean Modeling* 21(3-4):71-96
- Zhang Y, Baptista AM (2008b) An efficient and robust tsunami model on unstructured grids. Part I: Inundation Benchmarks. *Pure and Applied Geophysics* 165(11-12):2229-2248

Zhang Y, Witter RW, Priest GP (2011) Tsunami-tide interaction in 1964 Prince William Sound tsunami. *Ocean Modeling* 40(3-4):246-259

3. Meteotsunami Occurrences and Causes in Lake Michigan

The following is re-produced with permission from AGU. The final publication is available at:

<http://onlinelibrary.wiley.com/doi/10.1002/2015JC011317/full>

Bechle, A. J., Kristovich, D. A.R. and Wu, C. H. (2015), Meteotsunami occurrences and causes in Lake Michigan. *J. Geophys. Res. Oceans*. Accepted Author Manuscript. doi:10.1002/2015JC011317

3.1. Introduction

Meteotsunamis (or meteorological tsunamis) are propagating shallow water waves which exhibit many similarities to seismic tsunamis but are generated by a moving atmospheric disturbance [Nomitsu, 1935]. Meteotsunamis of up to 6 meters have occurred worldwide [Monserrat *et al.*, 2006; Vilibić *et al.*, 2014c], with single events capable of causing tens of millions of dollars in economic loss by inundating coastal towns [Vilibić *et al.*, 2004; Orlić *et al.*, 2010], damaging coastal structures [Mercer *et al.*, 2002; Tanaka, 2010; Whitmore and Knight, 2014], and sinking boats [Vilibić *et al.*, 2008; Asano *et al.*, 2012]. The human impact caused by meteotsunamis can be considerable, with numerous reported injuries [Churchill *et al.*, 1995; Vučetić *et al.*, 2009; Šepić *et al.*, 2015a] and deaths [Hibiya and Kajiura, 1982; Cho *et al.*, 2013]. The Laurentian Great Lakes have a particularly impactful meteotsunami history, illustrated by many events which have resulted in destruction [Donn, 1959; Irish, 1965; Murty and Freeman, 1973; As-Salek and Schwab *et al.*, 2004] and death [Ewing *et al.*, 1954]. In view of the threat posed by meteotsunamis, it is important to quantify the occurrence frequencies and characterize causes of meteotsunamis to better understand the risk posed by these coastal hazards.

A meteotsunami is generated by an atmospheric disturbance, typically associated with a combination of rapid atmospheric pressure perturbations and strong winds. Meteotsunamis can occur as non-trapped long waves or trapped edge waves. Non-trapped long waves are amplified under the condition of Proudman resonance, in which the generating atmospheric disturbance propagates with a speed U approximately equal to the non-dispersive long wave phase speed $C_{long} = \sqrt{g * \text{water depth}}$, where g is the acceleration due to gravity [Proudman, 1929]. Trapped edge waves propagate parallel to the coast and are amplified under the condition of Greenspan propagation resonance [Greenspan, 1956] which depends upon a match between both the speed and wavelength of the atmospheric disturbance and the edge wave [Munk *et al.*, 1956]. In Lake Michigan, past meteotsunamis have been caused by both Proudman and Greenspan resonances [Bechle and Wu, 2014]. For example, a deadly meteotsunami which struck Chicago on June 26, 1954 was revealed to be caused by Proudman resonance [Ewing *et al.*, 1954; Platzman, 1958]. Just 10 days later a significant meteotsunami occurred at Chicago as the result of Greenspan resonance [Donn and Ewing, 1956].

Atmospheric disturbances that have been recognized to induce meteotsunami propagation resonances are atmospheric gravity waves, frontal passages, cyclones, and mesoscale convective systems [Monserrat *et al.*, 2006]. Atmospheric gravity waves yield rapid atmospheric pressure and horizontal wind oscillations that have been the cause of many major meteotsunamis worldwide [Donn and McGuinness, 1960; Paxton and Sobien, 1998; Tanaka, 2010], especially in the Mediterranean Sea [Monserrat *et al.*, 1991; Jansa *et al.*, 2007; Šepić *et al.*, 2015b]. Tropical and extratropical cyclones can trigger both Proudman [Mercer *et al.*, 2002; Mecking *et al.*, 2009; Pasquet *et al.*, 2013] and Greenspan [Greenspan, 1956; Munk *et al.*, 1956] resonances, notably along the North American East Coast. Mesoscale convective storms can also produce

strong pressure and wind perturbations, leading to meteotsunamis in the United Kingdom [Tappin *et al.*, 2011], Finland [Pellikka *et al.*, 2014]; Australia [Pattiaratchi and Wijeratne, 2014], and the U.S. East Coast [Churchill *et al.*, 1995; Pasquet and Vilibić, 2013; Wertman *et al.*, 2014]. In the Great Lakes, meteotsunami events have been linked with strong convective storms [Ewing *et al.*, 1954; Donn and Ewing, 1956; As-Salek and Schwab, 2004; Šepić and Rabinovich, 2014], atmospheric gravity waves [Donn, 1959], and extratropical cyclones [As-Salek and Schwab, 2004]. Overall our knowledge of meteotsunami causative storm meteorology is typically based upon episodic analysis of individual large events whereas statistical characterization of the specific storms responsible for meteotsunamis is rare [Vilibić *et al.*, 2014b] and has yet to be conducted for the Great Lakes.

Statistical analysis of historical records can be used to quantify the occurrence frequency of meteotsunamis and associated risks. Typically, digitized water level records of high temporal resolution (<10 min) are of insufficient length to estimate meteotsunami probability with certainty [Geist and Parsons, 2011; Geist *et al.*, 2014]. While analog water level records of up to 55 years have been analyzed to identify and analyze large meteotsunami events [Šepić *et al.*, 2009b, 2012], tremendous efforts have to be made to digitize these records and perform good quality control procedures for use in an occurrence frequency analysis. Recently, Geist *et al.*, [2014] followed the Probabilistic Tsunami Hazard Assessment (PTHA) framework used in seismic tsunamis [Geist and Parsons, 2006; González *et al.*, 2009] to calculate squall line storm probabilities, simulate meteotsunami heights in response to stochastically sampled storms using a hydrodynamic model, and aggregate the simulation results into meteotsunami frequency-size distributions along the U.S. East Coast. Nevertheless, challenges in representatively characterizing the probability of meteotsunami associated with all possible atmospheric

disturbances are recognized [Geist *et al.*, 2014]. As a result, information on meteotsunami occurrence frequency remains a critical knowledge gap in determining meteotsunami-induced hazard risks.

The objective of this paper is to quantify the occurrence of meteotsunamis in terms of size-frequency statistics and characterize the associated causative storm structures. In particular, we aim to examine the Lake Michigan meteotsunami climate by answering the questions of how often, where, when, and why meteotsunamis occur. Water level records at a temporal resolution of 6 min that span up to 20 years are analyzed to quantify meteotsunami occurrence in terms of the size-frequency relationship, as well as the spatial and temporal distribution of meteotsunamis. Radar imagery is examined to determine the storm structures associated with the identified meteotsunamis. In the following, Section 3.2 details the study site of Lake Michigan. Observational data and analysis techniques are described in Section 3.3. Results of the analysis are then presented in Section 3.4 and discussed in Section 3.5, leading to suggestions for future work. Finally, conclusions are given in Section 3.6.

3.2. Study Site

Lake Michigan, one of the five Laurentian Great Lakes of North America, spans approximately 500 km in the north-south and 100 km in the east-west directions. The bathymetry of Lake Michigan, illustrated in Figure 1-1Figure 3-1, can be classified into three main basins based on water depth: a southern basin, a northern basin, and Green Bay. The Two Rivers Ridge divides the main basin of Lake Michigan into northern and southern basins along a latitude of approximately 44° N. In the southern basin, mid-lake water depths are between 50 m to 160 m, corresponding to Proudman resonant long wave speeds between $C = 22$ and 40 m/s. Average lake

shelf slopes calculated at the 50 m contour range from 0.007 to 0.0015. The northern basin is deeper than the southern basin, with mid-lake depths from 150 m to 270 m ($C = 38$ to 52 m/s). Shelf slopes are also steeper in the northern basin, ranging from 0.007 to 0.012. Green Bay, the northwest arm of the lake, is the shallowest basin, with depths ranging from 10 m to 30 m ($C = 10$ m/s to 17 m/s) and shelf slopes of 0.0005.

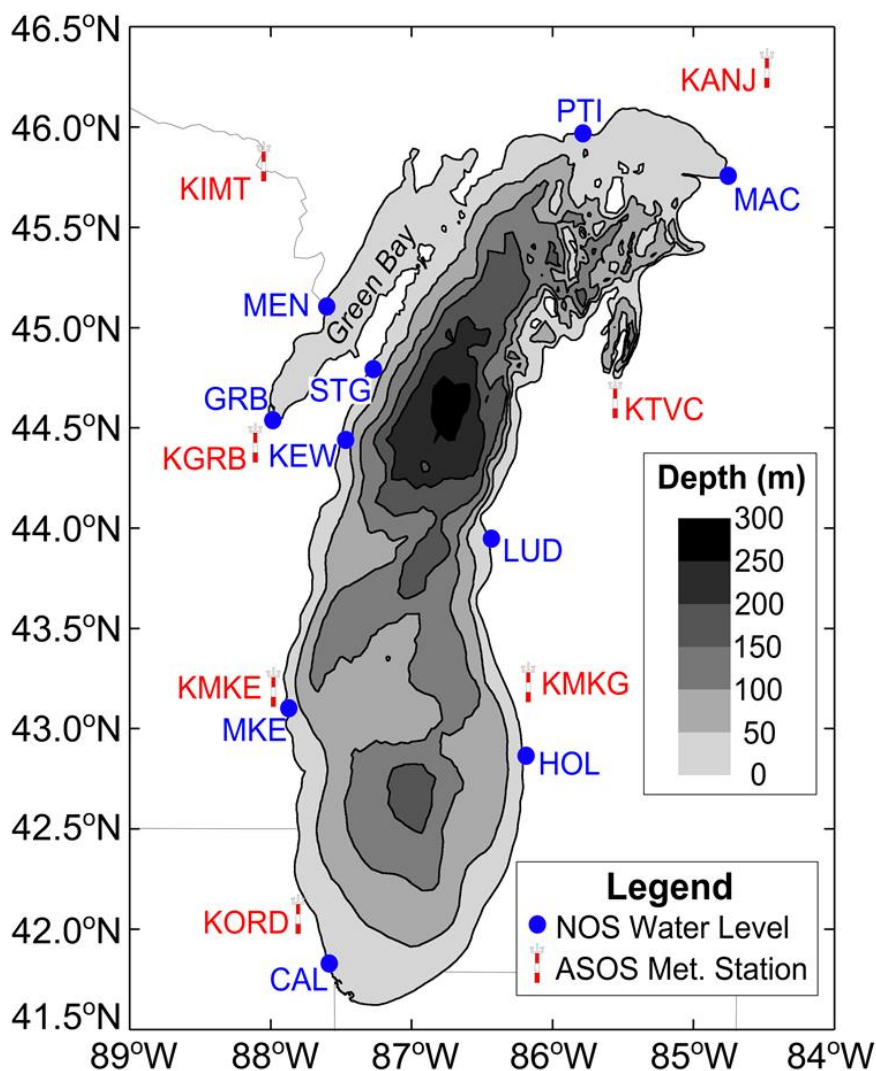


Figure 3-1: Lake Michigan bathymetry and locations of NOAA-NOS water level and NWS-ASOS surface meteorology stations.

As an enclosed basin, Lake Michigan is subject to basin-scale water level oscillations known as seiche [Rao *et al.*, 1976; As-Salek and Schwab, 2004]. A seiche is a standing wave which occurs at a free gravitational oscillation mode of the basin [Rabinovich 2009]. In contrast, for this study, a meteotsunami is defined as a sub-basin scale water level fluctuation which propagates similar to a seismic tsunami. Water level fluctuations with a dominant frequency that matches a natural seiche mode are not regarded as a meteotsunami. Rao *et al.*, [1976] and As-Salek and Schwab [2004] revealed that Lake Michigan water levels have the first five natural longitudinal seiche modes to have periods of 9.02, 5.20, 3.68, 3.11, and 2.52 hours whereas the fundamental transverse mode occurs at 2.12 hours and the second transverse mode at 1.26 hours. The Green Bay basin has distinct natural seiche modes at 10.67, 5.38, 4.16, and 3.42 hours [Rao *et al.*, 1976]. Meteotsunamis in this study are also distinguished from conventional storm surges on the Great Lakes, which classically refer to water level fluctuations in response to atmospheric disturbances which exceed the basin scale [Irish and Platzman, 1962; Rao, 1967]. In short, meteotsunami refers to waves at the sub-basin scale which behave more like seismic tsunamis than hurricane surges [Montserrat *et al.*, 2006].

3.3. Methods

3.3.1. Data Sources

Water level data are recorded at six-minute intervals at ten stations in Lake Michigan, operated by the National Ocean and Atmospheric Administration (NOAA) National Ocean Service (NOS). The location of gauges is illustrated by blue circles in Figure 1. Water level station names, abbreviations, and first full year of data are summarized in Table 1. All but one

water level station (Menominee) began operations by the year 2001, with the oldest record starting in 1995.

Meteorological data are analyzed to characterize the storms associated with Lake Michigan meteotsunamis. NEXRAD (WSR-88D) Base Reflectivity Radar composite imagery provide spatial depictions of storm structure and are made available by the Iowa Environmental Mesonet at 5-minute intervals with 1 km resolution. National Weather Service (NWS) Automated Surface Observing System (ASOS) stations provide wind speed, wind direction, and atmospheric pressure at 1-minute intervals starting January 1, 2001; prior to this date, ASOS hourly data are used to characterize the surface meteorological conditions. The ASOS stations used in this study are illustrated as red and white towers in Figure 1, selected based upon proximity to the water level gauges and data availability. Surface pressure maps are made available at 12-hour intervals from the National Weather Service Storm Prediction Center archives.

An example meteotsunami event at Calumet Harbor on August 4, 2008 is illustrated in Figure 3-2 using these data sources. Atmospheric pressure and wind speed records are obtained from the KORD ASOS station whereas the water level record is obtained from the CAL water level station. In this event, sudden rises in atmospheric pressure (Figure 3-2a) and wind speed (Figure 3-2b) were observed at 12:15 at the KORD station. These atmospheric perturbations preceded a 0.91 m meteotsunami observed at the CAL water level record (Figure 3-2c), which began at 14:30. Note that atmospheric pressure and water level data are high-pass filtered with a cutoff period of 6 hours to remove low frequency background oscillations. Radar imagery indicates a linear convective system crossed the lake shoreline at 10:00 (Figure 3-2d) and reached KORD at 12:15 (Figure 3-2e), consistent with rises in the atmospheric pressure and

wind speeds measured at KORD. Thus, the linear convective system is deemed to be the likely meteorological cause of the meteotsunami observed at CAL. Details of the data analysis involved in the meteotsunami identification and subsequent meteorological analysis are described in the following sections.

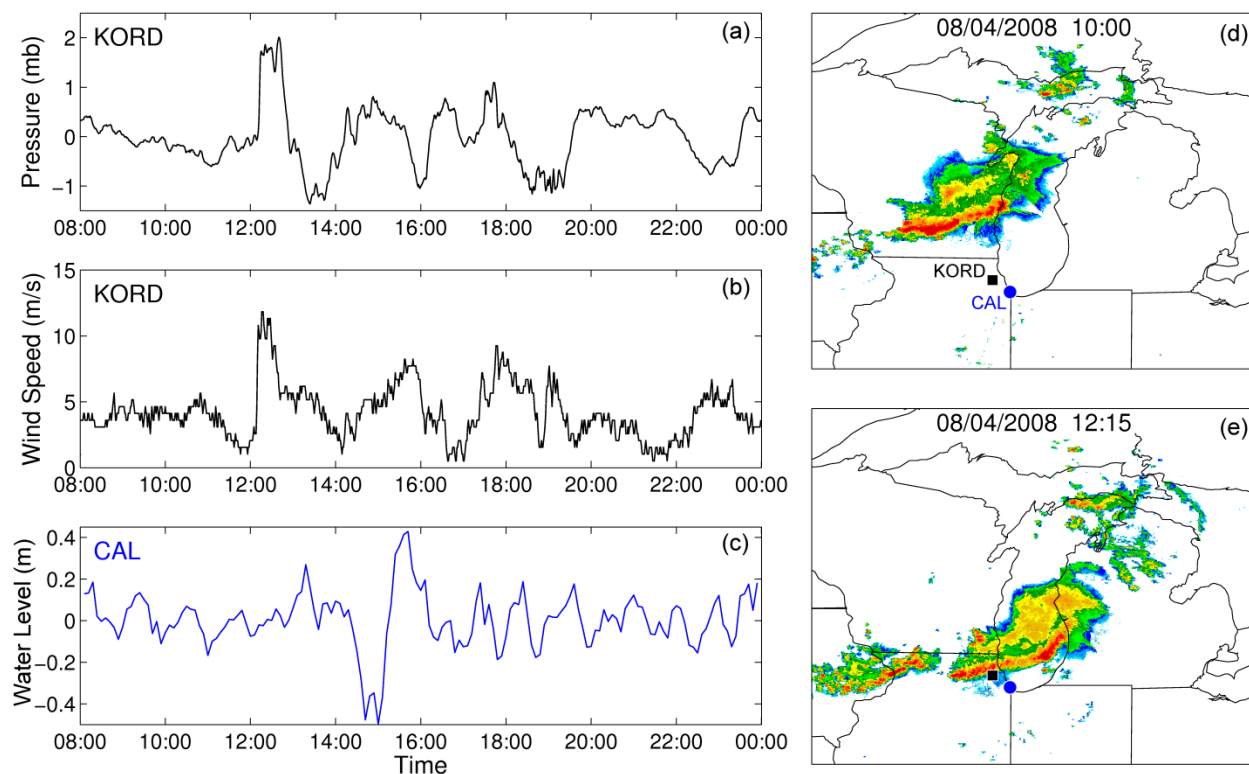


Figure 3-2: Observations of a meteotsunami event at Calumet Harbor (CAL) on August 4, 2008. At the KORD ASOS station, sudden rises in (a) atmospheric pressure and (b) wind speed occur at 12:15. At 14:30, (c) a 0.91 meter meteotsunami is observed in the CAL water level record. Note that atmospheric pressure and water level data are high-pass filtered with a cutoff period of 6 hr. Radar imagery indicates this meteotsunami is associated with a linear convective system which (d) crossed the lake shoreline at 10:00 and (e) reached KORD (black square) at 12:15, consistent with rises in the atmospheric pressure and wind speeds measured at KORD.

3.3.2. Meteotsunami Identification

Meteotsunami waves are identified based on criteria given by *Monserrat et al.* [2006]: period in the tsunami frequency band (2 minutes to 2 hours) and size exceeding a station-specific threshold. To isolate waves near the tsunami frequency band, the water level time series are high-pass filtered with a Kaiser-Bessel filter with a cutoff period of 6 hours [*Rabinovich and Monserrat, 1996*]. Individual waves in the filtered record are identified using the zero-crossing method [*Demirbilek and Vincent, 2002*]. A potential meteotsunami occurrence is indicated when a wave height exceeds an objective statistical meteotsunami height threshold, quantified as the smallest height wave for which a desired statistical distribution holds [*Coles, 2001*]. The Pareto Type 1 distribution is selected to describe the wave height statistics, consistent with seismic tsunami analysis [*Geist and Parsons, 2014*]. The height threshold, denoted as x_m , is determined from the failure-to-reject method [*Choulakian and Stephens, 2001*] by sorting the height observations, fitting the observations to the distribution, and iteratively deleting the lowest value observations until the distribution is no longer rejected by the Anderson-Darling test (*see Section 3.3.3 for detailed discussion*). Multiple oscillations that meet the meteotsunami threshold criteria within the same 12 hour period are consolidated to a single event represented by the largest wave. Events with a dominant frequency that matches one of the free gravitational oscillation periods for Lake Michigan [*Rao et al., 1976; As-Salek and Schwab, 2004*] are discarded. Figure 2c illustrates an example of a meteotsunami wave identified with these criteria on August 4, 2008, bounded by zero down-crossings (i.e. where the water level passes from positive to negative relative to the mean water level) at 14:30 and 16:18 with a height of 0.91 meters.

3.3.3. Cumulative Frequency Analysis

Cumulative frequency analysis is a statistical technique that uses past event magnitude data to estimate exceedance probability. To maximize usage of the available data, A Peaks Over Threshold (POT) approach [Coles, 2001] of extreme value statistics is chosen. For a random variable x , which in this case represents wave height, sampled events which exceed the locally defined height threshold x_m are sorted by magnitude to yield an empirical cumulative frequency distribution. To represent the event size-frequency relationship mathematically, the empirical cumulative frequency distribution is fit to a continuous probability distribution. In this paper, meteotsunami height data are fit to both the Pareto Type 1 (PT1) distribution, commonly used for seismic tsunami height statistics [Geist and Parsons, 2014], and the Generalized Pareto Distribution (GPD), typically used for extreme significant wind wave height statistics [Aarnes *et al.*, 2012; Anderson *et al.*, 2015b]. These two distributions are chosen for the meteotsunami size-frequency data because the physical behavior of meteotsunamis are similar to that of seismic tsunamis whereas the causative meteorological mechanisms of meteotsunamis are more closely related to extreme significant wave height events. Both distributions can be mathematically represented by a complimentary cumulative distribution function $\Phi(x)$, also known as a survivor function that gives the probability for an event exceeding a given magnitude. For example, the survivor function of the Pareto Type 1 distribution is given by:

$$\Phi_{PT1}(x) = \left(\frac{x_m}{x} \right)^\beta \quad (3-1)$$

where x is a wave height, x_m is the location parameter (i.e. height threshold), and β is the shape parameter. The PT1 imposes no upper limit so that wave height can increase to an infinite

magnitude for a finite probability. On the other hand, the survivor function for the Generalized Pareto Distribution is given by:

$$\Phi_{GPD}(x) = \left[1 + \xi \left(\frac{x - x_m}{\sigma} \right) \right]^{-1/\xi} \quad (3-2)$$

where x_m is the location parameter, σ is the scale parameter, and ξ is the shape parameter. The GPD contains the PT1 as a special case where $\xi = \beta^{-1}$ with the condition that $\sigma = x_m \xi$. The GPD is bounded by a wave height upper limit of $x_m - \sigma/\xi$ when $\xi < 0$ and unbounded when $\xi \geq 0$ [Coles, 2001]. The parameters of both distributions, i.e. Equations 4-1 and 4-2, are estimated using the Maximum Likelihood Estimate [Coles, 2001; Geist and Parsons, 2014].

Extreme event probabilities are often represented in terms of mean recurrence intervals (MRI), the inverse of which expresses the probability that a specified return level (RL) magnitude x_{RL} will be exceeded in any one year. For a given return level x_{RL} , the mean recurrence interval MRI is expressed as:

$$MRI = \left\{ \left[\Phi(x_{RL}) \right] \left[\frac{N_{exceed}}{N_{total}} \right] \left[\frac{N_{total}}{n_{years}} \right] \right\}^{-1} \quad (3-3)$$

where $\Phi(x_{RL})$ is the survivor function of the exceedance distribution, N_{total} is the total number of waves in the record, N_{exceed} is the total number waves in the record above the threshold x_m , and n_{years} is the length of the record in years. Meteotsunami occurrences at each station are assumed to be a stationary Poisson process such that the mean recurrence intervals do not change over time and meteotsunami occurrences are independent of past events [Geist et al., 2014].

To test the fit of the distributions, the Anderson-Darling Goodness-of-Fit test is used here. The Anderson-Darling test is particularly suited for extreme value statistics, as the test heavily weights the tails of the distribution. The test statistic is given by

$$A^2 = -N - \left(\frac{1}{N}\right) \sum_{i=1}^N \left\{ (2i-1) \left[\log(1-\Phi(x_i)) + \log(\Phi(x_{N+1-i})) \right] \right\} \quad (3-4)$$

where N is the total number of observations under consideration and $\Phi(x_i)$ is value of the survivor function for the i^{th} largest observation, calculated with Equation 1 or 2. Critical values for the Anderson-Darling test are derived from the tables provided by *Choulakian and Stephens* [2001]. The lower limit to x_m (i.e. a meteotsunami minimum height threshold) is obtained from the failure-to-reject method [*Choulakian and Stephens, 2001*] by sorting the observations and deleting the lowest value observations until the distribution is no longer rejected by the Anderson-Darling test at a significance level of $\alpha = 0.1$.

As the PT1 is a restricted special case of the GPD, the likelihood ratio test is used to determine if the difference in fit between the models is statistically significant. The likelihood ratio test statistic is

$$D = 2(l_{GPD} - l_{PT1}) \quad (3-5)$$

where l_{GPD} and l_{PT1} are the maximum log-likelihoods associated with the GPD and PT1 fits, respectively. With one degree of freedom from the reduction of one parameter from the GPD to PT1, the critical value for this likelihood ratio test is 3.84 at $\alpha = 0.05$ significance level.

3.3.4. Conditional Occurrence Analysis

To investigate spatial connections of meteotsunami events between stations, the percentage of meteotsunami events for which a meteotsunami occurs in close temporal proximity at a different station is quantified. We follow the method used by *Šepić et al.* [2009b] to identify meteotsunamis in the Adriatic Sea under the condition that a meteotsunami also occurred in close temporal proximity at the Balearic Islands. Specifically, for each event at a given station (termed

reference station), the other stations (termed *co-occurring stations*) are polled to identify a meteotsunami which also occurred within +/- 6 hours. A co-occurrence limit of 6 hours is chosen based upon the time needed for a wave to travel the long axis of the lake moving at a speed of 10 m/s, the minimum edge wave resonant speed for Lake Michigan [As-Salek and Schwab, 2004]. For each possible pair of reference and co-occurring stations, a conditional occurrence percentage is defined as the percent of events at the reference station for which a meteotsunami also occurs within 12 hours at a co-occurring station.

3.3.5. Monthly Occurrence Statistics

The monthly distribution of events is quantified to obtain seasonal patterns in meteotsunami occurrence. The monthly distribution of meteotsunami events at each station is calculated by binning the identified events by month. Monthly bins are subdivided into meteotsunami height quartiles to further examine seasonal distribution by event size. To reveal the seasonal patterns in causative storms, events are also binned monthly by storm structure classification (see *Section 3.6*). The overall monthly distribution of meteotsunami events for the entire lake is calculated by binning the total number of events at all stations.

3.3.6. Storm Structure Classification

Radar imagery analysis is used to classify the structure of the storm associated with each identified meteotsunami event. Storm structure is classified at the time the radar-measured reflectivity associated with the storm initially crosses the Lake Michigan shoreline. Based upon criteria for various types of events in the Great Lakes area [Fowle and Roebber, 2003; Gallus *et al.*, 2008; Kunkel *et al.*, 2012; Workoff *et al.*, 2012], storms are classified into one of seven

categories: cluster, complex, linear, bow, extratropical cyclone, frontal, or atmospheric gravity wave. Schematics of each storm structure are shown in Figure 3-3. Criteria for defining storm structures are described as follows.

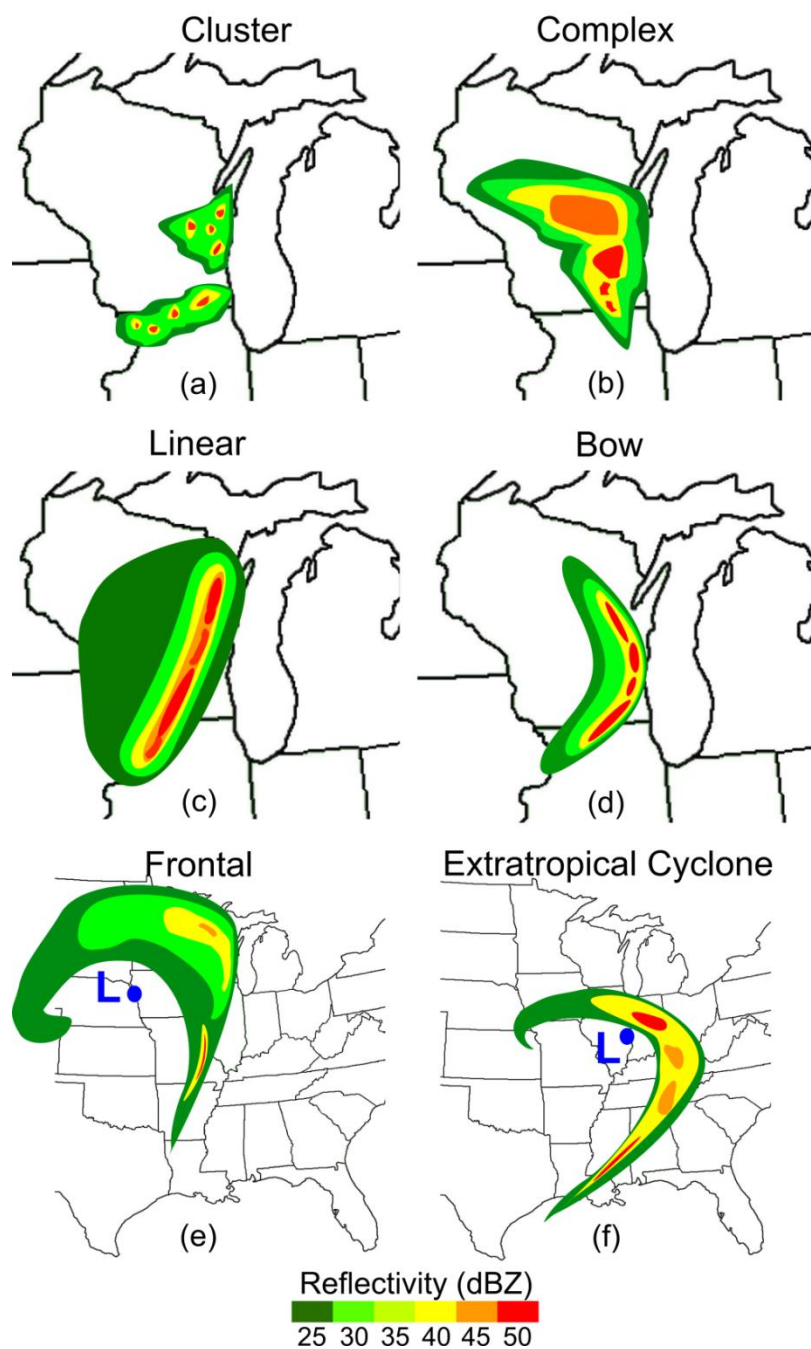


Figure 3-3 Schematics of common storm structures associated with meteotsunamis: (a) cluster, (b) complex, (c) linear, (d) bow, (e) frontal, and (f) extratropical cyclone.

Cluster (CL): “Areas of unorganized convection, with several (three or more) reflectivity maxima located within a distance equivalent of two diameters of the 45-dBZ reflectivity area of each individual storm; areas of >45-dBZ reflectivity were generally small (<40 km²) for individual storms and were separated by reflectivities >35 dBZ” [Workoff *et al.*, 2012] (Figure 3-3a). For convective structures, areas of high reflectivity exceeding 45 dBZ are likely to contain meteotsunami-causing surface wind and pressure perturbations, as the strongest pressure anomalies in developed mesoscale convective systems have been shown to be well correlated with areas of reflectivity greater than 40 dBZ [Wertman *et al.*, 2014].

Complex (C): “nonlinear, organized storm structure having an area of >500 km² with continuous reflectivity values of >45 dBZ” [Workoff *et al.*, 2012] (Figure 3-3b).

Linear (L): “an area with reflectivity values >45 dBZ organized in a curvilinear manner; storms were considered linear if they were organized in a line <50 km wide, exhibited a length–width ratio of at least 3:1 [Fowle and Roebber 2003], and areas of reflectivity >45 dBZ were separated by less than two of their diameters” [Workoff *et al.*, 2012] (Figure 3-3c).

Bow (B) – a convective structure organized similar to a linear storm system but with a curved region (bow) of less than 100 km diameter (distance from top to the bottom of the bowed segment), and the pinnacle of the bow is greater than 2 times the width of the area exceeding 45 dBZ reflectivity (Figure 3-3d).

Frontal (FRT): An area of reflectivity that does not match the convective structures above and is associated with an extratropical cyclone system. For the event to be considered frontal, the area reaching the Lake Michigan shoreline must be greater than 200 km from the center of low pressure as indicated by synoptic surface charts [Kunkel *et al.*, 2012] (Figure 3-3e).

Extratropical cyclone (ETC): A frontal event, except that the area reaching the Lake Michigan shoreline is less than 200 km from the center of low pressure [*Kunkel et al.*, 2012] (Figure 3-3f).

Atmospheric Gravity Waves (AGW): Strong pressure or wind fluctuations observed at ASOS stations which occur in the absence of convective or frontal systems. It is important to note that atmospheric gravity waves are commonly produced by and propagated with convective systems [*Belušić et al.*, 2007; *Šepić et al. 2009a*; *Vilibić et al.*, 2014a]. Detailed analyses of each storm would be required to determine the relative importance of AGW and meteorological systems, which is out of the scope of this climatological analysis. In this study, we choose to identify an event as AGW only for those propagating without a convective system.

In the cases where multiple storms move over Lake Michigan within several hours of a meteotsunami, we classify the storm propagating across the lake closest in time (within 3 hours) and location of the event. If a convective structure is situated near a frontal boundary, the storm is classified as the convective structure [*Kunkel et al.*, 2012]. If no reflectivity, frontal, or atmospheric gravity wave activity is observed within 3 hours of the potential meteotsunami, the possible meteotsunami event is deemed to be not directly meteorologically generated and was removed from further analysis.

3.4. Results

3.4.1. Exceedance Probability

Meteotsunamis are identified from the water level record using an absolute height threshold calculated from the failure-to-reject method with the Pareto Type 1 distribution. The resulting absolute height thresholds for each station are summarized in Table 3-1, with the

largest height threshold at Calumet Harbor of $x_m = 0.62$ m. The frequency of wave heights above this local absolute height threshold at Calumet Harbor is shown as a histogram in Figure 3-4a, with a total of 48 events for an average of 2.4 events per year. The largest meteotsunami height is at Calumet Harbor is 1.28 m, over twice the absolute threshold at this station. The smallest height threshold is observed at Menominee, with $x_m = 0.14$ m, yielding 5.8 events per year (Figure 3-4b). With a maximum height of 0.21 m, the ratio between the maximum height and threshold at Menominee is 1.5, the smallest among all stations. In contrast, the Green Bay station (Figure 3-4c) has a relatively low threshold of $x_m = 0.23$ m but a maximum height of 0.80 m, yielding the largest ratio between the maximum height and the threshold of 3.5.

Table 3-1: Summary of water level stations and probability distribution fits

Station	Abbrv.	Start Year	Pareto Distribution				GPD				
			x_m (m)	β	RMSE (m)	PPCC	x_m (m)	ξ	σ	RMSE (m)	PPCC
Menominee	MEN	2006	0.14	8.07	0.003	0.98	0.14	-0.221	0.026	0.003	0.99
Green Bay	GRB	1998	0.23	2.73	0.025	0.97	0.23	0.070	0.112	0.030	0.99
Port Inland	PTI	1995	0.32	5.54	0.015	0.98	0.32	-0.091	0.075	0.007	0.97
Mackinaw City	MAC	1998	0.19	5.12	0.009	0.98	0.19	0.084	0.041	0.011	0.97
Sturgeon Bay	STG	2000	0.25	6.29	0.010	0.97	0.25	-0.132	0.054	0.005	0.98
Kewaunee	KEW	2001	0.38	5.55	0.015	0.99	0.38	-0.053	0.088	0.010	0.97
Ludington	LUD	1998	0.43	6.68	0.011	0.96	0.43	-0.133	0.086	0.014	0.99
Holland	HOL	2001	0.17	3.47	0.017	0.98	0.17	0.122	0.062	0.014	0.99
Milwaukee	MKE	1996	0.38	6.73	0.017	0.97	0.38	-0.155	0.075	0.010	0.99
Calumet Harbor	CAL	1996	0.62	4.95	0.026	0.98	0.62	-0.041	0.162	0.033	0.97

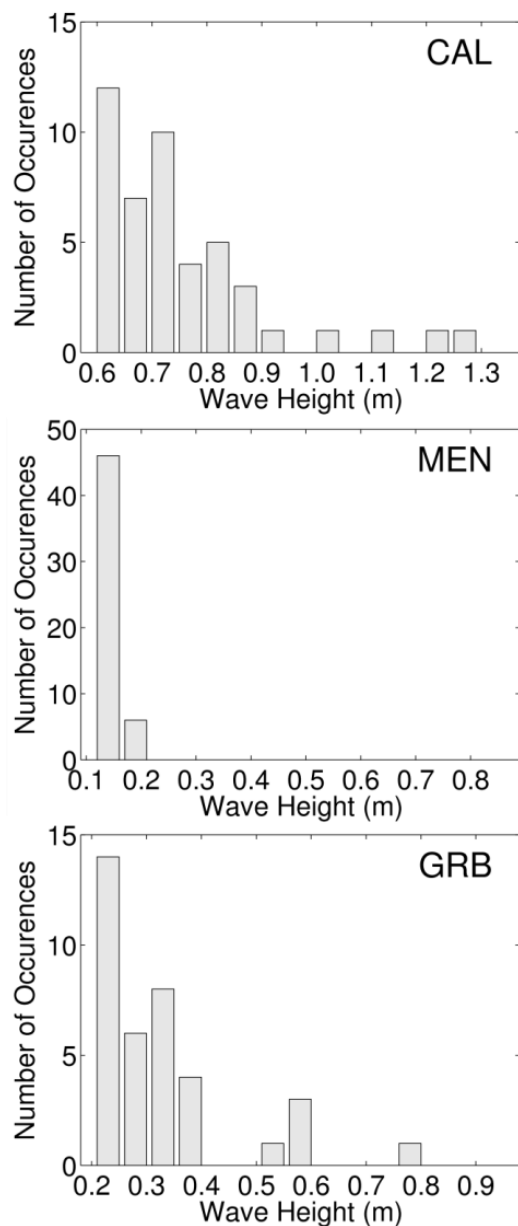


Figure 3-4: Histogram of events exceeding the absolute height threshold at Calumet Harbor, Menominee, and Green Bay. Note that the horizontal axis is scaled identically for each station with the y-intercept shifted to reflect differences in absolute thresholds.

Cumulative frequency distributions of sorted meteotsunami event sizes are plotted in Figure 3-5 for all stations. Both Pareto Type 1 (PT1) and Generalized Pareto Distributions (GPD) are chosen to fit to the data and plotted in Figure 5 as solid and dashed lines, respectively. All

distributions fail to be rejected by the Anderson-Darling goodness-of-fit test. Table 3-1 summarizes the probability distribution parameters for each station, as well as the root mean square error (RMSE) for the fits. The probability plot correlation coefficient (PPCC) is also reported, calculated as the Pearson correlation coefficient of the quantile-quantile plots corresponding to each fitted distribution(quantile-quantile plots not shown for brevity). The GPD tends to provide slightly larger wave height return levels for mean recurrence intervals less than 2 years whereas the PT1 yields much greater return levels for higher mean recurrence intervals. This is due to unbounded power law behavior of the PT1 such that wave height return levels grow infinitely with increasing mean recurrence interval while the GPD is upper bounded if the shape parameter is negative ($\xi < 0$). Based upon the RMSE and PPCC, the PT1 provides a slightly better fit for Green Bay, Mackinaw City, Ludington, and Calumet Harbor whereas the GPD provides a slightly better fit for Menominee, Port Inland, Sturgeon Bay, Kewaunee, Holland, and Milwaukee. All of the stations where the GPD give the best fit have negative GPD shape parameters except Holland, indicating the size-frequency relationships at these stations exhibit bounded growth for the observed data. In reality, meteotsunami size is physically limited by processes such as non-linear propagation, wave-breaking, strength of surface forcings, and duration of resonance [Korycansky and Lynett, 2005]. Nevertheless, the likelihood ratio test fails to reject the PT1 in favor of the GPD at the $\alpha = 0.05$ level for any station, indicating that the GPD does not provide a statistically significant better fit to the data than the PT1. This result suggests that longer historical records are needed to confidently determine an upper bound on meteotsunami size from statistics, consistent with findings for seismic tsunami size data [Geist and Parsons, 2014]. Thus, subsequent analysis will be based upon the Pareto Type 1 distribution, though similar conclusions can be drawn from the Generalized Pareto Distribution.

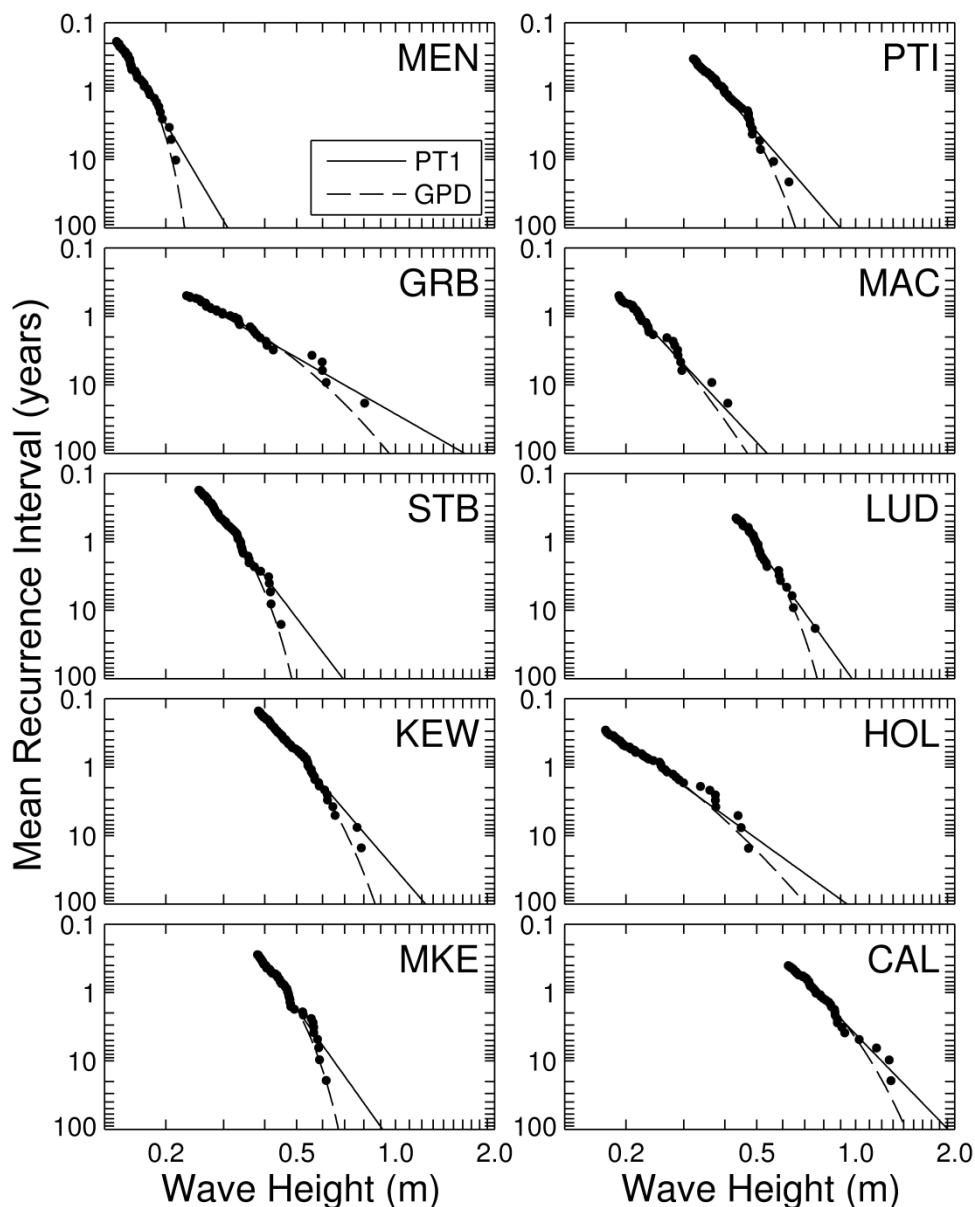


Figure 3-5: Meteotsunami size observations (dots) fit with the Pareto Type 1 (solid line) and Generalized Pareto Distributions (dashed line).

Return levels are calculated from the Pareto Type 1 distribution fits to represent meteotsunami probability at each station. The annual (1-year) meteotsunami height exceeds 0.25 meters for all stations except Menominee and Mackinaw City. Calumet Harbor has by far the

largest annual meteotsunami height of 0.75 m, nearly 50% greater than the next largest at Kewaunee (0.54 m). The 10-year mean recurrence interval exceeds 0.45 meters for all stations except Menominee and Mackinaw City. The largest 10-year return level occurs at Calumet Harbor at 1.2 m, indicating that Calumet Harbor is at risk of the largest meteotsunamis. The meteotsunami size-frequency distribution at Green Bay is of particular interest, as this station has only the 7th largest 1-year return level but the 3rd largest 10-year return level, demonstrating rapid growth in return level relative to the other stations. The character of these distributions and their implications for meteotsunami behavior at each station will be discussed in more detail in Section 5.5.2.

3.4.2. Conditional Meteotsunami Occurrence

The occurrence of meteotsunamis at multiple stations is calculated as the percentage of events at a given station (reference station) that satisfy the condition that a meteotsunami also occurs at another station (co-occurring station) within 6 hours [Šepić *et al.*, 2009b]. These conditional occurrence percentages are summarized in Table 3-2 for each combination of reference and co-occurring stations. Overall, 59% of the identified meteotsunamis occurred at only one station, 20% occurred at two stations, and 21% concurrently occurred at three or more stations. The largest conditional occurrence percentages are between Ludington-Sturgeon Bay (75%), Surgeon Bay-Kewaunee (66%), Ludington-Kewaunee (57%) and Kewaunee-Sturgeon Bay (52%). These three stations are located within closest spatial proximity of any three stations in the main basin of Lake Michigan. The next largest conditional occurrence percentages are between Calumet Harbor-Milwaukee (52%), Calumet Harbor-Sturgeon Bay (52%), and Calumet Harbor-Kewaunee (52%), with all stations located on the west shore of the main lake basin. The

strong conditional occurrence percentages between these stations suggest that one can “predict” the occurrence of a meteotsunami at the co-occurring station based upon meteotsunami arrival at the reference station [Marcos *et al.*, 2009; Šepić *et al.*, 2009b]. The only stations that have no conditional percentages in excess of 40% are Green Bay and Menominee, which are both located in the Green Bay basin. Despite the close spatial proximity between the Green Bay and Menominee stations, conditional occurrence percentages are not strong between these two stations. Overall, these results suggest that spatial proximity can be a considerable influence in the conditional occurrence of meteotsunamis between stations but other factors like bathymetry can also dictate the meteotsunami occurrence.

Table 3-2: Conditional occurrence of meteotsunamis between station pairs represented by the percent of meteotsunamis at a reference station for which meteotsunamis also occur at a co-occurring stations within +/- 6 hours.

Reference Station	Co-occurring Station									
	MEN	GRB	PTI	MAC	STG	KEW	LUD	HOL	MKE	CAL
MEN		12%	12%	12%	15%	6%	4%	21%	6%	8%
GRB	36%		19%	11%	24%	5%	3%	10%	14%	11%
PTI	22%	13%		27%	42%	41%	18%	16%	20%	12%
MAC	22%	13%	47%		39%	27%	7%	35%	17%	10%
STG	19%	7%	27%	17%		66%	23%	22%	25%	25%
KEW	7%	1%	23%	8%	52%		14%	23%	22%	18%
LUD	33%	3%	28%	11%	75%	57%		24%	44%	47%
HOL	18%	4%	13%	15%	30%	42%	8%		25%	19%
MKE	10%	9%	21%	9%	43%	50%	24%	35%		34%
CAL	21%	7%	17%	7%	52%	52%	33%	32%	52%	

3.4.3. Seasonal Occurrence

To examine seasonal trends in meteotsunami occurrence, events at each station are binned based upon the month of incidence. The monthly distribution of meteotsunamis is

illustrated in Figure 3-6, with events grouped into quartiles based upon wave height. In general, lake-wide, meteotsunamis primarily occur in the late spring and early summer, with 60% of the observed meteotsunamis occurring in the months of April, May, and June (AMJ). At each individual station, peak AMJ seasonality is shared by Port Inland, Mackinaw City, Kewaunee, Sturgeon Bay, Ludington, and Holland. Meteotsunami seasonality at Calumet Harbor is slightly later, peaking in May and June (MJ), while in Milwaukee the peak season extends from April to July (AMJJ). Peak meteotsunami occurrence at Green Bay is in the summer season, with nearly 80% of events reported in June, July, and August (JJA). A later seasonality for these three stations (Calumet Harbor, Milwaukee, and Green Bay) suggests that the causative atmospheric conditions may differ from those associated with the AMJ stations. Different from all other stations, Menominee does not have a clear meteotsunami season, with the most occurrences in May but also 44% of events in the fall and winter months. The monthly distributions of the height quartiles exhibit similar seasonality as the full collection of events, suggesting that the meteotsunami seasonality is irrespective of event size.

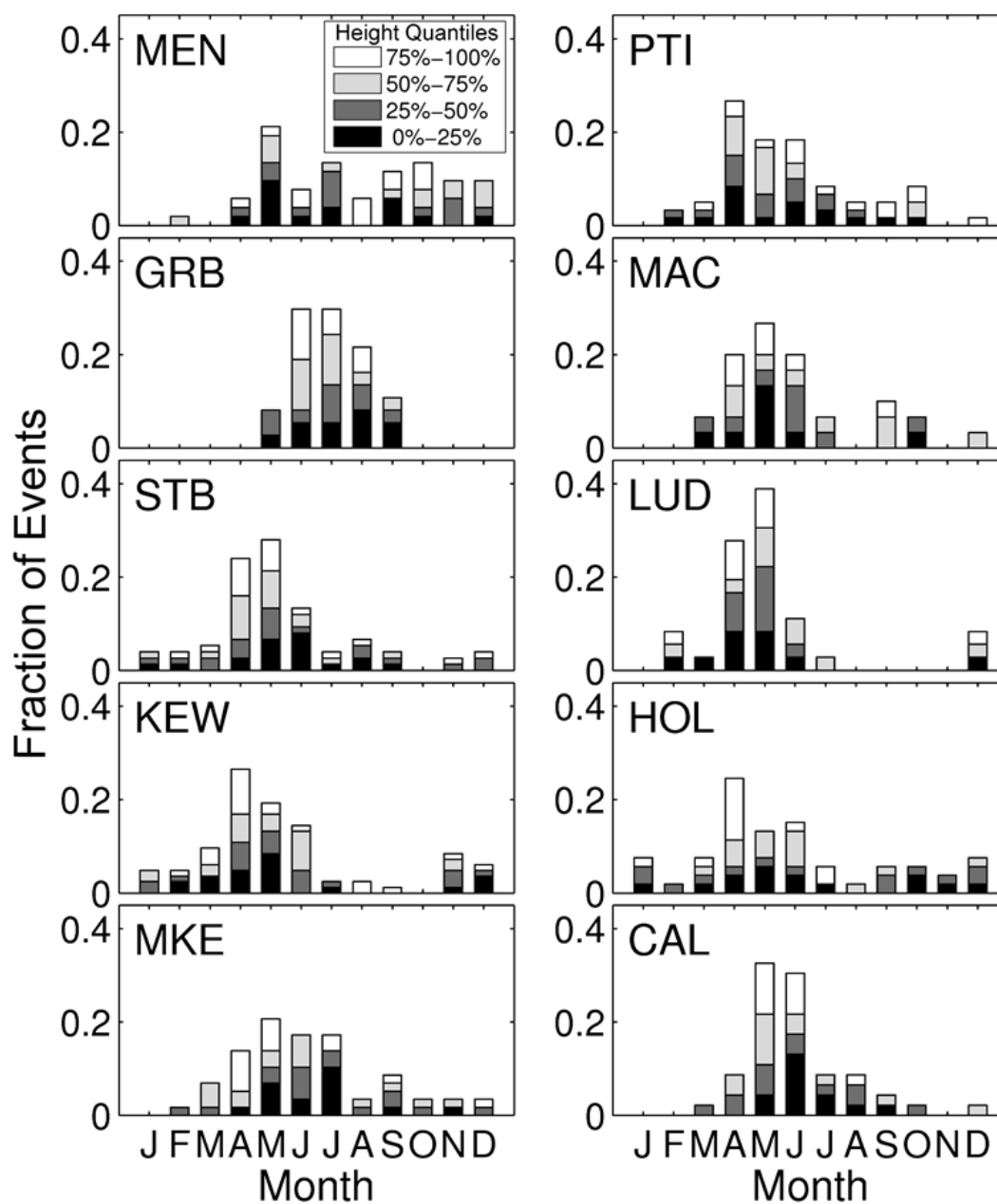


Figure 3-6: Monthly distributions of meteotsunamis at each station, with bars subdivided into height quantiles (i.e. 75% to 100% are the largest 25% of events at a given station).

3.4.4. Storm Structures Associated with Meteotsunamis

The cause of each identified meteotsunami is classified based upon storm structures (see Figure 3-3). The distribution of storm structures for each station is illustrated in Figure 3-7, with

warm colors (red, orange, and yellow) representing convective structures, cool colors (blues) representing frontal-type structures, and green representing atmospheric gravity waves. Generally, most meteotsunamis at every station are associated with convective activity, with meteotsunamis at Calumet Harbor and Milwaukee almost exclusively associated with convective structures at 94% and 84% of events, respectively. Complex convective systems are the most prevalent storm structure at every station except Green Bay and Calumet Harbor, where linear structures are most common. Linear structures also account for over 30% of meteotsunamis at Milwaukee and Holland. Cluster and bow structures are associated with no more than 13% of the meteotsunamis at any station. Frontal-type structures are associated with over 40% of the meteotsunamis at Menominee, Port Inland, Mackinaw City, and Kewaunee. Of the frontal-type structures, fronts are over twice as common as extratropical cyclones. Atmospheric gravity waves (in the absence of strong convective or frontal structures) are only associated with one meteotsunami, which occurred at Holland. Atmospheric gravity waves likely play a role in some of the meteotsunamis classified as convective structures, as convection can trigger atmospheric gravity waves and promote their ducting [Belušić *et al.*, 2007; Šepić *et al.*, 2009a; Vilibić *et al.*, 2014a]. Overall, meteotsunami events in Lake Michigan are strongly associated with convective and frontal activity, with convective structures generally more prevalent in southern Lake Michigan while frontal structures have increased importance in the north.

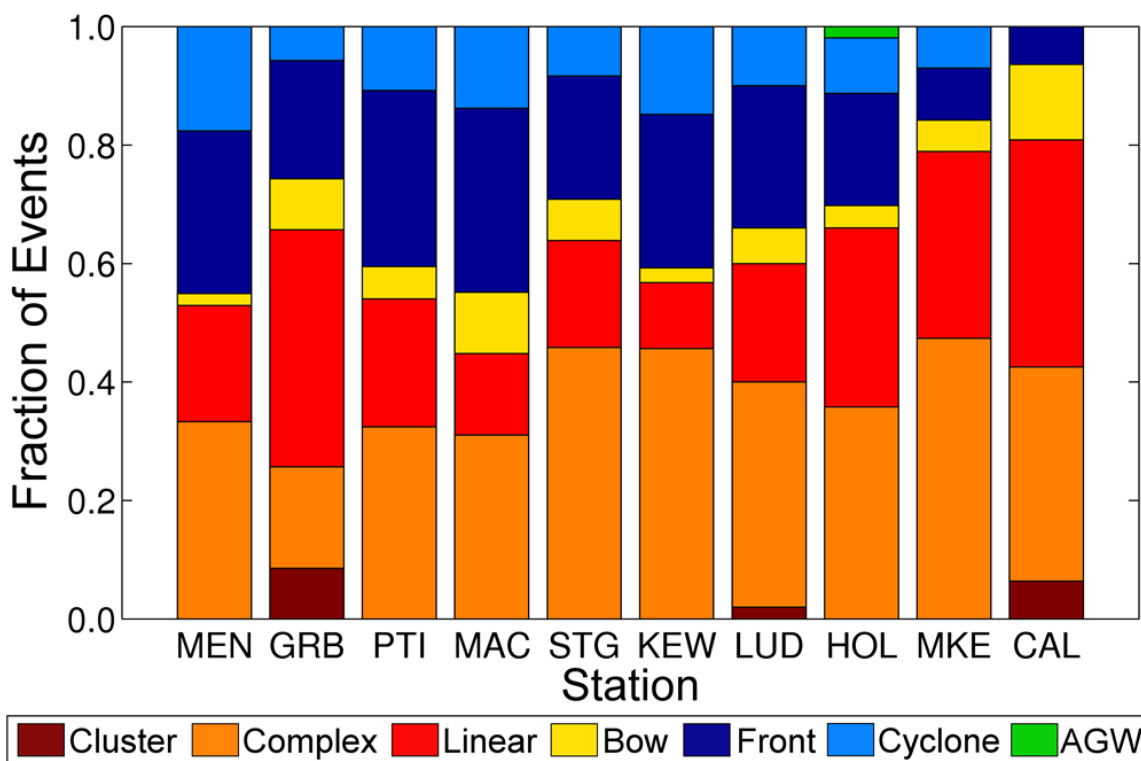


Figure 3-7: Distribution of storm structures associated with meteotsunamis at each station.

Seasonal trends in meteotsunami-causing storm structures are quantified by binning the storm classifications by month of occurrence. The monthly distribution of storm structures summed over all stations in Lake Michigan is shown in Figure 3-8. For this lake-wide aggregate, the storm structures associated with concurrent meteotsunamis at multiple stations (defined based upon the guidelines of Section 3.4) are only represented once. Meteotsunamis associated with convective storm structures occur primarily in the late spring to mid-summer, peaking between April and July (AMJJ). Meteotsunamis associated with complex convective structures occur primarily in April, May and June (AMJ), while those associated with linear structures peak later in the year from May through August (MJJA). The largest number of bow associated meteotsunamis occur in June while meteotsunamis associated with convective clusters do not

show a strong seasonal trend. Meteotsunamis associated with frontal-type structures occur primarily in the cold seasons between October through May, peaking in April and May before sharply dropping off in occurrence in the summer months. The only event classified as an atmospheric gravity wave, with no associated storm, occurred in April. This study presents statistics of the specific storm structures associated with meteotsunamis for the first time, as far as the authors are aware.

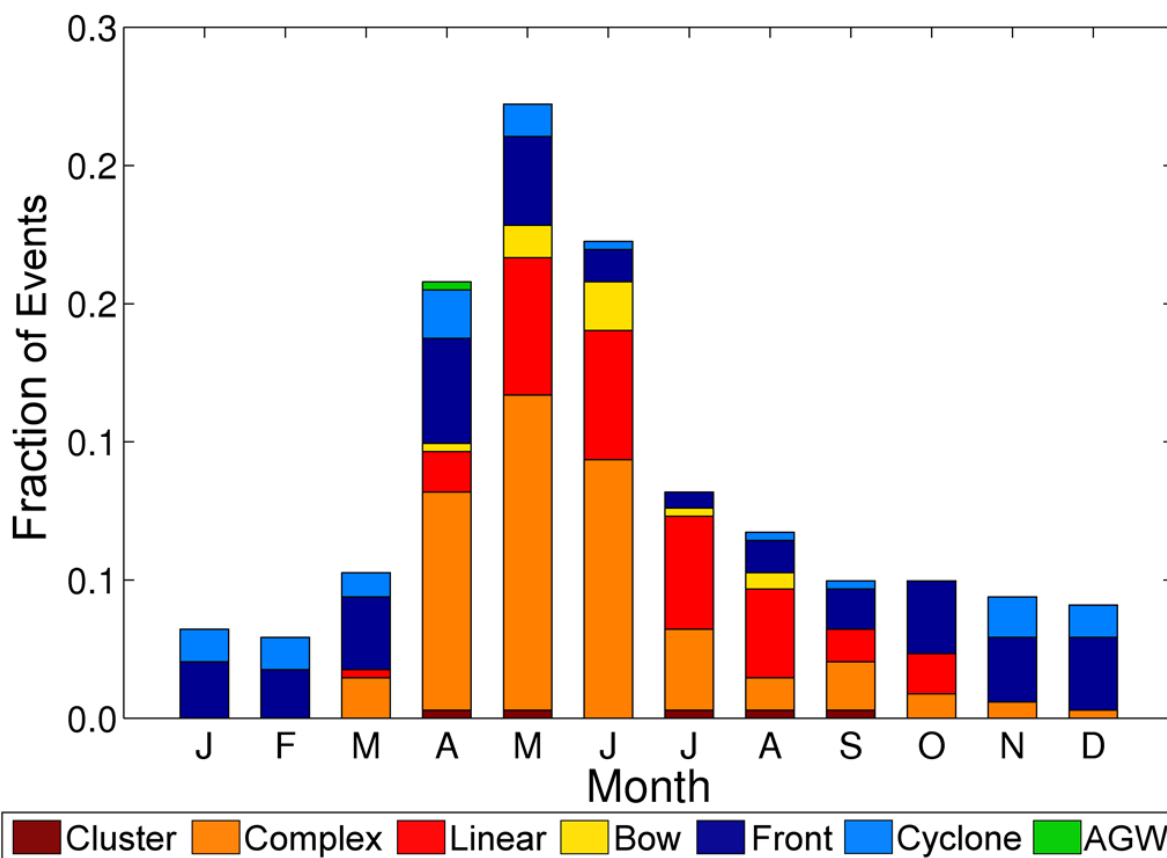


Figure 3-8: Monthly distribution of storm structures associated with meteotsunamis aggregated across all stations.

3.5. Discussion

3.5.1. Meteotsunami Statistics versus Storm Structure Statistics

To better understand the causative mechanisms of meteotsunamis in Lake Michigan, the spatial and temporal patterns in meteotsunami occurrence are compared with statistics of storms in the Great Lakes region. Meteotsunamis at Milwaukee and Calumet Harbor are caused almost exclusively by convective systems, including a much larger contribution from linear systems than any station besides Green Bay. Studies by *Johns and Hirt* [1987] and *Ashley and Mote* [2005] showed that intense and long-lived convective windstorms, also called derechos, exhibit a distinct corridor of activity that crosses southern Lake Michigan and drops off sharply over northern Lake Michigan. Conversely, northern Lake Michigan stations experience an increased proportion of meteotsunamis from frontal-type storms compared with southern Lake Michigan. Consistent with this spatial meteotsunami occurrence pattern, the average frequency of strong cyclones over Lake Michigan is highest in the north, owing to the origination of many of these cyclones from Canada [*Angel*, 1996].

The spatial differences in the observed storm structures associated with meteotsunamis in Lake Michigan have implications for the likely resonance mechanisms in meteotsunami generation. Observations by *Johns and Hirt* [1987] showed that derecho propagation speeds averaged 23 m/s with a top speed of 33 m/s. The median Great Lakes cyclone forward speeds observed by *Angel* [1996] ranged from 13 m/s in the winter to 10 m/s in the summer. The depth-based Proudman resonance speeds in the southern Lake Michigan basin range from 22 to 40 m/s. As a result, convective storms moving across southern Lake Michigan is a favorable situation for meteotsunami generation. In contrast, in the deeper northern basin Proudman resonant speeds range from 38 to 52 m/s, which rarely occurred in the convective storms observed in the Great

Lakes. In other words, Proudman resonance is not likely to generate meteotsunamis in the open waters of northern Lake Michigan. Instead, Greenspan edge wave resonance is possible throughout the entire Lake Michigan basin for convective and frontal storms traveling at speeds in excess of 10 m/s, based upon shelf slopes [As-Salek and Schwab, 2004]. Consequently, meteotsunamis in the northern basin of Lake Michigan are likely to be produced primarily through Greenspan resonance while southern basin experiences a combination of Greenspan and Proudman resonant meteotsunamis.

The monthly distribution of meteotsunami causative storms in Lake Michigan (Figure 3-8) indicates that convectively associated events occur primarily between April and July. Intense mesoscale convective systems over Lake Michigan have been observed to occur primarily in May, June, and July [Graham *et al.*, 2004]. In a study that is more representative of the storm structure classifications used in this paper, Workoff *et al.* [2012] found that both complex and linear convective storms over Lake Erie from 2001 to 2009 occurred primarily from May to August, peaking in July. The monthly occurrence of convectively associated meteotsunamis is earlier than the peak convective storm seasonality by approximately one month. This discrepancy could be related to climatological differences in storm speed and direction that may exist between the early and late convective season. Another possible explanation for the occurrence of convectively-caused meteotsunamis early in the convective storm season is the patterns in storm evolution over Lake Michigan. As observed by Graham *et al.* [2004], mesoscale convective systems which occurred earlier in the season (May and June) were more likely to maintain intensity whereas storms later in the summer were more likely to weaken or dissipate over the lake. In both Lakes Michigan and Erie, storms which maintained intensity were correlated with a strongly-stable overlake boundary layer [Graham *et al.*, 2004;

Workoff et al., 2012], which tends to be strongest in late spring and early summer when air temperatures are warm and the lake temperatures are still cool from winter. Nevertheless, the overall impact of overlake boundary layer physics on meteotsunami formation is unclear, which necessitates the further study. Future research is needed to compare meteotsunami-causing storms with those not causing meteotsunamis to better understand the discontinuity between peak meteotsunami and convective storm seasonality.

Meteotsunamis associated with frontal-type events occur from the late fall through spring, peaking in April and May (Figure 3-8). Strong cyclones over the Great Lakes occur primarily from November through April, with cyclone intensity peaking in January [*Angel*, 1996; *Angel and Isard*, 1998]. While meteotsunamis associated with frontal events do occur in the peak cyclone season, meteotsunami occurrences do not follow these increases in cyclone frequency or strength. Interestingly, in months when frontally-associated meteotsunamis occurrences peak, a reduction in cyclone frequency and intensity occurs between March and May during the transition to the warm season [*Angel and Isard*, 1997]. As with convectively associated meteotsunamis, future research which compares meteotsunami events with null frontal storms is needed to address these discrepancies in seasonal patterns.

3.5.2. Size-Frequency Distribution Parameters

The probability distribution fit parameters reveal insight into the behavior of meteotsunamis at each station. We focus on the PT1 parameters x_m and β for the following discussion though similar results can be drawn from the GPD parameters x_m and ξ . The height threshold x_m describes the minimum height for which a wave is considered a meteotsunami at each station. The height threshold likely indicates the strength of local processes such as the

harbor amplification, as a water level station located within a harbor with high amplification potential will consistently produce larger meteotsunamis than nearby harbors with lesser amplification potential [Marcos *et al.*, 2009]. As summarized in Table 1, the smallest height thresholds (in ascending order) occur at Menominee, Mackinaw City, Holland, Green Bay, and Sturgeon Bay. The water level stations at Green Bay and Mackinaw City are not located within harbors so no amplification is possible. Stations at Holland, Menominee, and Sturgeon Bay are located within small harbors which feed almost directly into river channels and are expected yield low amplification potential. On the other hand, the stations with the largest height thresholds (Calumet Harbor, Ludington, Milwaukee, and Kewaunee) are located in the four largest harbors among the stations of comparison with geometries that are more favorable to energy transmission and amplification. While other factors certainly impact the height threshold, the association with harbor configuration suggests that local processes can have a large influence on the meteotsunami height threshold x_m .

The PT1 shape parameter β describes the growth of the return levels, where a smaller shape parameter indicates a more tail-weighted distribution (i.e. return levels grow more rapidly). The shape parameter is indicative of the potential for meteotsunami generation at a station through processes such as propagation resonance and spatial focusing [Geist *et al.*, 2014]. As summarized in Table 1, the most tail-weighted distribution occurs at Green Bay, suggesting that this station may suffer from the most abnormally large meteotsunamis. Indeed, Green Bay has only the 7th largest 1-year return level but the 3rd largest 10-year return level, demonstrating the rapid growth in return level relative to the other stations. In contrast, Menominee has the least tail-weighted distribution, suggesting this station is the least sensitive to anomalously large meteotsunami events. Though the Menominee and Green Bay stations are located within in close

proximity of each other in the shallow basin of Green Bay, the difference in coastline shape between the two stations may explain the large discrepancy in shape parameter. Whereas Menominee is located along a straight reach of coast, the Green Bay station is at the end of Green Bay, where meteotsunami energy can be geometrically focused as the bay narrows [Rabinovich, 2009]. Furthermore, of the four most tail-weighted stations, three are located at the ends of the elongated lake (Mackinaw City and Calumet Harbor) and bay (Green Bay), suggesting the spatial focusing in these concave ends of the basins may lead to more extreme meteotsunami heights than along the open coast. In contrast, the five least tail-weighted stations are located in the middle of the basins along relatively straight stretches of coast.

3.5.3. Role of Wave Reflection

The frequent occurrence of large meteotsunamis along the west coast of Lake Michigan indicates the importance of meteotsunami wave reflection in the enclosed basin of Lake Michigan. As the propagation of both convective and frontal storms in the Great Lakes generally have a significant eastward component [Angel, 1996; Graham, 2004], the occurrence of meteotsunamis on the west coast is likely due to wave reflection off the east coast of the lake. This may explain why the largest 10-year return levels occur at Calumet Harbor and Kewaunee, both located on the west coast of the lake. Interestingly, meteotsunami wave reflection was a key mechanism in the fatal 1954 Lake Michigan meteotsunami which struck Chicago [Ewing *et al.*, 1954]. This reflection decoupled the damaging wave from the causative storms and recreational users returned to the coast after the passage of the storm, only to be struck with the non-coupled meteotsunami over an hour after the storm had passed. Furthermore, the enclosed basin retained wave energy that created hazardous conditions for over a day after the initial meteotsunami

[*Bechle and Wu, 2014*]. Recently, *Anderson et al., [2015a]* showed another example of a series of multiple wave reflections in the enclosed basin, leading to a dangerous, non-coupled meteotsunami in Lake Erie. Similar effects of meteotsunami wave reflection have also been observed in semi-enclosed basins [*Orlić et al., 2010; Šepić et al., 2015*]. Overall, the danger of non-coupled, reflected meteotsunami waves is recognized and ubiquitous with enclosed basins like the Great Lakes.

In comparison, along a non-enclosed sea coasts, meteotsunami wave reflection may occur in the onshore or offshore direction. In the case of a storm propagating towards the coastline, the meteotsunami wave is reflected off of the coast and radiates to the offshore [*Vilibić et al., 2004; 2008*]. Coastal reflection in non-enclosed water bodies leads to wave energy transmission into the open sea and typically does not add to the meteotsunami hazard. In the case of a storm propagating away from the coastline over a steep bathymetric change, some meteotsunami wave energy may reflect back onshore towards the coast [*Vennell, 2007; 2010*]. This topographic reflection is a significant factor in non-coupled meteotsunamis along the U.S. East Coast in response to storms moving eastward [*Mercer et al., 2002; Pasquet and Vilibić, 2013; Šepić and Rabinovich, 2014; Wertman et al., 2014*]. Nevertheless, along non-enclosed coasts much of the wave energy can leak out to the open ocean [*Vennell, 2007; 2010*]. Thus, meteotsunami wave energy is typically not as efficiently reflected and retained along non-enclosed coasts as compared with enclosed or semi-enclosed basins.

3.5.4. Comparisons with Worldwide Meteotsunami Occurrence

Lake Michigan meteotsunami occurrences peak in the late spring to early summer (April through June) and are primarily associated with convective storms and frontal systems. These

climatological characteristics for Lake Michigan meteotsunamis are compared with those derived from episodic analyses of meteotsunamis at major meteotsunami regions worldwide, including the U.S. East Coast, the Mediterranean, Northern Europe, and Japan. Along the U.S. East Coast, recent destructive meteotsunamis have been observed in the summer season (June and July) and are associated with strong convective activity [*Churchill et al.*, 1995; *Šepić and Rabinovich*, 2014; *Wertman et al.*, 2014] or atmospheric gravity waves [*Paxton and Sobien*, 1998; *Vilibić et al.*, 2014a]. A large number of East Coast meteotsunamis also occur in the winter and early spring and are associated with frontal storms [*Pasquet et al.*, 2013], a pattern that is similar to Lake Michigan. In the Mediterranean, peak meteotsunami seasonality is primarily in the summer months of June, July, and August [*Rabinovich and Monserrat*, 1996; *Šepić et al.*, 2009b; *Šepić et al.*, 2012], later than in Lake Michigan. Mediterranean meteotsunamis are commonly associated with atmospheric gravity waves [*Monserrat et al.*, 1991; *Jansa et al.*, 2007; *Šepić et al.*, 2012]. Future work to discern the effects of atmospheric gravity waves from convective storms in Lake Michigan may shed light on differences between the causative atmospheric processes in the Mediterranean and Great Lakes regions. In Northern Europe, damaging meteotsunamis in the United Kingdom and Finland occur mostly in the summer (June, July, August) and were attributed to strong convective activity [*Haslet and Bryant*, 2009; *Tappin et al.*, 2013; *Pelikka et al.*, 2014]. On the other hand, most meteotsunamis in Japan have been reported to occur in the winter and early spring [*Hibiya and Kajiura*, 1982; *Tanaka*, 2010; *Asano et al.*, 2012]. In general, most meteotsunami regions exhibit a peak season in the summer, though Lake Michigan has the earliest peak in meteotsunami occurrences among these regions. Convective activity is the dominant driver for many of these warm season meteotsunamis, consistent with the findings for Lake Michigan. As these comparisons were based upon collections of episodic analyses,

future work is desired to statistically characterize meteotsunami occurrence worldwide to improve the understanding of the differences in meteotsunami behavior and climatology around the world.

3.6. Summary and Conclusions

In this paper, the occurrence of meteotsunamis in Lake Michigan in terms of size-frequency statistics, seasonality, and meteorological cause is quantified. Historic water level records of up to 20 years are analyzed at ten sites around the lake to identify meteotsunamis using a statistically-based height threshold criterion. Meteotsunami height data are fit to Pareto Type 1 and Generalized Pareto Distributions, yielding estimates of meteotsunami probabilities that are crucial for hazard risk assessment. Return levels calculated from these distributions reveal that meteotsunamis in excess of 0.25 m are expected to occur annually throughout the lake, with the largest events at Calumet Harbor in southern Lake Michigan. A clear seasonal pattern exists in meteotsunami occurrence, with most events occurring in the late spring and early summer. Analysis of storm structure data reveals that strong convective and frontal storm structures are associated with the nearly all of the identified meteotsunamis, with convective structures generally more prevalent in southern Lake Michigan while frontal structures have increased importance in the north. The southern Lake Michigan basin has water depths ideal for Proudman resonance with convective storms whereas the northern basin, too deep for consistent Proudman resonance, is likely prone to meteotsunamis from Greenspan resonant edge waves. While there is a strong association between meteotsunamis and convective and frontal storm structures, the seasonality of these storms over the Great Lakes differs slightly from

meteotsunami seasonality, suggesting that storm patterns alone does not dictate meteotsunami occurrence.

Overall, this study presents meteotsunami statistics and associated causative storm structures for the first time, as far as the authors are aware. Specifically, the occurrences of Lake Michigan meteotsunamis occurrences peak in the late spring to early summer and primarily associated with convective storms and frontal systems. These climatological characteristics are compared with those derived from episodic analyses of meteotsunamis at major meteotsunami regions worldwide, including the U.S. East Coast, the Mediterranean, Northern Europe, and Japan. From another aspect, the statistical analysis of water level and storm structure records in Lake Michigan has revealed spatial and temporal patterns in meteotsunami occurrence that were previously unattainable through episodic event analysis. This information fills important knowledge gaps in the assessment meteotsunami-induced hazard risks.

3.7. Acknowledgements

This work was supported in part by the Cooperative Institute for Limnology and Ecosystems Research Long-term Great Lakes Fellowship, the UW-Madison/UW-Milwaukee Intercampus Research Incentive Grants Program, the University of Wisconsin Sea Grant Institute, and the ISWS/University of Illinois. In addition, the first author was supported by the National Science Foundation's Graduate Research Fellowship Program, All opinions are those of the authors and do not necessarily reflect those of the funding agencies or authors' institutions. The authors would like to thank Dr. David Schwab at the Graham Sustainability Institute, University of Michigan and Dr. Eric Anderson at NOAA-Great Lakes Environmental Research Laboratory for their valuable advice and discussion on meteotsunamis research in the Great

Lakes. Furthermore, the authors would like to acknowledge related agencies that grant access to observational data from the several public websites: <http://www.ndbc.noaa.gov>, <http://www.ncdc.noaa.gov>, and <https://mesonet.agron.iastate.edu/archive/data/>. Last but not least, the valuable suggestions and comments from the anonymous reviewer and the editor Dr. Andrey Proshutinsky to improve the paper are greatly appreciated.

3.8. References

- Aarnes, O.J., Ø. Breivik, M. Reistad (2012), Wave Extremes in the Northeast Atlantic, *J. Climate*, 25, 1529–1543.
- Anderson, E.J., Bechle, A.J., Wu, C.H., Schwab, D.J., Mann, G.E., and Lombardy, K.A. (2015a), Reconstruction of a meteotsunami in Lake Erie on 27 May 2012: Roles of atmospheric conditions on hydrodynamic response in enclosed basins. *J. Geophys. Res. Oceans*. Accepted Author Manuscript, doi: 10.1002/2015JC010883.
- Anderson, J. D., Wu, C. H. and Schwab, D. J. (2015b), Wave climatology in the Apostle Islands, Lake Superior. *J. Geophys. Res. Oceans*. 120(7), 4869-4890, doi:10.1002/2014JC010278.
- Angel, J.R. (1996), Cyclone climatology of the Great Lakes, *Misc. Publ. 172*, Midwestern Climate Center and Illinois State Water Survey, Champaign, IL.
- Angel, J.R., and Isard, S.A. (1998), The frequency and intensity of Great Lakes cyclones, *J. Climate*, 11, 61-71, doi: 10.1175/1520-0442(1998)011<0061:TFAIOG>2.0.CO;2.
- Asano, T., T. Yamashiro, and N. Nishimura (2012), Field observations of meteotsunami locally called “abiki” in Urauchi Bay, Kami-Koshiki Island, Japan, *Nat. Hazards*, 64, 1685–1706, doi:10.1007/s11069-012-0330-2.

- Ashley, W.S., and Mote, T.L. (2005), Derecho hazards in the United States, *Bull. Amer. Meteor. Soc.*, 86, 1577–1592, doi: 10.1175/BAMS-86-11-1577.
- As-Salek, J.A., and D.J. Schwab (2004), High-frequency water level fluctuations in Lake Michigan, *Journal of Waterway, Port, Coastal and Ocean Engineering*, 130(1), 45-53. doi: 10.1061/(ASCE)0733-950X.
- Bechle, A. J., and C. H. Wu (2014), The Lake Michigan meteotsunamis of 1954 revisited, *Nat. Hazards*, 74, 155–177, doi:10.1007/s11069-014-1193-5.
- Belušić, D., B. Grisogono, and Z. B. Klaić (2007), Atmospheric origin of the devastating coupled air-sea event in the east Adriatic, *J. Geophys. Res.*, 112, D17111, doi:10.1029/2006JD008204.
- Cho, K.-H., J.-Y. Choi, K.-S. Park, S.-K. Hyun, Y. Oh, and J.-Y. Park (2013), A synoptic study on tsunami-like sea level oscillations along the west coast of Korea using an unstructured-grid ocean model, *J. Coastal Res.*, 65, 678–683.
- Choulakian, V., and M. Stephens (2001), Goodness-of-fit test for the generalized Pareto distribution, *Technometrics*, 43, 478–485.
- Churchill, D.D., S.H. Houston, and N.A. Bond (1995), The Daytona Beach wave of 3-4 July 1992 – A shallow-water gravity-wave forced by a propagating squall line, *Bull. Amer. Meteor. Soc.*, 76(1), 21-32, doi: 10.1175/1520-0477(1995)076<0021:TDBWOJ>2.0.CO;2.
- Coles, S. (2001), *An Introduction to Statistical Modelling of Extreme Values*. Springer-Verlag, London.

- Demirbilek, Z., and C.L. Vincent (2002), Water Wave Mechanics, in Coastal Engineering Manual, Part II, Hydrodynamics, Chapter II-2, Engineer Manual 1110-2-1100, edited by L. Vincent and Z. Demirbilek, U.S. Army Corps of Engineers, Washington, D.C.
- Donn, W. L. (1959), The Great Lakes storm surge of May 5, 1952, *J. Geophys. Res.*, *64*(2), 191–198, doi:10.1029/JZ064i002p00191.
- Donn W.L., and W.T. McGuinness (1960), Air-coupled long waves in the ocean., *J. Meteor.*, *17*, 515–521, doi: 10.1175/1520-0469(1960)017<0515:ACLWIT>2.0.CO;2.
- Donn, W.L., and M. Ewing (1956), Stokes' edge waves in Lake Michigan, *Science*, *124*, 1238–1242, doi: 10.1126/science.124.3234.1238.
- Ewing, M., F. Press, and W. J. Donn (1954), An explanation of the Lake Michigan wave of 26 June 1954, *Science*, *120*, 684–686, doi:10.1126/science.120.3122.684.
- Fowle, M. A., and P. J. Roebber (2003), Short-range (0–48 h) numerical prediction of convective occurrence, mode, and location, *Weather Forecast.*, *18*, 782–794, doi:10.1175/1520-0434(2003)018<0782:SHNPOC>2.0.CO;2.
- Gallus, W. A., Jr., N. A. Snook, and E. V. Johnson (2008), Spring and summer severe weather reports over the Midwest as a function of convective mode: A preliminary study. *Weather Forecast.*, *23*, 101–113, doi: 10.1175/2007WAF2006120.1.
- Geist E.L., and T. Parsons (2006), Probabilistic analysis of tsunami hazards, *Nat. Hazards*, *37*, 277–314, doi: 10.1007/s11069-005-4646-z.
- Geist, E.L., and T. Parsons (2011), Assessing historical rate changes in global tsunami occurrence, *Geophys. J. Int.*, *187*, 497–509, doi: 10.1111/j.1365-246X.2011.05160.x.

- Geist, E.L., and T. Parsons (2014), Undersampling power-law size distributions: effect on the assessment of extreme natural hazards, *Nat. Hazards*, 72, 565-595, doi: 10.1007/s11069-013-1024-0.
- Geist EL, U.S. ten Brink, and M. Gove (2014), A framework for the probabilistic analysis of meteotsunamis. *Nat. Hazards*, 74(1), 123-142, doi: 10.1007/s11069-014-1294-1.
- González, F. I., E. L. Geist, B. Jaffe, U. Kânoğlu, H. Mofjeld, C. E. Synolakis, V.V. Titov, D. Arcas, D. Bellomo, D. Carlton, T. Horning, J. Johnson, J. Newman, T. Parsons, R. Peters, C. Peterson, G. Priest, A. Venturato, J. Weber, F. Wong, and A. Yalciner (2009), Probabilistic tsunami hazard assessment at Seaside, Oregon, for near- and far-field seismic sources, *J. Geophys. Res.*, 114, C11023, doi:10.1029/2008JC005132.
- Graham, R., M. Bentley, J. Sparks, B. Dukesherer, and J. Evans (2004), Lower Michigan MCS climatology: Trends, patterns types, and marine layer impacts, paper presented at 22nd Conference on Severe Local Storms, Amer. Meteor. Soc., Hyannis, MA.
- Greenspan, H. P. (1956), The generation of edge waves by moving pressure disturbances, *J. Fluid Mech.*, 1, 574–592.
- Haslett, S.K., H.E. Mellor, and E.A. Bryant (2009), Meteo-tsunami hazard associated with summer thunderstorms in the United Kingdom, *Phys. Chem. Earth*, 34, 1016-1022, doi: 10.1016/j.pce.2009.10.005.
- Hibiya, T., and K. Kajiura (1982), Origin of the Abiki phenomenon (a kind of seiche) in Nagasaki Bay, *J. Oceanogr. Soc. Jpn.*, 38, 172–182, doi:10.1007/BF02110288.
- Irish, S.M., and G.W. Platzman (1962), An investigation of meteorological conditions associated with extreme wind tides on Lake Erie, *Monthly Weather Rev.*, 90, 39–47, DOI: 10.1175/1520-0493(1962)090<0039:AIOTMC>2.0.CO;2.

- Irish, S.M. (1965), The prediction of surges in the southern basin of Lake Michigan: part II. A cases study of the surge of August 3, 1960, *Mon. Weather Rev.*, *93*(5), 275–281, doi: doi: 10.1175/1520-0493(1965)093<0282:TPOSIT>2.3.CO;2.
- Jansa, A., S. Monserrat, and D. Gomis (2007), The rissaga of 15 June 2006 in Ciutadella (Menorca), a meteorological tsunami, *Advances in Geosciences*, *12*, 1-4.
- Johns, R.H., and W.D. Hirt (1987), Derechos: Widespread Convectively Induced Windstorms. *Wea. Forecasting*, *2*, 32–49, doi: 10.1175/1520-0434(1987)002<0032:DWCIW>2.0.CO;2.
- Korycansky, D. G., and P. J. Lynett (2005), Offshore breaking of impact tsunami: The Van Dorn effect revisited, *Geophys. Res. Lett.*, *32*, L10608, doi:10.1029/2004GL021918.
- Kunkel, K.E., D.R. Easterling, D.A.R. Kristovich, B. Gleason, L. Stoecker, and R. Smith (2012), Meteorological Causes of the Secular Variations in Observed Extreme Precipitation Events for the Conterminous United States, *J. Hydrometeorol*, *13*, 1131–1141, doi: 10.1175/JHM-D-11-0108.1.
- Marcos, M., S. Monserrat, R. Medina, A. Orfila, and M. Olabarrieta (2009), External forcing of meteorological tsunamis at the coast of the Balearic Islands, *Phys. Chem. Earth*, *34*, 938-947, doi:10.1016/j.pce.2009.10.001.
- Mecking, J. V., C. T. Fogarty, R. J. Greatbatch, J. Sheng, and D. Mercer (2009), Using atmospheric model output to simulate the meteorological tsunami response to Tropical Storm Helene (2000), *J. Geophys. Res.*, *114*, C10005, doi:10.1029/2009JC005290.
- Mercer, D., J. Sheng, R. J. Greatbatch, and J. Bobanović (2002), Barotropic waves generated by storms moving rapidly over shallow water, *J. Geophys. Res.*, *107*(C10), 3152, doi:10.1029/2001JC001140.

- Monserrat S., A. Ibberson, and A.J. Thorpe (1991), Atmospheric gravity waves and the “rissaga” phenomenon, *Q. J. Roy. Meteorol. Soc.*, *117*, 553–570.
- Monserrat, S., I. Vilibić, and A. B. Rabinovich (2006), Meteotsunamis: Atmospherically induced destructive ocean waves in the tsunami frequency band, *Nat. Hazards Earth Syst. Sci.*, *6*, 1035–1051, doi:10.5194/nhess-6-1035-2006.
- Munk, W.H., F.E. Snodgrass, and G.F. Carrier (1956), Edge waves on the continental shelf, *Science*, *123*, 127–132, doi: 10.1126/science.123.3187.127.
- Murty, T. S., and N.G. Freeman (1973), Applications of the concepts of edge waves and numerical modelling to storm surge studies on Lake Huron, in Proc., 16th Conf. Great Lakes Research, pp. 533-548, Intl. Association of Great Lakes Research, Ann Arbor, Michigan.
- Nomitsu, T. (1935), A theory of tsunamis and seiches produced by wind and barometric gradient, *Mem. Coll. Sci. Imp. Univ. Kyoto A*, *18*(4), 201–214.
- Orlić, M., D. Belušić, I. Janeković, and M. Pasarić (2010), Fresh evidence relating the great Adriatic surge of 21 June 1978 to mesoscale atmospheric forcing, *J. Geophys. Res.*, *115*, C06011, doi:10.1029/2009JC005777.
- Pasquet, S., and I. Vilibić (2013), Shelf edge reflection of atmospherically generated long ocean waves along the central U.S East Coast, *Cont. Shelf Res.*, *66*, 1–8, doi:10.1016/j.csr.2013.06.007.
- Pasquet, S, I. Vilibić, and J. Šepić (2013), A survey of strong high-frequency sea level oscillations along the U.S. East Coast between 2006 and 2011, *Nat. Hazards Earth Syst. Sci.*, *13*, 473–482, doi:10.5194/nhess-13-473-2013.

- Pattiaratchi, C., and E. M. S. Wijeratne (2014), Observations of meteorological tsunamis along the south-west Australian coast, *Nat. Hazards*, 74, 281–302, doi:10.1007/s11069-014-1263-8.
- Paxton, C. H., and D. A. Sobien (1998), Resonant interaction between an atmospheric gravity wave and shallow water wave along Florida's west coast, *Bull. Am. Meteorol. Soc.*, 79, 2727–2732, doi:10.1175/1520-0477(1998)079<2727:RIBAAG>2.0.CO;2.
- Pellikka, H., J. Rauhala, K.K. Kahma, T. Stipa, H. Boman, and A. Kangas (2014), Recent observations of meteotsunamis on the Finnish coast, *Nat. Hazards*, 74(1), 197-215, doi: 10.1007/s11069-014-1150-3.
- Platzman, G.W. (1958), A numerical computation of the surge of 26 June 1954 on Lake Michigan, *Geophysica*, 6(1), 407–438.
- Proudman, J. (1929), The effects on the sea of changes in atmospheric pressure, *Mon. Not. R. Astron. Soc.*, 2, 197–209.
- Rabinovich, A.B. (2009), Seiches and harbor oscillations, in Handbook of Coastal and Ocean Engineering, edited by Kim, Y.C., 193-236, World Scientific Publishing Company, Toh Tuck Link, Singapore.
- Rabinovich, A.B. and S. Monserrat (1996), Meteorological tsunamis near the Balearic and Kuril Islands:descriptive and statistical analysis, *Nat. Hazards*, 13, 55-90.
- Rao, D.B. (1967), Response of a lake to a time-dependent wind stress, *J. Geophys. Res.*, 72(6), 1697–1708, doi:10.1029/JZ072i006p01697.
- Rao, D. B., C.H. Mortimer, and D.J. Schwab (1976), Surface normal modes of Lake Michigan: Calculations compared with spectra of observed water level fluctuations, *J. Phys. Oceanogr*, 6(4), 575–588. doi: 10.1175/1520-0485(1976)006<0575:SNMOLM>2.0.CO;2.

- Šepić, J., and A. B. Rabinovich (2014), Meteotsunami in the Great Lakes, Chesapeake Bay and on the Atlantic coast of the United States generated by the propagating 'derecho' of 29–30 June 2012, *Nat. Hazards*, *74*, 75–107, doi:10.1007/s11069-014-1310-5.
- Šepić, J., I. Vilibić, and D. Belušić (2009a), The source of the 2007 Ist meteotsunami (Adriatic Sea), *J. Geophys. Res.*, *114*, C03016, doi:10.1029/2008JC005092.
- Šepić, J., I. Vilibić, and S. Monserrat (2009b), Teleconnections between the Adriatic and the Balearic meteotsunamis, *Phys. Chem. Earth*, *34*, 928-937, doi:10.1016/j.pce.2009.08.007.
- Šepić, J., I. Vilibić, and N. Strelec Mahović (2012), Northern Adriatic meteorological tsunamis: Observations, link to the atmosphere, and predictability, *J. Geophys. Res.*, *117*, C02002, doi:10.1029/2011JC007608.
- Šepić, J., I. Vilibić, A. Lafon, L. Macheboeuf, and Z. Ivanović (2015a), High-frequency sea level oscillations in the Mediterranean and their connection to synoptic patterns, *Progress in Oceanography*, *137*, 284-298, doi:10.1016/j.pocean.2015.07.005.
- Šepić, J., I. Vilibić, A.B. Rabinovich, and S. Monserrat (2015b), Widespread tsunami-like waves of 23-27 June in the Mediterranean and Black Seas generated by high-altitude atmospheric forcing, *Scientific Reports*, *5*, 11682, doi:10.1038/srep11682.
- Tanaka, K. (2010), Atmospheric pressure-wave bands around a cold front resulted in a meteotsunami in the East China Sea in February 2009, *Nat. Hazards Earth Syst. Sci.*, *10*, 2599–2610, doi:10.5194/nhess-10-2599-2010.
- Tappin, D. R., A. Sibley, K. Horsburgh, C. Daubord, D. Cox, and D. Long (2013), The English Channel 'tsunami' of 27 June 2011 – a probable meteorological source, *Weather*, *68*, 144–152, doi: 10.1002/wea.2061.

- Vennell, R. (2007), Long barotropic waves generated by a storm crossing topography, *J. Phys. Oceanog.*, 37, 2809-2823, doi: <http://dx.doi.org/10.1175/2007JPO3687>.
- Vennell, R. (2010), Resonance and trapping of topographic transient ocean waves generated by a moving atmospheric disturbance, *J. Fluid Mech.*, 650, 427-442, doi:10.1017/S0022112009993739.
- Vilibić, I., N. Domijan, M. Orlić, N. Leder, and M. Pasarić (2004), Resonant coupling of a traveling air-pressure disturbance with the east Adriatic coastal waters, *J. Geophys. Res.*, 109, C10001, doi:10.1029/2004JC002279.
- Vilibić, I., S. Monserrat, A. B. Rabinovich, and H. Mihanović (2008), Numerical modelling of the destructive meteotsunami of 15 June, 2006 on the coast of the Balearic Islands, *Pure Appl. Geophys.*, 165, 2169–2195, doi:10.1007/s00024-008-0426-5.
- Vilibić, I., K. Horvath, N. Strelec Mahović, S. Monserrat, M. Marcos, Á. Amores, and I. Fine (2014a), Atmospheric processes responsible for generation of the 2008 Boothbay meteotsunami, *Nat. Hazards*, 74, 25–53, doi:10.1007/s11069-013-0811-y.
- Vilibić, I., H. Mihanović, and F. Charayre (2014b), Assessing meteotsunami potential of high-frequency air pressure oscillations observed in the middle Adriatic, *Nat. Hazards*, 74, 217-232, doi: 10.1007/s11069-013-0865-x.
- Vilibić, I., S. Monserrat, and A.R. Rabinovich (2014c), Meteorological tsunamis on the US East Coast and in other regions of the World Ocean, *Nat. Hazards*, 74, 1-9, doi:10.1007/s11069-014-1350-x.
- Vučetić, T., I. Vilibić, S. Tinti, and A. Maramai (2009), The Great Adriatic flood of 21 June 1978 revisited: An overview of the reports, *Phys. Chem. Earth*, 34, 894-903, doi: 10.1016/j.pce.2009.08.005.

- Wertman, C.A., R.M. Yablonsky, Y. Shen, J. Merrill, C.R. Kincaid, and R.A. Pockalny (2013), Mesoscale convective system surface pressure anomalies responsible for meteotsunamis along the U.S. East Coast on June 13th, 2013, *Scientific Reports*, 4, 7143 doi:10.1038/srep07143.
- Whitmore, P., and B. Knight (2014), Meteotsunami forecasting: Sensitivities demonstrated by the 2008 Boothbay, Maine, event, *Nat. Hazards*, 74, 11–23, doi:10.1007/s11069-014-1056-0.
- Workoff, T.E., D.A.R. Kristovich, N.F. Laird, R. LaPlante, and D. Leins (2012), Influence of the Lake Erie overlake boundary layer on deep convective storm evolution. *Weather Forecast.*, 27, 1279-1289. doi:10.1175/WAF-D-11-00076.1.

4. Regional Characteristics of Meteotsunamis in the Laurentian Great Lakes

The following is to be submitted to Geophysical Research Letters

4.1. Introduction

Meteotsunamis are water waves generated by perturbations in atmospheric pressure and wind [Monserrat *et al.*, 2006] and are similar to seismic tsunamis in both physical behavior and ability to cause disastrous effects to property and life [Nomitsu, 1935, Ewing *et al.*, 1954; Hibiya and Kajiura, 1982; Vilibić *et al.*, 2008; Haslett and Bryant, 2009; Orlić *et al.*, 2010; Cho *et al.*, 2013]. Individual large meteotsunamis have been investigated to understand the hydrodynamic processes of meteotsunamis [Vilibić *et al.*, 2004; 2008; 2010; Bechle and Wu, 2014; Anderson *et al.*, 2015] as well as the causative synoptic [Jansa *et al.*, 2007; Šepić *et al.*, 2008; 2015; Tanaka, 2012] and mesoscale atmospheric processes [Belušić *et al.*, 2007; Orlić *et al.*, 2010; Vilibić *et al.*, 2014]. While the study of individual events has revealed many detailed insights into meteotsunami causes and characteristics, the findings of episodic analyses may not be representative of the variety of possible meteotsunami conditions. Long-term water level records of up to 55 years at a single location have been examined to characterize site-specific occurrence statistics and the synoptic scale meteorological conditions typically associated with meteotsunamis at specific locations [Rabinovich and Monserrat, 1996; Šepić *et al.*, 2009b; 2012]. To evaluate meteotsunami events across a region, several studies have focused on identifying areas vulnerable to large meteotsunamis [Vilibić and Šepić, 2009; Šepić *et al.*, 2015a; 2015b] as well as the associated hydrodynamic [Pasquet and Vilibić, 2013] and atmospheric processes common to meteotsunamis in the region [Haslett *et al.*, 2009; Šepić *et al.*, 2009;

Pasquet et al., 2013; *Orlić et al.*, 2015]. To date, a comprehensive regional characterization of spatial patterns in meteotsunami occurrence, seasonality, and causes has yet to be carried out, particularly for the Laurentian Great Lakes region.

The characteristics of meteotsunamis can vary throughout a region due to local differences in climate and bathymetry, as meteotsunami formation is the result of interactions between an atmospheric disturbance and the water body [*Montserrat et al.*, 2006]. Meteotsunamis have been associated with the atmospheric pressure and wind perturbations of frontal passages [*Tanaka*, 2010], cyclones [*Mercer et al.*, 2002; *Pasquet et al.*, 2013], mesoscale convective systems [*Šepić and Rabinovich*, 2014; *Wertman et al.*, 2014], or atmospheric gravity waves [*Montserrat and Thorpe*, 1996; *Belušić et al.*, 2007]. The height of a meteotsunami wave can grow when the propagation speed of the atmospheric disturbance is approximately equal to the local free wave speed, which is dependent upon water depth for long waves [*Proudman*, 1929] and shelf slope for edge waves [*Greenspan*, 1956]. This hydrodynamic process, termed propagation resonance, allows atmospheric energy to constantly amplify the wave. Furthermore, meteotsunami heights can increase at the coast through local amplification mechanisms such as shoaling, shelf resonance, and harbor resonance [*Rabinovich*, 2009]. Long-term analysis of meteotsunami characteristics over a region may thereby shed light on the hydrodynamic and atmospheric conditions salient to meteotsunami generation in the region.

The Laurentian Great Lakes is a region with a long history of impactful meteotsunami events. As illustrated in Figure 4-1, numerous damaging or deadly meteotsunamis have been reported in each of the Great Lakes [*Ewing et al.*, 1954; *Donn et al.*, 1959; *Murty and Freeman*, 1973; *Chaston*, 1979; *Šepić and Rabinovich*, 2014; *Anderson et al.*, 2015] (*see Appendix A Table A1 for tabulated list of historic events reported in the literature and news articles*), with most

reported meteotsunamis near densely populated areas in the southern Great Lakes. It remains unclear whether this spatial distribution is representative of meteotsunamis in the Great Lakes or if it reflects a reporting bias towards population centers. Alternatively, the distribution of meteotsunami events may be the result of spatial variations in the physical features of the lake basins (i.e. locations, sizes, shape, water depths) and the storm climate of the region. As seen in Figure 1, bathymetry varies throughout the region in terms of both water depth and shelf slope. Convective storms, particularly strong storms, occur most frequently over the southern portion of the Great Lakes (Michigan and Erie) [Kelley *et al.*, 1985; Johns and Hirt 1987; Ashley *et al.*, 2005]. The greatest number of cyclones occur in the north-central portion of the Great Lakes (Michigan and Huron) [Angel, 1996] whereas frontal passages peak over the eastern lakes (Ontario and Erie) [Payer *et al.*, 2011]. Statistical analysis of long-term water level and radar data in the Lake Michigan basin has revealed spatial variations in seasonal occurrence and the associated storm structures throughout the lake [Bechle *et al.*, 2015]. To date, the meteotsunami occurrences and causes across the other Great Lakes basins have yet to be investigated to examine potential spatial patterns in meteotsunami characteristics throughout the region.

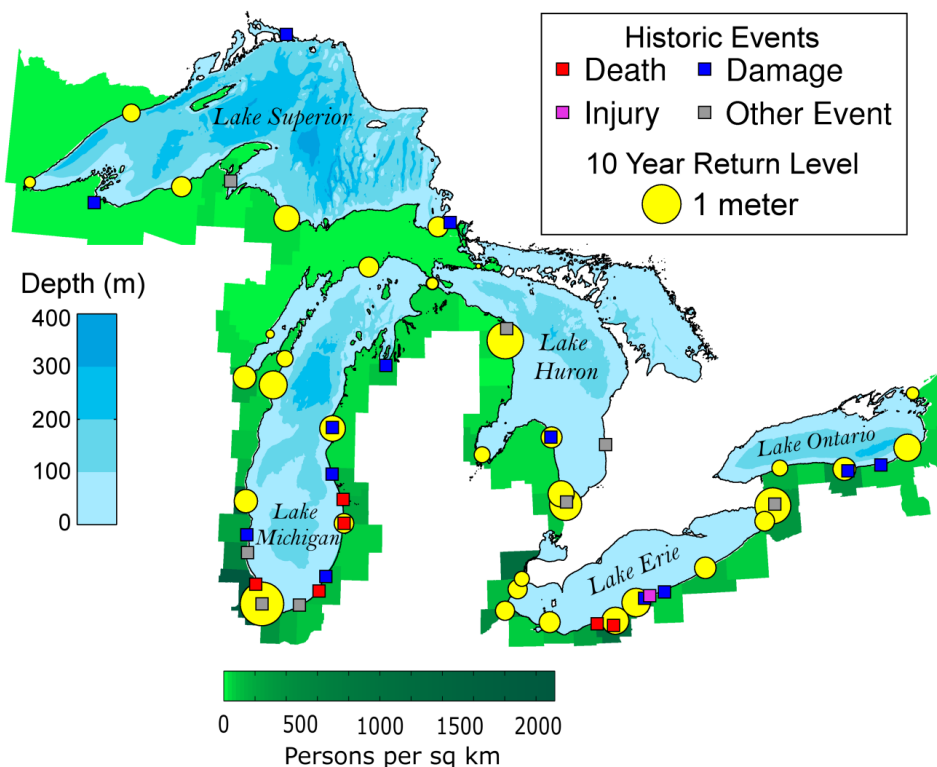


Figure 4-1: Map of Great Lakes meteotsunamis. Historic meteotsunami events from the literature and news reports are classified by impact. Meteotsunami 10-year return levels are calculated from fitting the Pareto Type 1 distribution to waves observed in NOAA/NOS water level records and plotted as scaled circles at the each station location. Also depicted are lake bathymetry contours and county-level population density.

The objective of this paper is to characterize regional patterns in Great Lakes meteotsunami magnitude, temporal occurrence, and causative storms. Water level and radar records are analyzed to quantify meteotsunami return levels, seasonal and annual distributions, and associated storm structure types. Great Lakes-wide patterns in meteotsunami characteristics are analyzed in the context of the physical and atmospheric settings of the region. Meteotsunami characteristics are also compared on a lake-by-lake basis to reveal similarities and differences in meteotsunami occurrence and causes between each of the lakes. The results of this study provide insight into the role physical features and storm climate have on the regional meteotsunami

characteristics of the Laurentian Great Lakes. Furthermore, the characterization of meteotsunamis at the regional scale would facilitate the comparison of meteotsunami climates throughout the world to identify areas which are most vulnerable to the meteotsunami threat.

4.2. Methods

Long-term water level data is obtained from 31 monitoring stations operated on the Great Lakes by the National Oceanic and Atmospheric Administration (NOAA) National Ocean Service (NOS), with gauge locations illustrated by yellow circles in Figure 1. Each station provides 6-minute water level records with an average record length of 17 years. The water level time series are high-pass filtered with a cutoff period of 6 hours [Rabinovich and Monserrat, 1996] and individual waves are identified using the zero-crossing method [Demirbilek and Vincent, 2002].

A Peaks Over Threshold (POT) approach of extreme value statistics is used to represent the meteotsunami size-frequency data [Bechle *et al.*, 2015]. Wave heights which exceed a station-specific height threshold x_m are fit to the Pareto Type 1 (PT1) distribution [Coles, 2001; Geist and Parsons, 2014] which is described by the shape parameter β . To establish x_m , a failure-to-reject method is employed by sorting the height observations and deleting the lowest value observations until the distribution is no longer rejected by the Anderson-Darling test ($\alpha = 0.1$) [Choulakian and Stephens, 2001]. Meteotsunami event probabilities are represented in terms of mean recurrence intervals (RI), the inverse of which expresses the probability that a specified return level (RL) magnitude will be exceeded in any one year.

NEXRAD base reflectivity radar imagery analysis is used to classify the structure of storms associated with meteotsunami events greater than the 1 year return level at each station.

Storms are classified as one of seven categories: convective cluster, convective complex, linear convection, bow convection, extratropical cyclone, frontal, or atmospheric gravity wave [Fowle and Roebber, 2003; Gallus *et al.*, 2008; Kunkel *et al.*, 2012; Workoff *et al.*, 2012]. Detailed descriptions of the criteria used to classify storm structures are given in *Bechle et al.* [2015].

Regional meteotsunami characteristics (occurrences, sizes, and causes) are analyzed using two approaches. First, a Great Lakes basin-wide analysis is employed that aggregates the observed meteotsunami characteristics from all water level stations in the region. Linear regression analysis [Seber and Lee, 2003] is used to examine relationships between these meteotsunami characteristics (response variables) versus the physical features and atmospheric storm occurrences at the station location (explanatory variables). Specifically, the response variables used are 10 year return level, mean month of occurrence, the fraction of events associated with a linear storm structures, and fraction of events associated with a convective complex storm structures. Explanatory variables include the physical location, bathymetry, and frequency of storm occurrence at each gauge stations. The location of each station is represented by the latitude, longitude, and relative location along each lake's major axis. Similar to fetch for wind waves, the location along the lake axis is quantified as the distance a station is from the eastern (for east-west orientation) or northern (for north-south orientation) end of the lake divided by the length of the major axis of the lake. The bathymetry at each station is defined by both the depth of the lake sub-basin the station is located in as well as the bottom slope along the coast, calculated at 20 km offshore. Convective storm environment is represented by the annual frequency of strong thunderstorms wind gusts in excess of 28.5 m/s [Kelley *et al.*, 1985]; other measures of convective storm occurrence were also considered, including lightning strikes [Zajac *et al.*, 2001] and average annual days with severe thunderstorm potential [Brooks *et al.*,

2003]. Similarly, the frontal-type storm environment at each station is quantified from contours of cyclone storm counts composed by Angel [1996]. The Pearson correlation coefficient is used as a measure of the degree of linear relationship between response and explanatory variables. Linear relationships are considered statistically significant at the $\alpha = 0.05$ level. To check relationships against the influence of outliers, regressions are calculated both with and without outliers, which are defined in this study as data points with a Cook's distance which exceeds three times the mean Cook's distance. Relationships which are not statistically significant upon removal of outliers are not considered for further analysis.

Second, a lake-by-lake comparison is conducted where the identified meteotsunami events are aggregated for each individual lake to compare distributions of meteotsunami size, occurrence, and cause between the lakes. To address concerns with treating a meteotsunami which impacts multiple stations as numerous independent events, meteotsunamis that occurred in the same lake within the same 12 hour period are consolidated to a single event represented by the largest wave [Bechle *et al.*, 2015]. Meteotsunami magnitude data for each lake are fit with the Pareto Type 1 distribution to establish event size return levels. The seasonal distribution of meteotsunami events is calculated by binning the identified events by month, with a meteotsunami season defined as the consecutive three month period which experiences the largest number of meteotsunamis. Annual distributions of meteotsunami occurrences are obtained by binning events by year. The fraction of events associated with each storm structure is also calculated on a lake-by-lake basis.

4.3. Results

4.3.1. Great Lakes Basin-Wide Characteristics

Figure 1 shows the 10-year return levels of meteotsunami magnitude calculated at each station (as a yellow circle scaled by return level magnitude). Calumet Harbor, IL in Lake Michigan has the largest return level (1.2 m). Other stations with large 10-year return levels are Alpena, MI in Lake Huron (0.98 m), Buffalo, NY in Lake Erie (0.88 m). The mean month of meteotsunami occurrence is between April and August for all but three stations (Appendix A Figure A1). Convective storm structures are the dominant atmospheric cause of meteotsunamis at each station and are associated with 78% of the events overall (see Appendix A Figure A2). Overall, complex (39%) and linear (33%) convective storm structures are the two most common storm structures (see supplemental material in Appendix A Figure A3 and Figure S4, respectively). Linear regressions are fit between the meteotsunami characteristics at each station (response variables) and explanatory physical and atmospheric variables of the water level stations, with the associated Pearson correlation coefficient for each regression is given in Table 4-1. Significant linear relationships ($\alpha=0.05$) are highlighted in bold in Table 1 and discussed in the following.

Table 4-1: Pearson correlation coefficients of the linear regressions between meteotsunami characteristics (columns) and parameters which describe of the physical and atmospheric settings of each station (rows). Linear trends that are significant at the 95% level are in bold.

	10 Year Return Level	Mean Month	Convective Storm Events	Linear Storm Events	Complex Storm Events
Latitude	-0.30	-0.19	-0.11	-0.30	0.24
Longitude	-0.03	0.36	-0.11	0.54	-0.51
Lake Axis Pos.	0.41	0.32	0.01	0.36	-0.21
Depth of Basin	0.01	-0.32	-0.02	-0.28	0.35
Shelf Slope	-0.05	-0.41	-0.04	-0.08	0.19
T-Storm Freq.	0.28	0.11	0.32	0.11	0.15
Cyclone Freq.	0.12	-0.41	-0.04	-0.49	0.13

The 10 year return level has a positive relationship with the relative location of a station along the lake's major axis ($r = 0.41$, $p = 0.024$, Figure 4-2a). This relationship indicates that meteotsunamis tend to be larger for the eastern-most stations of east-west oriented lakes (Superior, Erie, Ontario) and the southern-most stations of north-south oriented lakes (Michigan, Huron). For east-west oriented lakes, meteotsunami size growth eastward along the major axis of the lake is consistent with the prevailing storm direction in the region, which has a significant easterly component for both convective storms [Johns and Hirt, 1987; Graham, 2004] and cyclones [Angel, 1996]. Indeed, as a storm propagates along a water body, the meteotsunami wave amplification from propagation resonance grows with the distance traveled [Hibiya and Kajiura, 1982; Greenspan, 1956]. Thus, based on propagation resonance mechanisms, water level stations in the leeward direction of storm propagation would be expected to experience larger meteotsunamis, consistent with the observed relationship.

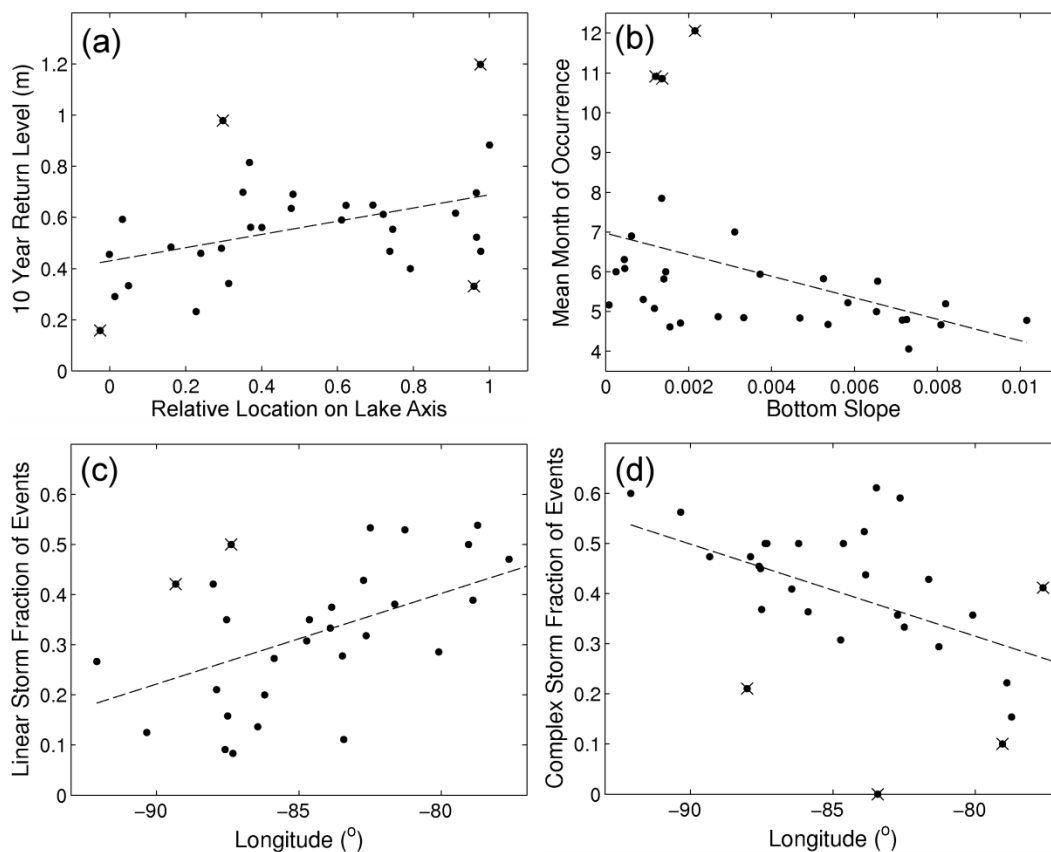


Figure 4-2: Scatterplots of (a) lake axis location vs 10 year return level, (b) bottom slope vs mean month of occurrence, (c) longitude vs the fraction of events associated with linear storms, and (d) longitude vs the fraction of events associated with complex convective storms. The observed data from each station are plotted as dots (●), the regression line as a dashed line (---). Identified outliers are denoted with a cross (x) but remain included in the regressions.

The mean month of meteotsunami occurrence has a negative relationship with lake bottom slope ($r = -0.41$, $p = 0.024$, Figure 4-2b). This relationship indicates that meteotsunamis tend to occur earlier in the year at water level stations which are located on steeper bottom slopes. In terms of meteotsunami mechanisms, as bottom slope increases, the speed at which edge waves travel along the shoreline also increases [Ursell, 1952]. In turn, propagation resonance of edge waves over steeper bottom slopes requires faster storm propagation speeds [Greenspan, 1956]. Thus, meteotsunamis tend to occur earlier in the year at locations where

faster moving storms are likely to cause propagation resonance. Indeed, cloud level winds (300 mb to 850 mb), which are positively related to convective storm speed [Corfidi et al., 1996], tend to be greatest early in the year and decrease to a minimum in the mid-summer according to observed Great Lakes-region upper air sounding climatologies compiled by the NOAA Storm Prediction Center. Thus, variations in the monthly occurrence of meteotsunamis in the Great Lakes region may be explained by the propagation resonance characteristics of local bathymetry and seasonal patterns in storm speed.

The fraction of events which are associated with linear storm structures has a positive relationship with the longitude of the water level station ($r = 0.54$, $p = 0.002$, Figure 4-2c) and a negative relationship with cyclone frequency at the water level station ($r = -0.49$, $p = 0.006$, not shown for brevity). Thus, meteotsunamis tend to be associated with a greater fraction of linear storms in the eastern portion of the Great Lakes as well as in areas where cyclone frequencies decrease. The fraction of events associated with complex convective storm structures has a negative relationship with the longitude of the water level station ($r = -0.51$, $p = 0.003$, Figure 4-2d). While studies which compare linear and complex storms at the sub-regional scale are rare, the distribution of linear-type and complex-type storms through the Great Lakes region provide insight into these relationships. Contours of mesoscale convective complex activity vary longitudinally across the Great Lakes with peak activity in the west [Ashley et al., 2003]. On the other hand, derechos, which are intense convective windstorms that are typically arranged in a linear manner, have a primarily latitudinal variation in activity across the Great Lake, with peak activity located to the south [Ashley and Mote, 2005]. Thus, spatial variations in mesoscale convective complex activity may explain the longitudinal patterns in linear and complex storm structures associated with meteotsunamis in the Great Lakes.

4.3.2. Lake-by-Lake Comparisons

Meteotsunami size-frequency distributions for each lake are shown in Figure 4-3. Overall, Lake Michigan experiences the largest meteotsunamis with a 10 year return level of 1.3 m. Lakes Superior and Ontario experience the smallest meteotsunamis, with 10 year return levels of 0.65 m and 0.70 m, respectively. Lakes Erie and Huron have nearly identical 10-year return levels at 0.96 m and 0.98 m, respectively, though the distribution of Lake Huron meteotsunami sizes is more tail-weighted. This difference is evident in the shape parameter β at each lake, which is inversely related to the in growth of return level [*Geist and Parsons, 2014*]. Amongst the five lakes, Lake Erie has the least tail-weighted distribution of meteotsunami heights ($\beta = 6.5$) whereas Lake Huron has the most tail-weighted distribution ($\beta = 4.2$). A similar difference can also be seen between the distributions of Lake Superior ($\beta = 6.1$) and the less tail-weighted Lake Ontario ($\beta = 5.0$).

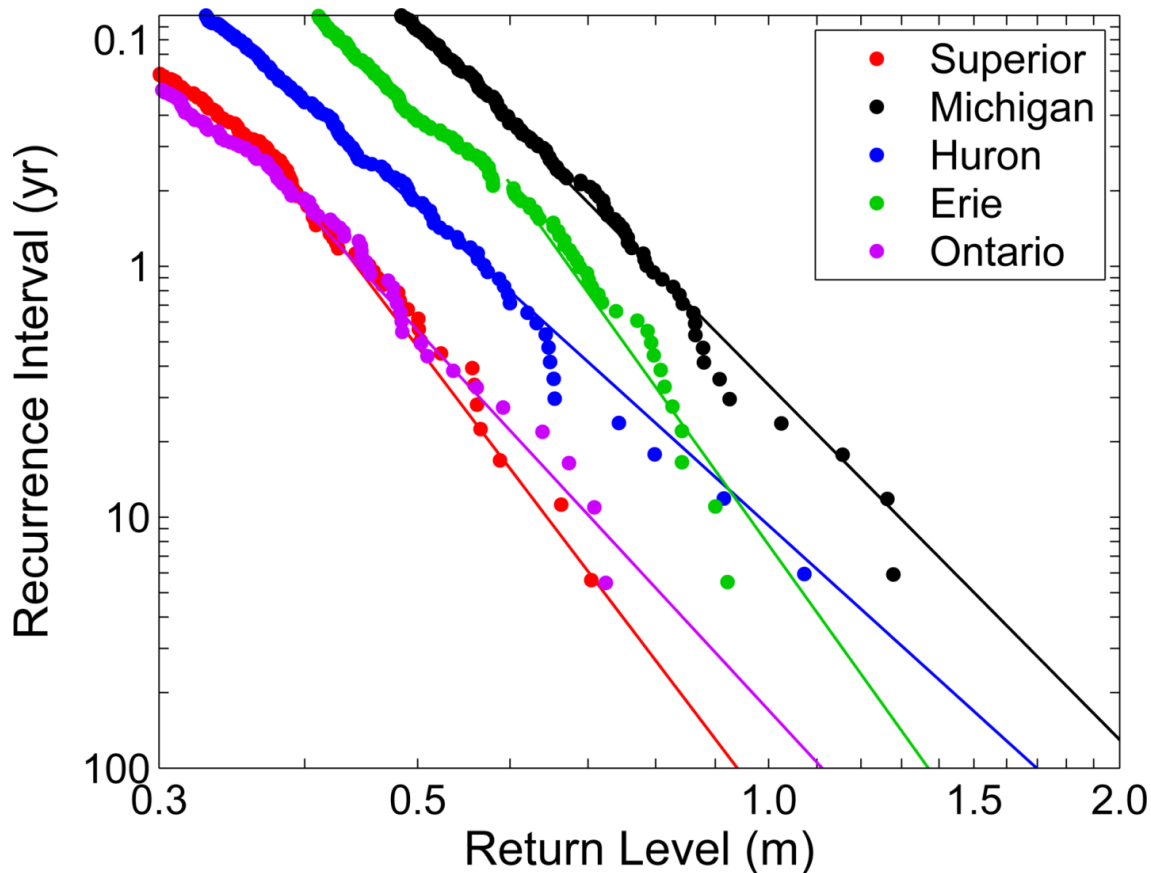


Figure 4-3: Lake-wide meteotsunami height observations (dots) fit with the Pareto Type 1 distribution (solid line).

The monthly distribution of meteotsunami occurrences in the Great Lakes is illustrated in Figure 4-4a-f. Great Lakes meteotsunami occurrences as a whole rise sharply in April, reach a maximum in May, and gradually decrease in frequency until October, yielding a peak three month season of April, May, and June. Meteotsunamis in Lake Michigan were revealed by *Bechle et al.* [2015] to occur primarily in the spring and early summer (April, May, and June). Lakes Huron and Ontario exhibit similar seasonality as Lake Michigan (April, May, June). Lake Superior meteotsunamis occur later in the year (May, June, July), with a peak in June. Of all the Great Lakes, meteotsunamis in Lake Erie occur latest in the year (May, June, July) with maxima in June and July. Interestingly, Lakes Michigan, Huron, and Ontario, which

share a peak three month meteotsunami season, also have similar average depths (85 m, 59 m, and 86 m) when compared with Lake Superior (147 m) and Lake Erie (19m). Thus, similar to the results of the Great Lakes-basin wide regression analysis, bathymetry may be associated with the monthly occurrence of meteotsunamis.

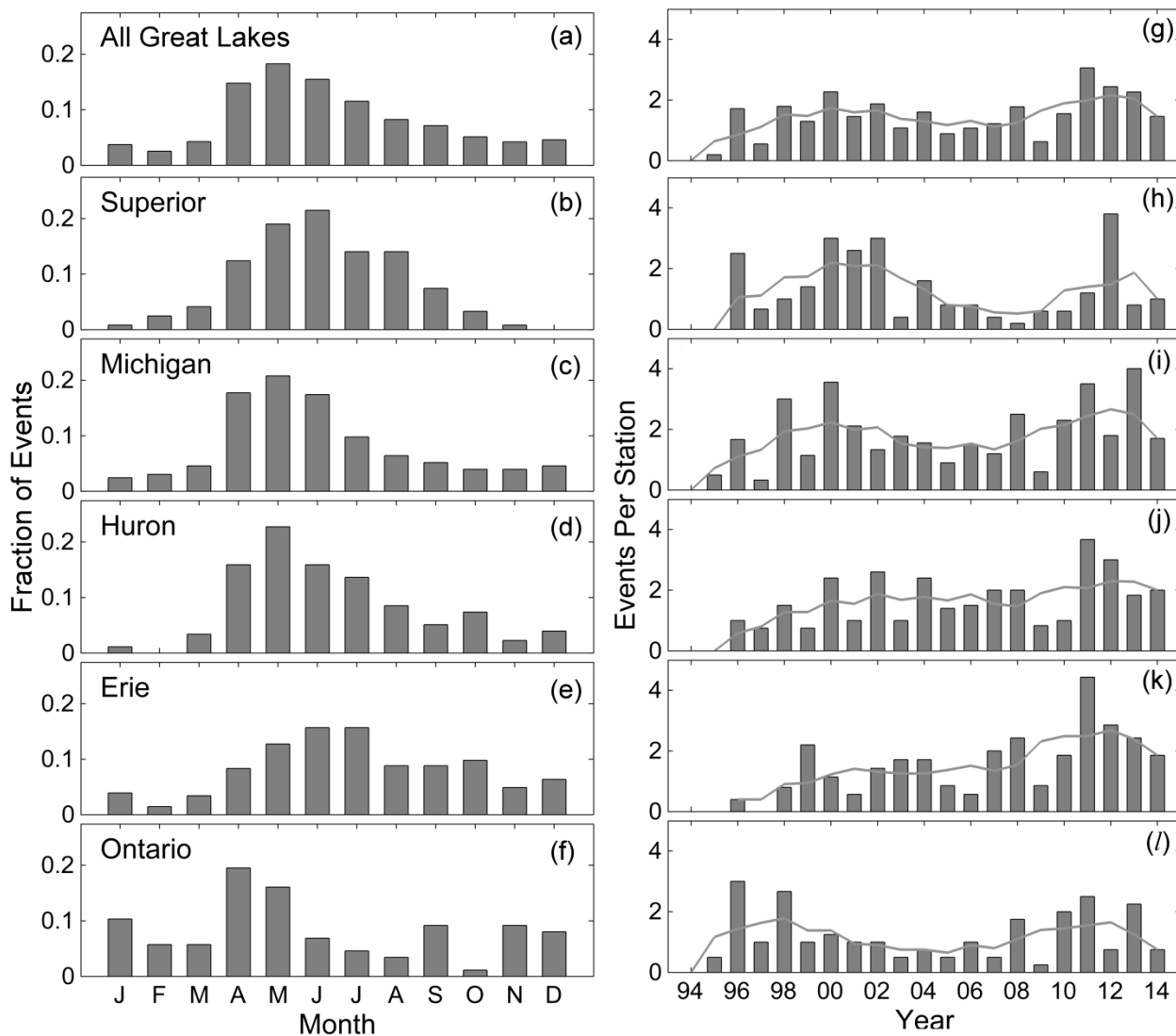


Figure 4-4: (a)-(f) Monthly distributions of meteotsunamis observed in each lake. (g)-(l) Annual distribution of meteotsunamis observed in each lake, normalized for the number of stations operational in each year. A five year moving average in annual meteotsunami occurrences is also plotted.

The annual distribution of meteotsunami events is illustrated for each lake in Figure 4-4f. For all lakes, individual years with the greatest number of meteotsunami are between 1996 to 2002 and 2011 to 2013. A five-year moving average is calculated to visualize longer-term trends. For the entire Great Lakes as a whole, there is a bimodal annual distribution with local maxima in five-year moving average at 2000 and 2012 and a local minima at 2006. Lakes Superior, Michigan, and Ontario all have a bimodal distributions in the five-year moving average of annual occurrence, with a shared local maxima in 2012, another local maxima in 2000, 2000, and 1998, respectively, and a local minima in 2008, 2007, and 2005, respectively. Lakes Huron and Erie have maxima in the five year moving average of annual occurrence in 2012. The source of these annual variations in meteotsunami occurrences is yet unknown, as the temporal trends are not correlated well with climactic oscillations such as the El Nino Southern Oscillation, Pacific Decadal Oscillation, or the North Atlantic Oscillation. In general, frequent meteotsunami activity occurred in the Great Lakes in the late 1990s to early 2000s, decreased through the mid to late 2000s, and increased again in the 2010s.

The storm types associated with meteotsunamis classified for each lake are illustrated in Figure 4-5. For all lakes, convective storm structures are associated with at least 70% of meteotsunamis. Lake Superior meteotsunamis has the largest portion of convective structures (87%). Convective complexes are associated with the greatest number of meteotsunamis for all lakes except for Lake Ontario, where linear structures are associated with nearly 43% of the meteotsunamis. This lake-by-lake comparison agrees with the longitudinal pattern in storm structures observed in the Great Lakes-wide regression analysis. For non-convective events, the fraction of meteotsunamis associated with frontal storms is the greatest in Lake Ontario, which also has been observed to experience the largest density of frontal passages among the five lakes

[Payer et al., 2011]. Lakes Michigan and Huron experience the greatest fraction of events associated with cyclones, consistent with peaks in the frequency of strong cyclones over the Great Lakes [Angel et al., 1996]. Atmospheric gravity waves in the absence of convective or frontal systems are a minor contributor to Great Lakes meteotsunamis, consistent with *Bechle et al.*, [2015]. Overall, meteotsunamis in the Great Lakes are primarily associated with complex and linear convective storm structures, with a secondary contribution from frontal-type structures.

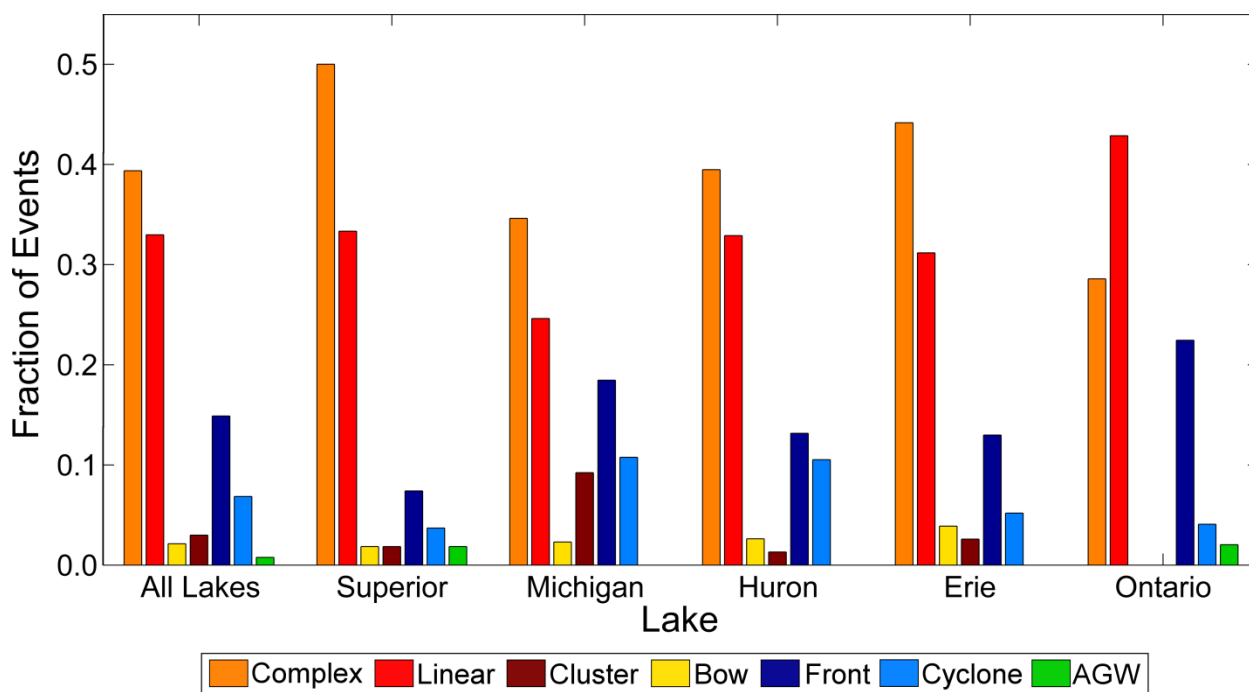


Figure 4-5: Distribution of storm structures associated with meteotsunamis which exceed the 1-year return level, with warm colors (red, orange, and yellow) representing convective structures, cool colors (blues) representing frontal-type structures, and green representing atmospheric gravity waves.

4.4. Discussion and Conclusions

Regional analysis of Laurentian Great Lakes water level records and radar data reveal that meteotsunamis in generally occur from the late-spring to mid-summer and are associated primarily with convective storms. Regional patterns in meteotsunami magnitude, season, and causative storms are examined with both a Great Lakes-wide regression analysis and a lake-by-lake comparison. Across the region, meteotsunami height tends to increase along the major axis of the lake in the leeward direction of storm propagation, consistent with the propagation resonance mechanism in which amplification grows with the distance traveled by the wave [Greenspan, 1956; Hibiya and Kajiura, 1982]. The monthly distribution of meteotsunamis is found to be negatively related with lake bottom slope in the regression analysis. In a lake-by-lake perspective, similarities in the seasonal distribution of meteotsunamis were found between lakes with comparable average depths. As bottom slope and water depth dictate propagation speed for edge [Greenspan, 1956] and long waves [Proudman, 1929], respectively, these relationships suggest that the seasonal distribution of meteotsunamis may be related to the resonance characteristics of the water body. Linear and complex convective storms are the dominant storm structures associated with meteotsunamis in the Great Lakes. The role of complex convective storms tends to increase westward across the region whereas the role of linear storms decreases along the same direction. This pattern is consistent with longitudinal variations in mesoscale convective complex storms across the region [Ashley et al, 2003].

Interestingly, while meteotsunamis in the Great Lakes are strongly connected with convective storms, the peak season for meteotsunami occurrence in the Great Lakes precedes that of the mid-summer peak in convective activity [Kelley et al., 1985]. Bechle et al. [2015] noted that the late-spring to early summer meteotsunami seasonality in Lake Michigan

corresponded well with the occurrence of the strongly-stable overlake boundary layer [Graham, 2004; Workoff *et al.*, 2012], though a mechanistic connection of boundary layer physics to meteotsunami formation was unclear. Analysis of meteotsunamis in the Great Lakes at the regional scale has revealed another possible explanation for this disconnect between peak meteotsunami and convective activity. Both the positive relationship between monthly occurrence of meteotsunamis and lake bottom slopes as well as shared meteotsunami seasonality for lakes of similar depth suggest that the propagation resonant characteristics of the lake may control the seasonal occurrence of meteotsunamis. While convective activity may peak in the mid-summer, storm speeds in the late-spring and early summer may be more conducive to propagation resonance with Great Lakes bathymetry than storm speeds in the mid-summer. Further study into the storm velocities of meteotsunami-causing storms compared with null cases which do not cause meteotsunamis is needed to address this relationship in detail. Overall, the regional-scale analysis of meteotsunamis in the Great Lakes reveals valuable insight into the role of physical and atmospheric setting on meteotsunami occurrence which can be useful to identify both the times and locations which may be most vulnerable to destructive meteotsunami events.

4.6. References

- Anderson, E.J., Bechle, A.J., Wu, C.H., Schwab, D.J., Mann, G.E., and Lombardy, K.A. (2015a), Reconstruction of a meteotsunami in Lake Erie on 27 May 2012: Roles of atmospheric conditions on hydrodynamic response in enclosed basins. *J. Geophys. Res. Oceans*. Accepted Author Manuscript, doi: 10.1002/2015JC010883.

- Angel, J.R. (1996), Cyclone climatology of the Great Lakes, *Misc. Publ. 172*, Midwestern Climate Center and Illinois State Water Survey, Champaign, IL.
- Ashley, W.S., and Mote, T.L. (2005), Derecho hazards in the United States, *Bull. Amer. Meteor. Soc.*, 86, 1577–1592, doi: 10.1175/BAMS-86-11-1577.
- Ashley, W.S., T.L. Mote, P.G. Dixon, S.L. Trotter, E.J. Powell, J.D. Durkee, and A.J. Grundstein, Distribution of mesoscale convective complex rainfall in the United States, *Monthly Weather Review*, 131, 3003-3017.
- Bechle, A. J., and C. H. Wu (2014), The Lake Michigan meteotsunamis of 1954 revisited, *Nat. Hazards*, 74, 155–177, doi:10.1007/s11069-014-1193-5.
- Bechle, A. J., Kristovich, D. A.R. and Wu, C. H. (2015), Meteotsunami occurrences and causes in Lake Michigan. *J. Geophys. Res. Oceans*. Accepted Author Manuscript. doi:10.1002/2015JC011317
- Belušić, D., B. Grisogono, and Z. B. Klaić (2007), Atmospheric origin of the devastating coupled air-sea event in the east Adriatic, *J. Geophys. Res.*, 112, D17111, doi:10.1029/2006JD008204.
- Brooks, H.E., J.W. Lee, and J.P. Craven (2003) The spatial distribution of severe thunderstorm and tornado environments from global reanalysis data. *Atmos. Res.*, 67–68, 73–94.
- Chaston, P.R. (1979) An unusual weather phenomenon: The Rochester Seiche, *Weatherwise*, 32(5), 211.
- Cho, K.-H., J.-Y. Choi, K.-S. Park, S.-K. Hyun, Y. Oh, and J.-Y. Park (2013), A synoptic study on tsunami-like sea level oscillations along the west coast of Korea using an unstructured-grid ocean model, *J. Coastal Res.*, 65, 678–683.

- Choulakian, V., and M. Stephens (2001), Goodness-of-fit test for the generalized Pareto distribution, *Technometrics*, 43, 478–485.
- Coles, S. (2001), *An Introduction to Statistical Modelling of Extreme Values*. Springer-Verlag, London.
- Demirbilek, Z., and C.L. Vincent (2002), Water Wave Mechanics, in *Coastal Engineering Manual, Part II, Hydrodynamics, Chapter II-2, Engineer Manual 1110-2-1100*, edited by L. Vincent and Z. Demirbilek, U.S. Army Corps of Engineers, Washington, D.C.
- Donn, W. L. (1959), The Great Lakes storm surge of May 5, 1952, *J. Geophys. Res.*, 64(2), 191–198, doi:10.1029/JZ064i002p00191.
- Donn, W.L., and M. Ewing (1956), Stokes' edge waves in Lake Michigan, *Science*, 124, 1238–1242, doi: 10.1126/science.124.3234.1238.
- Ewing, M., F. Press, and W. J. Donn (1954), An explanation of the Lake Michigan wave of 26 June 1954, *Science*, 120, 684–686, doi:10.1126/science.120.3122.684.
- Fowle, M. A., and P. J. Roebber (2003), Short-range (0–48 h) numerical prediction of convective occurrence, mode, and location, *Weather Forecast.*, 18, 782–794, doi10.1175/1520-0434(2003)018<0782:SHNPOC>2.0.CO;2.
- Gallus, W. A., Jr., N. A. Snook, and E. V. Johnson (2008), Spring and summer severe weather reports over the Midwest as a function of convective mode: A preliminary study. *Weather Forecast.*, 23, 101–113, doi: 10.1175/2007WAF2006120.1.
- Geist, E.L., and T. Parsons (2014), Undersampling power-law size distributions: effect on the assessment of extreme natural hazards, *Nat. Hazards*, 72, 565-595, doi: 10.1007/s11069-013-1024-0.

- Geist EL, U.S. ten Brink, and M. Gove (2014), A framework for the probabilistic analysis of meteotsunamis. *Nat. Hazards*, 74(1), 123-142, doi: 10.1007/s11069-014-1294-1.
- Graham, R., M. Bentley, J. Sparks, B. Dukesherer, and J. Evans (2004), Lower Michigan MCS climatology: Trends, patterns types, and marine layer impacts, paper presented at 22nd Conference on Severe Local Storms, Amer. Meteor. Soc., Hyannis, MA.
- Greenspan, H. P. (1956), The generation of edge waves by moving pressure disturbances, *J. Fluid Mech.*, 1, 574–592.
- Haslett, S.K., H.E. Mellor, and E.A. Bryant (2009), Meteo-tsunami hazard associated with summer thunderstorms in the United Kingdom, *Phys. Chem. Earth*, 34, 1016-1022, doi: 10.1016/j.pce.2009.10.005.
- Hibiya, T., and K. Kajiura (1982), Origin of the Abiki phenomenon (a kind of seiche) in Nagasaki Bay, *J. Oceanogr. Soc. Jpn.*, 38, 172–182, doi:10.1007/BF02110288.
- Jansa, A., S. Monserrat, and D. Gomis (2007), The rissaga of 15 June 2006 in Ciutadella (Menorca), a meteorological tsunami, *Advances in Geosciences*, 12, 1-4.
- Johns, R.H., and W.D. Hirt (1987), Derechos: Widespread Convectively Induced Windstorms. *Wea. Forecasting*, 2, 32–49, doi: 10.1175/1520-0434(1987)002<0032:DWCIW>2.0.CO;2.
- Kelly, D.L., J. T. Schaefer, and C.A. Doswell (1985), Climatology of nontornadic severe thunderstorm events in the United States, *Monthly Weather Review*, 113, 1997-2014.
- Kunkel, K.E., D.R. Easterling, D.A.R. Kristovich, B. Gleason, L. Stoecker, and R. Smith (2012), Meteorological Causes of the Secular Variations in Observed Extreme Precipitation Events for the Conterminous United States, *J. Hydrometeorol*, 13, 1131–1141, doi: 10.1175/JHM-D-11-0108.1.

- Mercer, D., J. Sheng, R. J. Greatbatch, and J. Bobanović (2002), Barotropic waves generated by storms moving rapidly over shallow water, *J. Geophys. Res.*, *107*(C10), 3152, doi:10.1029/2001JC001140.
- Monserrat S., A. Ibberson, and A.J. Thorpe (1991), Atmospheric gravity waves and the “rissaga” phenomenon, *Q. J. Roy. Meteorol. Soc.*, *117*, 553–570.
- Monserrat, S., I. Vilibić, and A. B. Rabinovich (2006), Meteotsunamis: Atmospherically induced destructive ocean waves in the tsunami frequency band, *Nat. Hazards Earth Syst. Sci.*, *6*, 1035–1051, doi:10.5194/nhess-6-1035-2006.
- Murty, T. S., and N.G. Freeman (1973), Applications of the concepts of edge waves and numerical modelling to storm surge studies on Lake Huron, in Proc., 16th Conf. Great Lakes Research, pp. 533-548, Intl. Association of Great Lakes Research, Ann Arbor, Michigan.
- Nomitsu, T. (1935), A theory of tsunamis and seiches produced by wind and barometric gradient, *Mem. Coll. Sci. Imp. Univ. Kyoto A*, *18*(4), 201–214.
- Orlić, M., D. Belušić, I. Janeković, and M. Pasarić (2010), Fresh evidence relating the great Adriatic surge of 21 June 1978 to mesoscale atmospheric forcing, *J. Geophys. Res.*, *115*, C06011, doi:10.1029/2009JC005777.
- Orlić, M. (2015), The first attempt at cataloguing tsunami-like waves of meteorological origin in Croatian coastal waters, *Acta Adriatica*, *56*(1), 83-96.
- Pasquet, S., and I. Vilibić (2013), Shelf edge reflection of atmospherically generated long ocean waves along the central U.S East Coast, *Cont. Shelf Res.*, *66*, 1–8, doi:10.1016/j.csr.2013.06.007.

- Pasquet, S, I. Vilibić, and J. Šepić (2013), A survey of strong high-frequency sea level oscillations along the U.S. East Coast between 2006 and 2011, *Nat. Hazards Earth Syst. Sci.*, *13*, 473–482, doi:10.5194/nhess-13-473-2013.
- Payer, M., N.F. Laird, R.J. Maliawco, and E.G. Hoffman (2011), Surface fronts, troughs, and baroclinic zones in the Great Lakes Region, *Weather and Forecasting*, *26*, 555-563.
- Proudman, J. (1929), The effects on the sea of changes in atmospheric pressure, *Mon. Not. R. Astron. Soc.*, *2*, 197–209.
- Rabinovich, A.B. (2009), Seiches and harbor oscillations, in *Handbook of Coastal and Ocean Engineering*, edited by Kim, Y.C., 193-236, World Scientific Publishing Company, Tuck Link, Singapore.
- Rabinovich, A.B. and S. Monserrat (1996), Meteorological tsunamis near the Balearic and Kuril Islands: descriptive and statistical analysis, *Nat. Hazards*, *13*, 55-90.
- Seber, G.A.F. and A.J. Lee (2003), *Linear Regression Analysis*, Second Edition, John Wiley, Hoboken, N. J., doi: 10.1002/9780471722199.
- Šepić, J., and A. B. Rabinovich (2014), Meteotsunami in the Great Lakes, Chesapeake Bay and on the Atlantic coast of the United States generated by the propagating 'derecho' of 29–30 June 2012, *Nat. Hazards*, *74*, 75–107, doi:10.1007/s11069-014-1310-5.
- Šepić, J., M. Orilić, and I. Vilibić (2008) The Bakar Bay seiches and their relationship with atmospheric processes, *Acta Adriatica*, *49*(2), 107-123.
- Šepić, J., I. Vilibić, and D. Belušić (2009a), The source of the 2007 Ist meteotsunami (Adriatic Sea), *J. Geophys. Res.*, *114*, C03016, doi:10.1029/2008JC005092.
- Šepić, J., I. Vilibić, and S. Monserrat (2009b), Teleconnections between the Adriatic and the Balearic meteotsunamis, *Phys. Chem. Earth*, *34*, 928-937, doi:10.1016/j.pce.2009.08.007.

- Šepić, J., I. Vilibić, and N. Strelec Mahović (2012), Northern Adriatic meteorological tsunamis: Observations, link to the atmosphere, and predictability, *J. Geophys. Res.*, *117*, C02002, doi:10.1029/2011JC007608.
- Šepić, J., I. Vilibić, A. Lafon, L. Macheboeuf, and Z. Ivanović (2015a), High-frequency sea level oscillations in the Mediterranean and their connection to synoptic patterns, *Progress in Oceanography*, *137*, 284-298, doi:10.1016/j.pocean.2015.07.005.
- Šepić, J., I. Vilibić, A.B. Rabinovich, and S. Monserrat (2015b), Widespread tsunami-like waves of 23-27 June in the Mediterranean and Black Seas generated by high-altitude atmospheric forcing, *Scientific Reports*, *5*, 11682, doi:10.1038/srep11682.
- Tanaka, K. (2010), Atmospheric pressure-wave bands around a cold front resulted in a meteotsunami in the East China Sea in February 2009, *Nat. Hazards Earth Syst. Sci.*, *10*, 2599–2610, doi:10.5194/nhess-10-2599-2010.
- Tanaka K (2012), On meteotsunami around Tsushima Strait generated by the Baiu front, *Natural Hazards*, *63*, 805–822.
- Vilibić, I., and J.Šepić (2009), Destructive meteotsunamis along the eastern Adriatic coast: Overview, *Phys. Chem. Earth*, *34*, 904–917.
- Vilibić, I., N. Domijan, M. Orlić, N. Leder, and M. Pasarić (2004), Resonant coupling of a traveling air-pressure disturbance with the east Adriatic coastal waters, *J. Geophys. Res.*, *109*, C10001, doi:10.1029/2004JC002279.
- Vilibić, I., S. Monserrat, A. B. Rabinovich, and H. Mihanović (2008), Numerical modelling of the destructive meteotsunami of 15 June, 2006 on the coast of the Balearic Islands, *Pure Appl. Geophys.*, *165*, 2169–2195, doi:10.1007/s00024-008-0426-5.

- Vilibić, I., J. Šepić, B. Rangelov, and N. Strelec Mahovic (2010), Possible atmospheric origin of the 7 May 2007 western Black Sea shelf tsunami event. *Journal of Geophysical Research*, 115, C07006, doi:10.1029/2009JC005904.
- Vilibić, I., K. Horvath, N. Strelec Mahović, S. Monserrat, M. Marcos, Á. Amores, and I. Fine (2014a), Atmospheric processes responsible for generation of the 2008 Boothbay meteotsunami, *Nat. Hazards*, 74, 25–53, doi:10.1007/s11069-013-0811-y.
- Wertman, C.A., R.M. Yablonsky, Y. Shen, J. Merrill, C.R. Kincaid, and R.A. Pockalny (2013), Mesoscale convective system surface pressure anomalies responsible for meteotsunamis along the U.S. East Coast on June 13th, 2013, *Scientific Reports*, 4, 7143 doi:10.1038/srep07143.
- Workoff, T.E., D.A.R. Kristovich, N.F. Laird, R. LaPlante, and D. Leins (2012), Influence of the Lake Erie overlake boundary layer on deep convective storm evolution. *Weather Forecast.*, 27, 1279-1289. doi:10.1175/WAF-D-11-00076.1.
- Zajac, B.A., and S.A. Rutledge (2001), Cloud-to-ground lightning activity in the contiguous United States from 1995 to 1999, *Monthly Weather Review*, 129, 999-1019.

5. Worldwide Meteotsunami Occurrence

The following is to be submitted to Nature Geoscience

5.1 Introduction

Meteotsunamis occur throughout the world's ocean and large lakes, where individual meteotsunami events have reached heights of 6 meters [Vučetić *et al.*, 2009], inflicted millions of dollars in damage [Vilibić *et al.*, 2008; Orlić *et al.*, 2010; Tanaka, 2010], and claimed numerous lives [Ewing *et al.*, 1954; Hibiya and Kajiura, 1982; Haslett and Bryant, 2009; Cho *et al.*, 2013]. The formation of a destructive meteotsunami involves three main processes: wave generation by an atmospheric disturbance, propagation resonance with the atmospheric disturbance [Proudman, 1929; Greenspan, 1956], and local amplification at the coast through shoaling, shelf resonance, and harbor resonance [Rabinovich, 2009]. Owing to the dependence on multiple resonant mechanisms, meteotsunamis are considered a local process much like landslide tsunamis [Lynett and Liu, 2002] compared with the potential transoceanic scale of seismic tsunamis [Titov *et al.*, 2005]. Nevertheless, atmospheric disturbances can yield a tsunami threat to regions which are not traditionally recognized as seismically tsunamigenic [ten Brink *et al.*, 2014]. Owing to their local scale, meteotsunamis have been studied primarily on an episodic basis [Wang *et al.*, 1987; Akamatsu, 1982; Rabinovich and Monserrat, 1996; Šepić *et al.*, 2009; Šepić *et al.*, 2011] or more recently at a regional scale [Bechle *et al.*, 2015; Orlić, 2015; Šepić *et al.*, 2015]. While meteotsunamis are recognized worldwide [Pattiaratchi and Wijeratne, 2015], meteotsunami occurrences have yet to be assessed in global perspective. Here the spatial and temporal occurrence of meteotsunamis recorded throughout the world is investigated to identify

regions of meteotsunami activity, seasonal patterns in meteotsunami occurrence, and relations to local storm climate.

5.2. Methods

A database of historic meteotsunami events is aggregated from the published literature, National Geophysical Data Center (NGDC)/World Data Service Global Historical Tsunami Database, the Novosibirsk Tsunami Laboratory (NTL) Historical Tsunami Databases for the World Ocean, and unpublished anecdotal accounts. Tsunamis of meteorological origin were selected from the NGDC and NTL databases based upon the reported cause code. Events from the NGDC database are categorized based upon reported numbers of deaths, injuries, or damages whereas events from the NTL database only report a damage code. As many events appear in both the NGDC and NTL databases, events were cross-referenced by date and location to remove coincident reports. Unpublished reports of meteotsunamis were collected from a survey of newspaper databases, web search engines, and social media (Twitter, YouTube) using keywords “meteotsunami”, “meteo-tsunami”, and “meteorological tsunami”. Furthermore, a targeted search of newspaper databases was performed with expanded search terms including “tidal wave” and “tsunami”, similar to the work of *Haslet and Bryant* [2009] in the United Kingdom. Identified meteotsunami events are mapped based on impact (i.e. death, injury, or damage, or no reported impact) and compared with bathymetry and climate. Zones of high meteotsunami activity are identified based upon event groupings in close geographic proximity and hydrodynamic connectivity. Seasonal distributions of meteotsunamis are obtained by binning events by month of occurrence.

5.3. Results

The occurrence of reported meteotsunamis throughout the world is illustrated in Figure 5-1. To date, reported meteotsunamis are primarily located in the northern hemisphere. The majority of meteotsunamis occur in relatively shallow water ($H < 200\text{m}$) along wide shelves ($> 100\text{ km}$) (see Appendix B Figure B1). Depths in this range correspond to long wave speeds less than 45 m/s, which would allow for long wave resonance on the shelf to occur at realistic atmospheric disturbance speeds [*Proudman, 1929*]. In contrast, significant propagation resonance is unlikely to occur in deeper water or over narrow shelf slopes. For example, meteotsunamis in the Mediterranean Sea tend to occur in shallower sub-basins such as the Adriatic [*Šepić et al., 2012*] and Aegean Seas [*Papadopoulos, 1993*] rather than the much deeper Laguarian, Tyrrhenian, and Ionian Seas. The majority of meteotsunamis occur in the temperate and continental Köppen climate zones, [*Chen and Chen, 2013*], whereas very few events occur in tropical, dry, or polar climates (see Appendix B Figure B2). While dry and polar climates do not frequently experience convective storms, a common atmospheric disturbance type associated with meteotsunamis [*Belušić et al., 2007; Šepić et al. 2009; Bechle et al., 2015*], many tropical regions experience high convective activity [*Brooks et al., 2003; Christian et al., 2003; Zipser et al., 2006*]. Nevertheless, the lack of reported meteotsunami occurrences in tropical regions suggests that these storms may not meet the resonant criteria of the water bodies, which coincidentally tend to have greater depths and narrower shelves compared with the water bodies in the temperate and continental climate zones (see Appendix B, Figure B2). Overall, the spatial distribution of meteotsunamis throughout the World Ocean demonstrates the importance of both the bathymetry and atmospheric setting of the water body in meteotsunami formation.

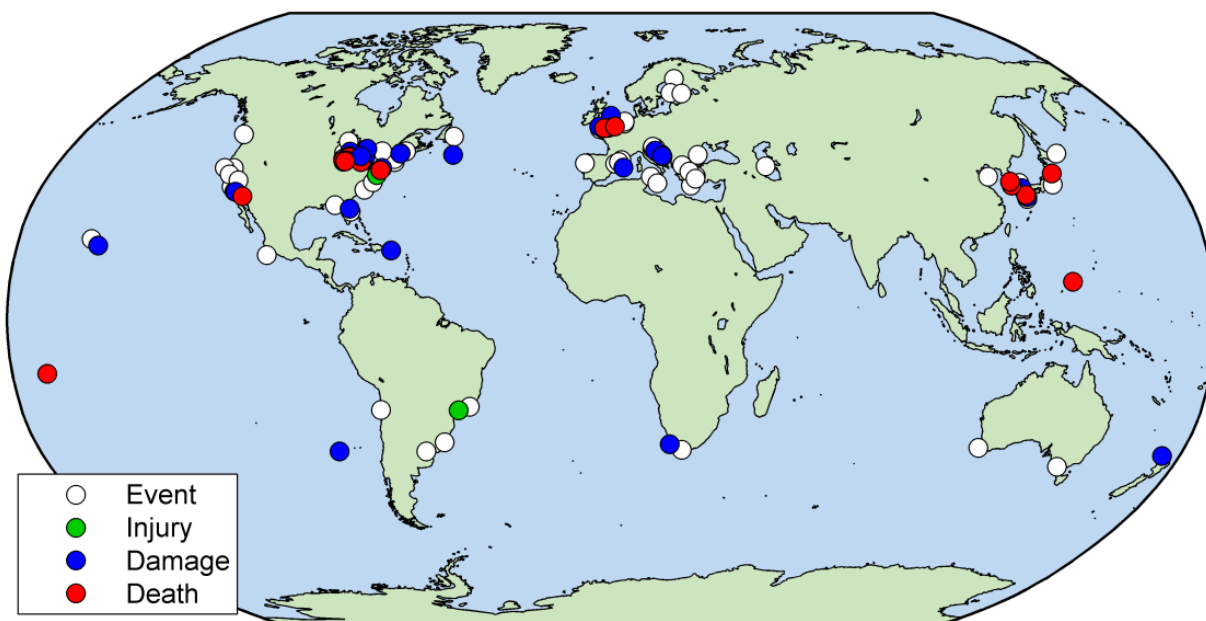


Figure 5-1: Occurrence and impact of meteotsunamis worldwide

The seasonal distribution of reported meteotsunamis is illustrated in Figure 5-2 as a histogram of monthly occurrences. Overall, worldwide meteotsunami occurrences peak from May to August, during the warm season for the northern hemisphere. To examine the seasonal meteotsunami occurrence in different parts of the world, the monthly distribution are broken into six major meteotsunami regions: the Laurentian Great Lakes, the North American East Coast, the North American West Coast, the Mediterranean, Northern Europe, and Eastern Asia (see Appendix B Figure B3 for a map of these regions). The overall pattern of warm season meteotsunamis is consistent in the Mediterranean, Northern Europe, and the Great Lakes regions (note that the Great Lakes monthly distribution of reported meteotsunamis has a higher percentage of events in May compared with the distribution derived from water level records in Chapter 5). In all three of these regions, meteotsunamis are typically associated with convection [Belušić and Strelec Mahovic, 2009; Haslett et al., 2009; Bechle et al., 2015]. In each of these regions, convective activity also peaks during the mid-summer (June, July, August) [Morel and

Sensi, 2002; Kolios and Feidas, 2010; Mikus et al., 2012; Workoff et al., 2012]. Interestingly, Great Lakes meteotsunami seasonality precedes peak convective seasonality [*Bechle et al., 2015*] whereas Mediterranean and Northern European meteotsunami seasons align well with the convective season. Cold season peaks in reported meteotsunamis occur along the North American East and West coasts as well as Eastern Asia. Meteotsunamis reported along the North American East Coast are primarily linked with tropical and extratropical cyclones in the cold season [*Mercer et al., 2002; Pasquet et al., 2013*] and convective storms in the warm season [*Churchill et al., 1995; Pasquet and Vilibić, 2013; Wertman et al., 2014*]. The origins of cold season meteotsunamis along the North American West Coast are less clear [*Thomson et al., 2009*], though some events are associated with extratropical cyclones [*Rabinovich and Stephenson, 2004*]. Similarly, cold season meteotsunamis in Eastern Asia are associated with a variety of sources, including cyclones [*Tanaka et al., 2012*], fronts [*Tanaka, 2010; 2012*], and convection [*Cho et al., 2013; Tanaka et al., 2013*].

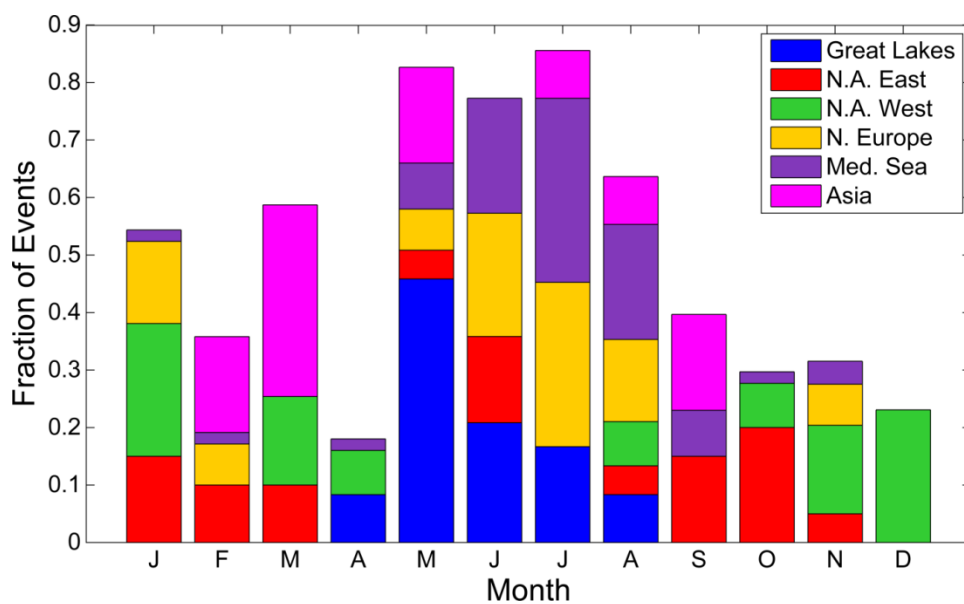


Figure 5-2: Monthly distribution of meteotsunami events reported in the literature, databases, and news reports.

5.4. Discussion and Conclusions

Meteotsunamis are potentially damaging and deadly water waves that have been reported worldwide. Overall, these destructive waves have been reported mostly in the northern hemisphere in water depths below 200 meters and in temperate or continental climates. Consistent with meteotsunami generation mechanisms, these characteristics allow for propagation resonance with relatively fast moving storms. Reported meteotsunamis occur primarily in the warm season and are associated with convective storms, though some regions experience a meteotsunami peak in the cold season, associated with cyclone activity. Owing to their dependence on atmospheric processes, it is possible that meteotsunami patterns will shift under a changing climate. For example, simulations of future climate scenarios over the United States indicate a likely increase in the number of days favorable to severe thunderstorm formation over both the Great Lakes and East Coast, particularly in the spring season [Trapp *et al.*, 2007; Diffenbaugh *et al.*, 2013; Seeley and Romps, 2015]. This would suggest that the convectively associated meteotsunamis in these regions may see an overall increase in occurrence frequency or a temporal shift in occurrence to earlier in the warm season. On the other hand, the frequency of tropical and extratropical cyclones may decrease under a changing climate [Christensen *et al.*, 2013], suggesting that meteotsunamis associated with cyclones may become less prevalent. In summary, a growing body of research has revealed that meteotsunamis pose a clear risk to many regions of the world, particularly those areas located in temperate or continental climates with wide areas of water depths less than 200 meters. While these general patterns are revealed from reported meteotsunamis, ongoing efforts are required both to characterize meteotsunami climatology and predict damaging events in order to mitigate the threat from these coastal hazards.

5.5. References

- Bechle, A. J., Kristovich, D. A.R. and Wu, C. H. (2015), Meteotsunami occurrences and causes in Lake Michigan. *J. Geophys. Res. Oceans*. Accepted Author Manuscript. doi:10.1002/2015JC011317
- Belušić, D. and N. Strelec Mahović (2009) Detecting and following atmospheric disturbances with a potential to generate meteotsunamis in the Adriatic, *Physics and Chemistry of the Earth*, 34, 918-927.
- Belušić, D., B. Grisogono, and Z. B. Klaić (2007), Atmospheric origin of the devastating coupled air-sea event in the east Adriatic, *J. Geophys. Res.*, 112, D17111, doi:10.1029/2006JD008204.
- Brooks, H.E., J.W. Lee, and J.P. Craven (2003) The spatial distribution of severe thunderstorm and tornado environments from global reanalysis data. *Atmos. Res.*, 67–68, 73–94.
- Chen, D. and H.W. Chen (2013) Using the Köppen classification to quantify climate variation and change: An example for 1901-2010, 6, 69-79, doi: 10.1016/j.envdev.2013.03.007.
- Cho, K.-H., J.-Y. Choi, K.-S. Park, S.-K. Hyun, Y. Oh, and J.-Y. Park (2013), A synoptic study on tsunami-like sea level oscillations along the west coast of Korea using an unstructured-grid ocean model, *J. Coastal Res.*, 65, 678–683.
- Christensen and co-authors (2013) Climate Phenomena and their Relevance for Future Regional Climate Change. In: *Climate Change 2013: The Physical Science Basis. Contribution of Working Group I to the Fifth Assessment Report of the Intergovernmental Panel on Climate Change* [Stocker, T.F., D. Qin, G.-K. Plattner, M. Tignor, S.K. Allen, J. Boschung, A.

Nauels, Y. Xia, V. Bex and P.M. Midgley (eds.)]. Cambridge University Press, Cambridge, United Kingdom and New York, NY, USA.

Christian, H. J., and coauthors (2003) Global frequency and distribution of lightning as observed from space by the Optical Transient Detector. *J. Geophys. Res.*, 108,4005, doi:10.1029/2002JD002347

Churchill, D.D., S.H. Houston, and N.A. Bond (1995), The Daytona Beach wave of 3-4 July 1992 – A shallow-water gravity-wave forced by a propagating squall line, *Bull. Amer. Meteor. Soc.*, 76(1), 21-32, doi: 10.1175/1520-0477(1995)076<0021:TDBWOJ>2.0.CO;2.

Diffenbaugh, N.S., M. Scherer, and R.J. Trapp (2013) Robust increases in severe thunderstorm environments in response to greenhouse forcing, *Proc Natl Acad Sc*, 110(41), 16361-16366.

Donn, W.L., and M. Ewing (1956), Stokes' edge waves in Lake Michigan, *Science*, 124, 1238–1242, doi: 10.1126/science.124.3234.1238.

Ewing, M., F. Press, and W. J. Donn (1954), An explanation of the Lake Michigan wave of 26 June 1954, *Science*, 120, 684–686, doi:10.1126/science.120.3122.684.

Greenspan, H. P. (1956), The generation of edge waves by moving pressure disturbances, *J. Fluid Mech.*, 1, 574–592.

Haslett, S.K., and E.A. Bryant (2009) Meteorological tsunamis in southern Britain: an historical review. *The Geographical Review* 99, 146–163.

Haslett, S.K., H.E. Mellor, and E.A. Bryant (2009), Meteo-tsunami hazard associated with summer thunderstorms in the United Kingdom, *Phys. Chem. Earth*, 34, 1016-1022, doi: 10.1016/j.pce.2009.10.005.

Hibiya, T., and K. Kajiura (1982), Origin of the Abiki phenomenon (a kind of seiche) in Nagasaki Bay, *J. Oceanogr. Soc. Jpn.*, 38, 172–182, doi:10.1007/BF02110288.

- Kolios, S. and H. Feidas (2010), A warm season climatology of mesoscale convective systems in the Mediterranean basin using satellite data, *Theor. Appl. Climatol.*, 102, 29-42, doi: 10.1007/s00704-009-0241-7.
- Lynett, P., and Liu, P.L. (2002) A numerical study of submarine-landslide-generated waves and run-up, *Proceedings: Mathematical, Physical and Engineering Sciences*, 458, 2885-2910.
- Mercer, D., J. Sheng, R. J. Greatbatch, and J. Bobanović (2002), Barotropic waves generated by storms moving rapidly over shallow water, *J. Geophys. Res.*, 107(C10), 3152, doi:10.1029/2001JC001140.
- Mikus, P., M.T. Prtenjak, and N. Strelec Mahovic (2012) Analysis of the convective activity and its synoptic background over Croatia, *Atmospheric Research*, 104-105, 139–153.
- Monserrat, S., I. Vilibić, and A. B. Rabinovich (2006), Meteotsunamis: Atmospherically induced destructive ocean waves in the tsunami frequency band, *Nat. Hazards Earth Syst. Sci.*, 6, 1035–1051, doi:10.5194/nhess-6-1035-2006.
- Morel, C. and S. Senesi (2002) A climatology of mesoscale convective systems over Europe using satellite infrared imagery . II: Characteristics of European mesoscale convective systems. *Q. J. R. Meteorol. Soc.* , 128, 1973– 1995.
- Orlić, M., D. Belušić, I. Janeković, and M. Pasarić (2010), Fresh evidence relating the great Adriatic surge of 21 June 1978 to mesoscale atmospheric forcing, *J. Geophys. Res.*, 115, C06011, doi:10.1029/2009JC005777.
- Papadopoulos, G.A. (1993) On some exceptional seismic(?) sea waves in the Greek archipelago, *International Journal of the Tsunami Society*, 11(1), 25-34.

- Pasquet, S., and I. Vilibić (2013), Shelf edge reflection of atmospherically generated long ocean waves along the central U.S East Coast, *Cont. Shelf Res.*, 66, 1–8, doi:10.1016/j.csr.2013.06.007.
- Pasquet, S, I. Vilibić, and J. Šepić (2013), A survey of strong high-frequency sea level oscillations along the U.S. East Coast between 2006 and 2011, *Nat. Hazards Earth Syst. Sci.*, 13, 473–482, doi:10.5194/nhess-13-473-2013.
- Pattiaratchi, C.B. and E.M.S. Wijeratne (2015), Are meteotsunamis and underrated hazard? *Phil.Trans.R.Soc.A*, 373, 20140377, <http://dx.doi.org/10.1098/rsta.2014.0377>.
- Proudman, J. (1929), The effects on the sea of changes in atmospheric pressure, *Mon. Not. R. Astron. Soc.*, 2, 197–209.
- Rabinovich, A.B. (2009), Seiches and harbor oscillations, in Handbook of Coastal and Ocean Engineering, edited by Kim, Y.C., 193-236, World Scientific Publishing Company, Toh Tuck Link, Singapore.
- Rabinovich, A.B. and S. Monserrat (1996), Meteorological tsunamis near the Balearic and Kuril Islands:descriptive and statistical analysis, *Nat. Hazards*, 13, 55-90.
- Rabinovich, A.B., and F.E. Stephenson (2004). Longwave measurements for the coast of British Columbia and improvements to the tsunami warning capability. *Natural Hazards* 32 (3), 313–43.
- Seeley, J.T. and D.M. Romps (2015) The Effect of Global Warming on Severe Thunderstorms in the United States, *Journal of Climate*, 2443-2458.
- Šepić, J., I. Vilibić, and D. Belušić (2009a), The source of the 2007 Ist meteotsunami (Adriatic Sea), *J. Geophys. Res.*, 114, C03016, doi:10.1029/2008JC005092.

- Šepić, J., I. Vilibić, and S. Monserrat (2009b), Teleconnections between the Adriatic and the Balearic meteotsunamis, *Phys. Chem. Earth*, *34*, 928-937, doi:10.1016/j.pce.2009.08.007.
- Šepić, J., and I. Vilibić (2011) The development and implementation of a real-time meteotsunami warning network for the Adriatic Sea. *Natural Hazards and Earth Systems Science*, *11*(1), 83-91.
- Šepić, J., I. Vilibić, and N. Strelec Mahović (2012), Northern Adriatic meteorological tsunamis: Observations, link to the atmosphere, and predictability, *J. Geophys. Res.*, *117*, C02002, doi:10.1029/2011JC007608.
- Šepić, J., I. Vilibić, A. Lafon, L. Macheboeuf, and Z. Ivanović (2015a), High-frequency sea level oscillations in the Mediterranean and their connection to synoptic patterns, *Progress in Oceanography*, *137*, 284-298, doi:10.1016/j.pocean.2015.07.005.
- Tanaka, K. (2010), Atmospheric pressure-wave bands around a cold front resulted in a meteotsunami in the East China Sea in February 2009, *Nat. Hazards Earth Syst. Sci.*, *10*, 2599–2610, doi:10.5194/nhess-10-2599-2010.
- Tanaka K, Yamada F, Asano T (2012) Toward the prediction of meteotsunamis propagating over the East China Sea with downscaling approach. In: Proceedings of the International Conference on Disaster Management 2012, The 8th Annual Conference of the International Institute for Infrastructure, Renewal and Reconstruction (IIIRR), 24–26 Aug 2012, Kumamoto, pp 205–214.
- Tanaka, K. S. Gohara, T. Koga, R. Yamaguchi, and F. Yamada (2014) Abiki oscillations in Sakitsu Bay, west Kyushu, Japan, *Natural Hazards*, *74*(1), 233-250.

- ten Brink, U.S., J.D. Chaytor, E.L. Geist, D.S. Brothers, and B.D. Andrews, (2014) Assessment of tsunami hazard to the U.S. Atlantic margin, *Marine Geology*, 353, 31-54.
- Thomson, R.E., A.B. Rabinovich, I.V. Fine, D.C. Sinnott, A. McCarthy, N.A.S. Sutherland, and L.K. Neil (2009) Meteorological tsunamis on the coasts of British Columbia and Washington, *Physics and Chemistry of the Earth*, 34, 971-988.
- Titov, V., A.B. Rabinovich, H.O. Mofjeld, R.E. Thomson, and F.I. Gonzalez (2005) The Global Reach of the 26 December 2004 Sumatra Tsunami, *Science*, 309, 2045-2048, doi:10.1126/science.1114576.
- Trapp RJ, N.S. Diffenbaugh, H.E. Brooks, M.E. Baldwin, E.D. Robinson, and J.S. Pal (2007) Changes in severe thunderstorm environment frequency during the 21st century caused by anthropogenically enhanced global radiative forcing. *Proc Natl Acad Sci USA*104(50):19719–19723.
- Vilibić, I. (2008), Numerical simulations of the Proudman resonance, *Continental Shelf Research*, 28, 574– 581, doi:10.1016/j.csr.2007.11.005.
- Vilibić, I., S. Monserrat, A. B. Rabinovich, and H. Mihanović (2008), Numerical modelling of the destructive meteotsunami of 15 June, 2006 on the coast of the Balearic Islands, *Pure Appl. Geophys.*, 165, 2169–2195, doi:10.1007/s00024-008-0426-5.
- Vučetić, T., I. Vilibić, S. Tinti, and A. Maramai (2009), The Great Adriatic flood of 21 June 1978 revisited: An overview of the reports, *Phys. Chem. Earth*, 34, 894-903, doi: 10.1016/j.pce.2009.08.005.
- Wang, X., K. Li, Z. Yu, and J. Wu (1987) Statistical characteristics of seiches in Longkou Harbor, *Journal of Physical Oceanography*, 17, 1063-1065.

- Wertman, C.A., R.M. Yablonsky, Y. Shen, J. Merrill, C.R. Kincaid, and R.A. Pockalny (2013), Mesoscale convective system surface pressure anomalies responsible for meteotsunamis along the U.S. East Coast on June 13th, 2013, *Scientific Reports*, *4*, 7143 doi:10.1038/srep07143.
- Workoff, T.E., D.A.R. Kristovich, N.F. Laird, R. LaPlante, and D. Leins (2012), Influence of the Lake Erie overlake boundary layer on deep convective storm evolution. *Weather Forecast.*, *27*, 1279-1289. doi:10.1175/WAF-D-11-00076.1.
- E. J. Zipser, C. Liu, D.J. Cecil, S.W. Nesbitt, and D.P. Yorty (2006) Where are the most intense thunderstorms on earth?. *Bull. Amer. Meteor. Soc.*, **87**, 1057–1071.
doi: <http://dx.doi.org/10.1175/BAMS-87-8-1057>

6. Conclusion

6.1 Summary

The Laurentian Great Lakes are a region with an active and impactful meteotsunami history, illustrated by many events which have resulted in destruction, injury, and death [Ewing *et al.*, 1954; Donn and Ewing, 1956; Irish 1965; Murty and Freeman, 1973; As-Salak and Schwab, 2004; Šepić and Rabinovich, 2014; Anderson *et al.*, 2015]. Nevertheless, many detailed meteotsunami processes in these large events remain unclear. Beyond these large events, the meteotsunami climate of the Great Lakes is also unknown in terms of size frequency, seasonal occurrence, and causative storms. In view of these knowledge gaps, the objective of this research was to characterize Great Lakes meteotsunamis in terms of both physical mechanisms as well as historic meteotsunami occurrence statistics.

In Chapter 2, two large meteotsunami events on Lake Michigan were simulated with a numerical model to investigate the detailed behavior of these events. Both atmospheric pressure and wind perturbations were found to be essential to explain the magnitude of the wave activity. Long waves and edge waves were found to be critical to each event, with the superposition of edge and long waves responsible for the greatest meteotsunami height observed in the second event. The relative importance of long and edge waves in these events was shown to be sensitive to changes in the atmospheric disturbance speed and direction. The findings of this analysis demonstrate that the enclosed Lake Michigan basin retained and focused wave energy, leading to the large magnitude, long duration, and destructive nature of the events.

In Chapter 3, the occurrence of meteotsunamis in Lake Michigan was quantified at 10 locations from up to 20 years of historical water level records. The Pareto Type 1 distribution was used to estimate meteotsunami exceedance probabilities in the lake, with the largest annual return level found at Calumet Harbor, IL (0.62 m). Analysis of radar imagery indicates that Lake Michigan meteotsunamis are associated primarily with convective storm structures, with a secondary contribution from frontal storms. Meteotsunami events occur primarily in the late spring and early summer, which precedes the peak convective storm season over the lake. Overall, this statistical analysis provides valuable insight into the spatial and temporal occurrence of meteotsunamis in Lake Michigan.

In Chapter 4, a regional analysis of meteotsunami characteristics across the Great Lakes was performed, expanding upon the results of Chapter 3. Meteotsunamis generally occur in the Great Lakes from the late-spring to mid-summer and are associated primarily with convective storms. Across the region, meteotsunami height tends to increase along the major axis of the lake in the leeward direction of storm propagation. The monthly distribution of meteotsunamis is found to be negatively related with lake bottom slope which suggests that the seasonal distribution of meteotsunamis may be related to the resonance characteristics of the water body [*Proudman, 1929; Greenspan, 1956*]. Complex convective storms tend to be the dominant storm structure associated with meteotsunamis in the western Great Lakes whereas linear storm structures tend to dominate in the eastern Great Lakes. Overall, the regional-scale analysis of meteotsunamis in the Great Lakes reveals valuable insight into the role of physical and atmospheric setting on meteotsunami occurrence.

In Chapter 5, a worldwide data base of reported meteotsunami events is compiled to examine global patterns in meteotsunami occurrence. In general, reported meteotsunamis are located in temperate or continental climates of the northern hemisphere that have wide shelves (>100 km) with water depths below 200 m. Meteotsunamis in the Great Lakes, Mediterranean, and Northern Europe tend to occur in the warm season and are associated with convection whereas meteotsunamis on the North American East Coast, North American West Coast, and Eastern Asia tend to occur in the cold season in response to cyclone or frontal-type events. This global assessment of meteotsunamis provides insight into the physical and atmospheric characteristics that make regions vulnerable to meteotsunamis.

6.2 Conclusions

- **Atmospheric pressure perturbations and wind stress are both important to meteotsunami formation in the Great Lakes**

While the potential of wind stress to significantly contribute to meteotsunami height has been recognized [*Platzman, 1965; Vilibić et al., 2005; Orlić et al., 2010*], to date wind stress has been viewed as a secondary meteotsunami forcing compared to atmospheric pressure [*Šepić et al., 2008; Orlić et al., 2010; Renault et al., 2011*]. Previous studies of the Lake Michigan meteotsunami events did not consider wind stress in their analysis [*Ewing et al., 1954; Platzman, 1958; Donn and Ewing, 1956*]. The model results in Chapter 2 indicate that wind stress was responsible for 40% and 68% of the wave heights in the June 26, 1954 and July 6, 1954 Lake Michigan meteotsunami events, respectively. Clearly, wind stress can play a significant role in generating meteotsunamis in Lake Michigan. It is also important to note that the observed wind speeds of 25 and 32 m/s for June 26, 1954 and July 6, 1954 events, respectively, are much

greater than that of any other meteotsunami that had been discussed in the literature. Recent work by *Anderson et al.* [2015] also revealed that both pressure and wind perturbations were responsible for the formation of a 2012 Lake Erie meteotsunami. This suggests that the role of wind stress in Great Lakes meteotsunamis may be unique compared with the rest of the world.

- **Long waves and edge waves can interact to create large meteotsunamis, especially in enclosed basins**

The simulation results of Chapter 2 reveal that long waves and edge waves were generated simultaneously in the two historic Lake Michigan meteotsunami events studied. While edge waves did not play a major role in the destructive wave that struck Chicago in the June 26, 1954 event, significant oscillations ($H > 0.5$ m) due to edge waves occurred hours after the initial wave. The enclosed nature of the Lake Michigan allowed this edge wave energy to remain in the basin and propagate for over a day, hindering rescue efforts. In the July 6, 1954 event, the largest wave observed was the result of edge wave and long wave superposition, with a height 60% larger than the other waves in the lake. Nevertheless, the presence of the long wave was not considered in the original analysis of *Donn and Ewing* [1956]. Furthermore, the enclosed nature of the Lake Michigan basin enabled edge waves generated on both the east and west coasts of the lake to meet and superpose to heights in excess of 1 meter along the coast. The role of edge waves and long waves in these meteotsunamis is sensitive to storm speed and direction. Long waves and edge waves were also found to both have significant role in the 2012 Lake Erie meteotsunami studied by *Anderson et al.* [2015]. Overall, the hydrodynamic model results presented in this dissertation indicate that edge waves and long waves can be generated simultaneously and interact to create a large meteotsunami.

- **Great Lakes meteotsunamis occur primarily in the late-spring to mid-summer and are associated with convective storm structures**

Long term analysis of Great Lakes meteotsunami water level records reveals that meteotsunamis primarily occur from April to June. The majority (78%) of meteotsunamis are associated with convective storm structures, particularly convective complexes and linearly organized convection. Frontal-type storms have a secondary contribution to meteotsunami generation in the Great Lakes. Interestingly, while meteotsunamis in the Great Lakes are strongly connected with convective storms, the peak season for meteotsunami occurrence in the Great Lakes precedes that of the mid-summer peak in convective activity [*Kelley et al.*, 1985]. Compared with two other warm season meteotsunami regions (Mediterranean and Northern Europe), the Great Lakes is the only region where this disconnect in meteotsunami and convective season is apparent. Possible explanations for this discrepancy include the strength of the strongly-stable overlake boundary layer [*Workoff et al.*, 2012] and seasonal variations in convective storm speed over the lakes.

- **Patterns in Great Lakes meteotsunami characteristics are associated with physical and atmospheric features of the Great Lakes region**

Regional patterns in Great Lakes meteotsunami magnitude, season, and causative storm characteristics exhibit relationships with the physical and atmospheric features of the region. Across the region, meteotsunami height tends to increase along the major axis of the lake in the leeward direction of storm propagation, consistent with the propagation resonance mechanism in which amplification grows with the distance traveled by the wave [*Greenspan*, 1956; *Hibiya and Kajiura*, 1982]. Across the region, mean month of meteotsunami occurrence has a significant

negative linear relationship with lake bottom slope whereas lakes of comparable average depths were found to have similar monthly distributions in meteotsunami occurrence. As bottom slope and water depth dictate propagation speed for edge and long waves, respectively, these relationships suggest that the seasonal distribution of meteotsunamis may be related to the propagation resonance characteristics of the water body [*Proudman, 1929; Greenspan, 1956*]. The role of complex convective storms tends to increase westward across the region whereas the role of linear storms decreases along the same direction, consistent with longitudinal variations in the historical occurrence frequency of mesoscale convective complex storms across the region [*Ashley et al, 2003*]. These regional patterns in Great Lakes meteotsunamis reveal valuable insight into the role of the physical and atmospheric setting of the region on meteotsunami occurrence.

6.3 Recommendations for Future Work

A future detailed investigation into the storms which cause meteotsunamis in the Great Lakes could explain patterns observed in this research. While this dissertation revealed the storm types responsible for meteotsunamis in the Great Lakes, an assessment of the associated storm propagation speed, direction, atmospheric pressure perturbations, and surface wind stress would reveal how these storms interact with the water surface to generate the meteotsunamis. An analysis of the null storms which do not generate meteotsunamis over this same period would provide further information to better identify the storm motion and surface perturbations favorable to meteotsunamis in the Great Lakes. Seasonal variations in meteotsunamigenic and non-meteotsunamigenic storms could be used to shed light on the seasonal patterns in

meteotsunami occurrence observed in this dissertation. Specifically, this analysis would reveal if seasonal variations in storm speed could explain why the monthly distribution of meteotsunamis precedes the months of peak convective storm activity in the region. Furthermore, detailed analysis of the atmospheric environment during these meteotsunamis would shed light into the role of atmospheric gravity waves in Great Lakes meteotsunamis. While atmospheric gravity waves are recognized as a main cause of meteotsunamis in the Mediterranean [*Montserrat et al.*, 1991; *Šepić et al.*, 2009, 2012], the level of analysis required to attribute surface perturbations to atmospheric gravity waves was out of the scope of the climatological analysis performed in this dissertation. Nevertheless, understanding the role of atmospheric gravity waves in Great Lakes meteotsunamis remains important in order to compare the Great Lakes meteotsunami processes to those in other regions.

A probabilistic tsunami hazard assessment (PTHA) type study [*Geist and Parsons*, 2006; *González et al.*, 2009] could provide spatial depiction of meteotsunami occurrence frequency throughout the Great Lakes that goes beyond the discrete return levels established in this dissertation. PTHA uses probabilities of tsunami source parameters to stochastically simulate tsunami events using a numerical model to estimate tsunami return levels. *Geist et al.* [2014] applied this concept to estimate the meteotsunami probabilities along the U.S. East Coast, though source probabilities were limited to squall line thunderstorms, which were recognized as a limited subset of possible meteotsunami sources. To apply PTHA for meteotsunami in the Great Lakes, the probability of causative atmospheric disturbance parameters such as speed, direction, and surface perturbations would need to be estimated for all storm structure types identified in this dissertation to be associated with meteotsunamis. This probability space could be built from the comprehensive storm analysis recommended earlier in this section. Hydrodynamic models

such as Lake Michigan model employed in Chapter 2 would be used to simulate the meteotsunami response throughout the lakes in response to a stochastically sampled set of storm conditions. This approach would provide return levels at a higher spatial resolution than the empirical analysis of Chapter 3 and 4 of this dissertation to improve estimates of the meteotsunami threat in the Great Lakes. Nevertheless, the empirical analysis performed in this dissertation would be critical to validate the return levels established in a PTHA study of meteotsunamis in the Great Lakes.

Great Lakes risk and vulnerability to meteotsunamis could also be assessed based on meteotsunami probabilities. Meteotsunami heights at specified return levels would be used to assess potential damage to coastal infrastructure using software such as Hazus-HM, the FEMA standard for estimating economic losses due to earthquakes, floods, and hurricanes. While Hazus-MH has default generic flood depth-to-damage relationships, these relationships may need to be modified for meteotsunamis to account for the large currents and dynamic velocities of meteotsunamis [Vilibić *et al.*, 2008; Asano *et al.*, 2012] in addition to their inundation potential. The resulting spatial assessment of the impacts of meteotsunamis on infrastructure would provide decision makers risk-based information to develop mitigation and resiliency strategies.

Finally, short-term meteotsunami forecasts should be developed to provide warning of imminent events to coastal users. An empirical warning system could be created in which real-time storm conditions such as propagation speed, direction, and pressure and wind perturbations could be compared against the database of historic meteotsunamigenic storms to assess whether a storm with those characteristics has produced meteotsunamis in the past. Furthermore, a heuristic model could be created which invokes analytical solutions to propagation resonance

and an understanding of local wave transformations to provide a rapid estimate of potential meteotsunami height. To provide a more complete forecast of a potential meteotsunami, a real time hydrodynamic model could be developed, though two major barriers exist. First, the computational costs of running a high-resolution hydrodynamic model that resolves detailed meteotsunami processes would be prohibitive to real-time simulation. A “forecast laboratory” could be used to simulate historic events to determine the necessary balance between model resolution and accuracy to achieve real-time meteotsunami simulation. Second, current real-time meteorological conditions used to force Great Lakes operational hydrodynamic models are not of high spatial and temporal resolution to faithfully represent meteotsunami processes [Anderson *et al.*, 2015]. High-resolution meteorological simulations (space~1 km, time~6 sec) have been shown to provide reasonable forcing conditions for hydrodynamic models to simulate meteotsunami processes [Horvath and Vilibić, 2014; Anderson *et al.*, 2015]. The development of a real-time hydrodynamic meteotsunami simulation system requires close collaboration with researchers who develop and implement state-of-the-art weather forecasts models.

6.4. References

- Anderson, E.J., Bechle, A.J., Wu, C.H., Schwab, D.J., Mann, G.E., and Lombardy, K.A. (2015a), Reconstruction of a meteotsunami in Lake Erie on 27 May 2012: Roles of atmospheric conditions on hydrodynamic response in enclosed basins. *J. Geophys. Res. Oceans*. Accepted Author Manuscript, doi: 10.1002/2015JC010883.

- Asano, T., T. Yamashiro, and N. Nishimura (2012), Field observations of meteotsunami locally called “abiki” in Urauchi Bay, Kami-Koshiki Island, Japan, *Nat. Hazards*, 64, 1685–1706, doi:10.1007/s11069-012-0330-2.
- Ashley, W.S., T.L. Mote, P.G. Dixon, S.L. Trotter, E.J. Powell, J.D. Durkee, and A.J. Grundstein, (2003) Distribution of mesoscale convective complex rainfall in the United States, *Monthly Weather Review*, 131, 3003-3017.
- As-Salek, J.A., and D.J. Schwab (2004), High-frequency water level fluctuations in Lake Michigan, *Journal of Waterway, Port, Coastal and Ocean Engineering*, 130(1), 45-53. doi: 10.1061/(ASCE)0733-950X.
- Donn, W. L. (1959), The Great Lakes storm surge of May 5, 1952, *J. Geophys. Res.*, 64(2), 191–198, doi:10.1029/JZ064i002p00191.
- Donn, W.L., and M. Ewing (1956), Stokes’ edge waves in Lake Michigan, *Science*, 124, 1238–1242, doi: 10.1126/science.124.3234.1238.
- Ewing, M., F. Press, and W. J. Donn (1954), An explanation of the Lake Michigan wave of 26 June 1954, *Science*, 120, 684–686, doi:10.1126/science.120.3122.684.
- Geist E.L., and T. Parsons (2006), Probabilistic analysis of tsunami hazards, *Nat. Hazards*, 37, 277–314, doi: 10.1007/s11069-005-4646-z.
- Geist EL, U.S. ten Brink, and M. Gove (2014), A framework for the probabilistic analysis of meteotsunamis. *Nat. Hazards*, 74(1), 123-142, doi: 10.1007/s11069-014-1294-1.
- González, F. I., E. L. Geist, B. Jaffe, U. Kânoğlu, H. Mofjeld, C. E. Synolakis, V.V. Titov, D. Arcas, D. Bellomo, D. Carlton, T. Horning, J. Johnson, J. Newman, T. Parsons, R. Peters, C. Peterson, G. Priest, A. Venturato, J. Weber, F. Wong, and A. Yalciner (2009), Probabilistic

- tsunami hazard assessment at Seaside, Oregon, for near- and far-field seismic sources, *J. Geophys. Res.*, *114*, C11023, doi:10.1029/2008JC005132.
- Greenspan, H. P. (1956), The generation of edge waves by moving pressure disturbances, *J. Fluid Mech.*, *1*, 574–592.
- Hibiya, T., and K. Kajiura (1982), Origin of the Abiki phenomenon (a kind of seiche) in Nagasaki Bay, *J. Oceanogr. Soc. Jpn.*, *38*, 172–182, doi:10.1007/BF02110288.
- Horvath, K., and I. Vilibić (2014), Atmospheric mesoscale conditions during the Boothbay meteotsunami: a numerical sensitivity study using a high-resolution mesoscale model, *Natural Hazards*, *74*, 55-74, doi: 10.1007/s11069-014-1055-1.
- Irish, S.M. (1965), The prediction of surges in the southern basin of Lake Michigan: part II. A cases study of the surge of August 3, 1960, *Mon. Weather Rev.*, *93*(5), 275–281, doi: doi: 10.1175/1520-0493(1965)093<0282:TPOSIT>2.3.CO;2.
- Kelly, D.L., J. T. Schaefer, and C.A. Doswell (1985), Climatology of nontornadic severe thunderstorm events in the United States, *Monthly Weather Review*, *113*, 1997-2014.
- Monserrat S., A. Ibberson, and A.J. Thorpe (1991), Atmospheric gravity waves and the “rissaga” phenomenon, *Q. J. Roy. Meteorol. Soc.*, *117*, 553–570.
- Murty, T. S., and N.G. Freeman (1973), Applications of the concepts of edge waves and numerical modelling to storm surge studies on Lake Huron, in *Proc., 16th Conf. Great Lakes Research*, pp. 533-548, Intl. Association of Great Lakes Research, Ann Arbor, Michigan.
- Orlić, M., D. Belušić, I. Janeković, and M. Pasarić (2010), Fresh evidence relating the great Adriatic surge of 21 June 1978 to mesoscale atmospheric forcing, *J. Geophys. Res.*, *115*, C06011, doi:10.1029/2009JC005777.

- Platzman, G.W. (1958), A numerical computation of the surge of 26 June 1954 on Lake Michigan, *Geophysica*, 6(1), 407–438.
- Platzman, G.W. (1965), The prediction of surges in the southern basin of Lake Michigan: Part I, The dynamical basis for prediction, *Monthly Weather Review*, 93(5), 275-281.
- Proudman, J. (1929), The effects on the sea of changes in atmospheric pressure, *Mon. Not. R. Astron. Soc.*, 2, 197–209.
- Renault L, G. Vizoso, A. Jansá, J. Wilkin, J. Tintoré (2011), Toward the predictability of meteotsunamis in the Balearic Sea using regional nested atmosphere and ocean models, *Geophysical Research Letters*, 38, doi:10.1029/2011GL047361.
- Šepić, J., and A. B. Rabinovich (2014), Meteotsunami in the Great Lakes, Chesapeake Bay and on the Atlantic coast of the United States generated by the propagating 'derecho' of 29–30 June 2012, *Nat. Hazards*, 74, 75–107, doi:10.1007/s11069-014-1310-5.
- Šepić J, M. Orlić, and I. Vilibić (2008), The Bakar Bay seiches and their relationship with atmospheric processes, *Acta Adriatica*, 49(2),107-123.
- Šepić, J., I. Vilibić, and S. Monserrat (2009), Teleconnections between the Adriatic and the Balearic meteotsunamis, *Phys. Chem. Earth*, 34, 928-937, doi:10.1016/j.pce.2009.08.007.
- Šepić, J., I. Vilibić, and N. Strelec Mahović (2012), Northern Adriatic meteorological tsunamis: Observations, link to the atmosphere, and predictability, *J. Geophys. Res.*, 117, C02002, doi:10.1029/2011JC007608.
- Vilibić I, N. Domijan, and S. Cupic (2005), Wind versus air pressure seiche triggering in the Middle Adriatic Coastal waters, *Journal of Marine Sciences*, 57(1-2),189-200.

Vilibić, I., S. Monserrat, A. B. Rabinovich, and H. Mihanović (2008), Numerical modelling of the destructive meteotsunami of 15 June, 2006 on the coast of the Balearic Islands, *Pure Appl. Geophys.*, *165*, 2169–2195, doi:10.1007/s00024-008-0426-5.

Workoff, T.E., D.A.R. Kristovich, N.F. Laird, R. LaPlante, and D. Leins (2012), Influence of the Lake Erie overlake boundary layer on deep convective storm evolution. *Weather Forecast.*, *27*, 1279-1289. doi:10.1175/WAF-D-11-00076.1.

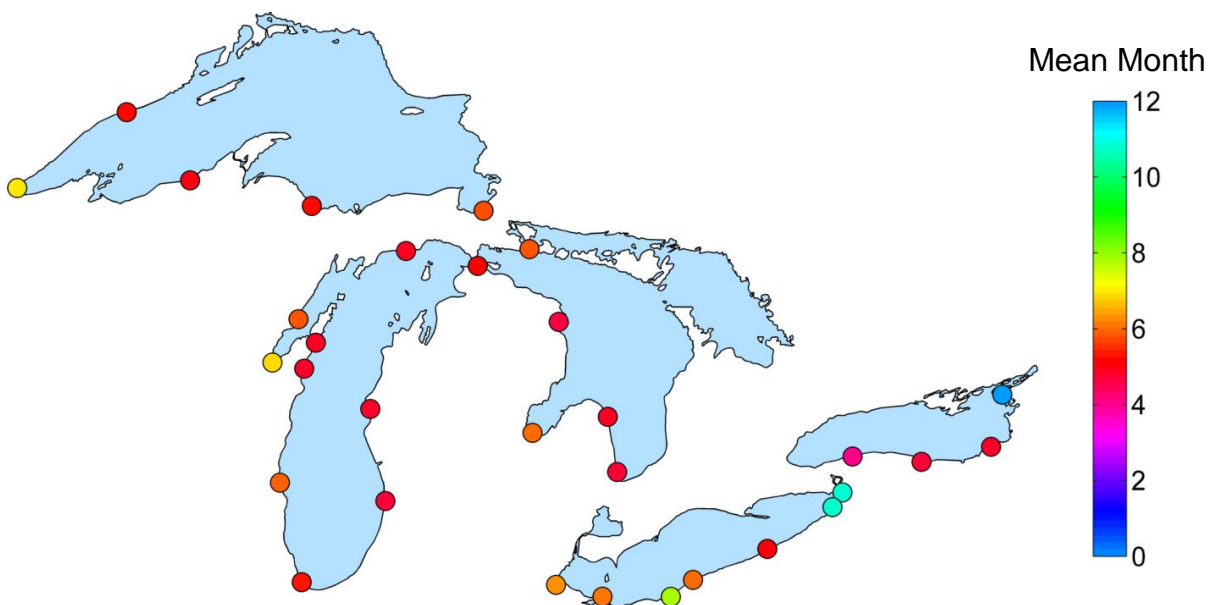
Appendix A Supplemental Material for Chapter 4

Figure A1: Map of the mean month of meteotsunami occurrence at each water level station

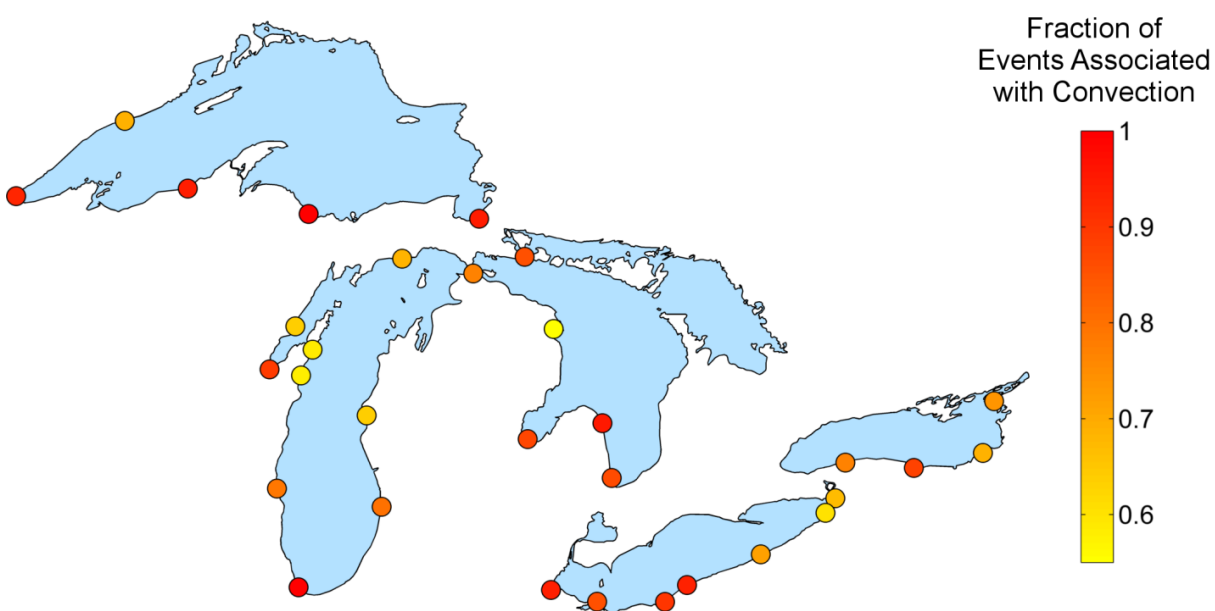


Figure A2: Map of the fraction of meteotsunami events associated with convective storm structures observed at each water level station

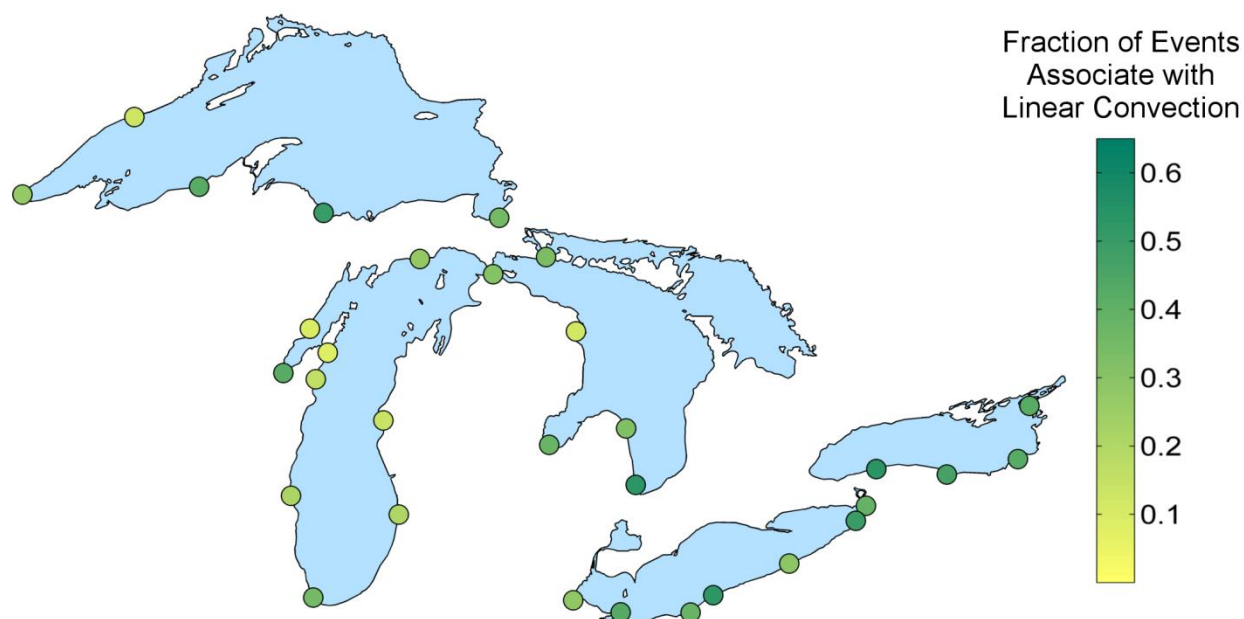


Figure A3: Map of the fraction of meteotsunami events associated with linear convective storms structures observed at each water level station

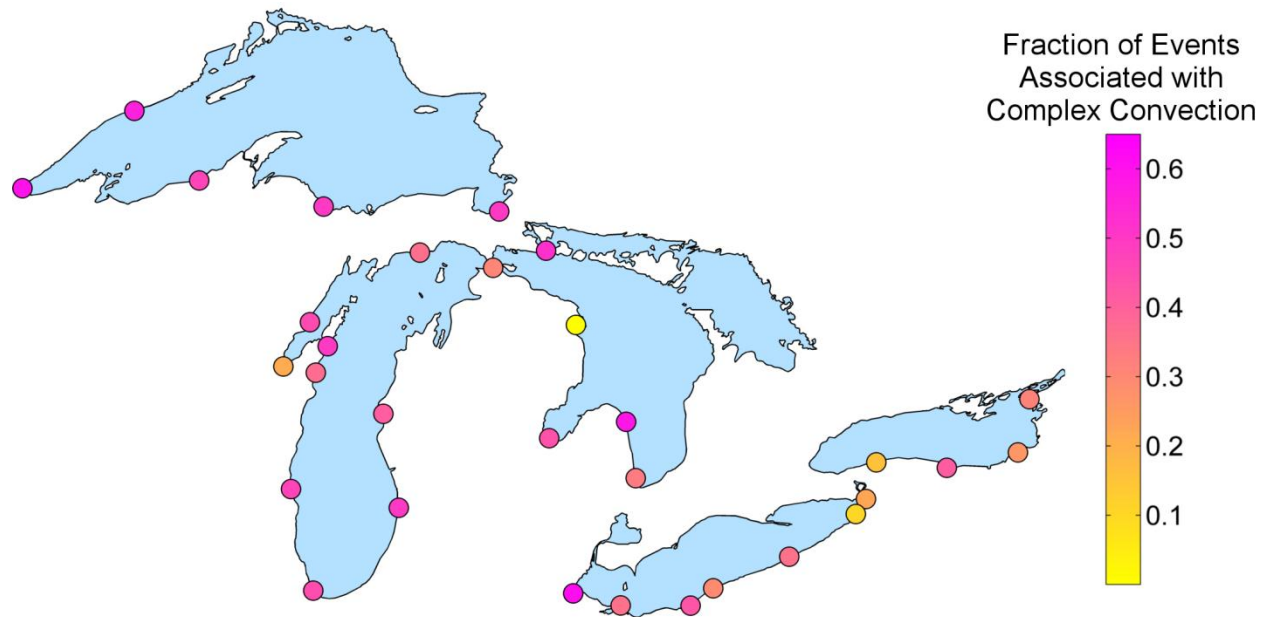


Figure A4: Map of the fraction of meteotsunami events associated with complex convective storm structures observed at each water level station

A.2 Supplemental Tables

Table A1: Historic Great Lakes meteotsunamis from literature and news reports

Lake	Location	Date	Height (m)	Injury	Damage	Deaths	Reference
Superior	Ashland, WI	1895/09/14	2.0		Y		Quebec Saturday Budget [1895]
Superior	Rosspport, ON	1933/10/03	-		Y		Montreal Gazette [1933]
Superior	Keweenaw Bay, MI	2011/05/31	1.0				https://youtu.be/bYI1zljJr4g [2011]
Superior	Sault St. Marie	2014/09/04	1.0		Y		www.sootoday.com [2014]
Michigan	St. Joseph, MI	1893/04/07	1.5		Y		Mortimer [2004]
Michigan	Chicago, IL	1954/06/26	3.0			7	Ewing et al. [1954]
Michigan	Michigan City, IN	1954/06/26	1.0				Harris [1957]
Michigan	Calumet Harbor	1998/05/31	1.7				As-Salek and Schwab [2004]
Michigan	White Lake, MI	1998/05/31	1.7		Y		As-Salek and Schwab [2004]
Michigan	Waukegan, IL	1960/08/03	1.5				Donn and Ewing [1956]
Michigan	Grand Haven, MI	1929/07/04	6.0			10	Grand Haven Daily Tribune [1929]
Michigan	Holland, MI	1938/07/13	3.0			3	Joint Archives of Holland [2001]
Michigan	Warren Dunes, IN	2003/07/04	1.5			7	Guenther [2003]
Michigan	Kenosha, WI	1912/05/12	1.5		Y		Sandusky Star Journal [1905]
Michigan	Ludington, MI	1956/07/01	3.0		Y		Ludington Daily News [1956] www.mlive.com [2015]
Michigan	Traverse City, MI	2015/06/10	-		Y		
Huron	Presque Isle, MI	1925/05/23	3.0				Ludington Daily News [1925]

Lake	Location	Date	Height (m)	Injury	Damage	Deaths	Reference
Huron	Harbor Beach, MI	1952/05/05	1.5		Y		Donn [1959]
Huron	Goderich, ON	1971/08/22	0.5				Murty and Freeman [1973]
Huron	Fort Gratiot, MI	1971/08/22	1.0				Murty and Freeman [1973]
Erie	Cleveland, OH	1882/06/23	4.0	Y	Y	1	Cleveland Plain Dealer [1882]
Erie	Ashtabula, OH	1912/04/12	-		Y		New York Times [1912]
Erie	Cleveland, OH	1942/05/31	5.0			7	Toledo Blade [1942]
Erie	Cleveland, OH	1952/05/05	0.5				Donn [1959]
Erie	Buffalo, NY	1952/05/05	1.0				Donn [1959]
Erie	Madison, OH	2012/05/27	2.0	Y			Anderson et al. [2015]
Erie	Perry, OH	2012/05/27	-		Y		Anderson et al. [2015]
Ontario	Sodus Point, NY	1925/05/23	1.3		Y		Montreal Gazette [1925]
Ontario	Rochester, NY	1979/08/07	1.5		Y		Chaston [1979]
Ontario	Greece, NY	2012/07/07	1.3				13WHAM Rochester, NY [2012]

A.3 References

- Anderson, E.J., Bechle, A.J., Wu, C.H., Schwab, D.J., Mann, G.E., and Lombardy, K.A. (2015), Reconstruction of a meteotsunami in Lake Erie on 27 May 2012: Roles of atmospheric conditions on hydrodynamic response in enclosed basins. *J. Geophys. Res. Oceans*. Accepted Author Manuscript, doi: 10.1002/2015JC010883.
- As-Salek, J.A., and D.J. Schwab (2004), High-frequency water level fluctuations in Lake Michigan, *Journal of Waterway, Port, Coastal and Ocean Engineering*, 130(1), 45-53. doi: 10.1061/(ASCE)0733-950X.
- Chaston, P.R. (1979) An unusual weather phenomenon: The Rochester Seiche, *Weatherwise*, 32(5), 211.
- Daniels, Joyce, ed. "Rip Currents: Be Aware, Swim with Care." *Upwellings* 27 (June 2004): 4-7. Print.
- Donn, W. L. (1959), The Great Lakes storm surge of May 5, 1952, *J. Geophys. Res.*, 64(2), 191–198, doi:10.1029/JZ064i002p00191.
- Donn, W.L., and M. Ewing (1956), Stokes' edge waves in Lake Michigan, *Science*, 124, 1238–1242, doi: 10.1126/science.124.3234.1238.
- Ewing, M., F. Press, and W. J. Donn (1954), An explanation of the Lake Michigan wave of 26 June 1954, *Science*, 120, 684–686, doi:10.1126/science.120.3122.684.
- Fifth body recovered from lake today. 1929, July 5. Grand Haven Daily Tribune.
- Freak Tidal Wave Sweeps Lake Erie Shoreline; Eight Believed Drowned, *Toledo Blade*, May 31, 1942.

Harris DL (1957), The effect of a moving pressure disturbance on the water level in a lake, *Meteorological Monographs*, 2(10), 46-57.

Homes evacuated after Lake Superior surge, 2014, September 5, *Soo Today*,

www.sootoday.com/content/news/details.asp?c=78052

Lake Port Damaged – Strange tidal wave carries away fishing docks, *The Montreal Gazette*, October 4, 1933.

Mortimer, C.H. (2004), *Lake Michigan in Motion*, University of Wisconsin Press, Madison, WI, pp 304.

Murty, T. S., and N.G. Freeman (1973), Applications of the concepts of edge waves and numerical modelling to storm surge studies on Lake Huron, in *Proc., 16th Conf. Great Lakes Research*, pp. 533-548, Intl. Association of Great Lakes Research, Ann Arbor, Michigan.

Reynolds, G.D. (2001), Fatal wave: The “Seiche”, *The Joint Archives of Holland*, 10(2), 1-4.

Šepić, J., and A. B. Rabinovich (2014), Meteotsunami in the Great Lakes, Chesapeake Bay and on the Atlantic coast of the United States generated by the propagating 'derecho' of 29–30 June 2012, *Nat. Hazards*, 74, 75–107, doi:10.1007/s11069-014-1310-5.

Tidal wave rolled up along shores of Lake Ontario, *The Montreal Gazette*, May 25, 1925.

A tidal wave sweeps the lake front doing considerable damage – docks four feet under water – hundreds of fish washed ashore, *Cleveland Plain Dealer*, June 24, 1882.

Tidal wave sweeps Erie, *New York Times*, April 14, 1912.

A tidal wave swept over Lake Superior, *The Quebec Saturday Budget*, September, 21, 1895.

Wind, water on rampage, *Ludington Daily News*, July 2, 1956.

Weather stages acrobatic stunt, *Ludington Sunday Morning News*, May 24, 1925.

Appendix B Supplemental Material for Chapter 5

B.1 Supplemental Figures

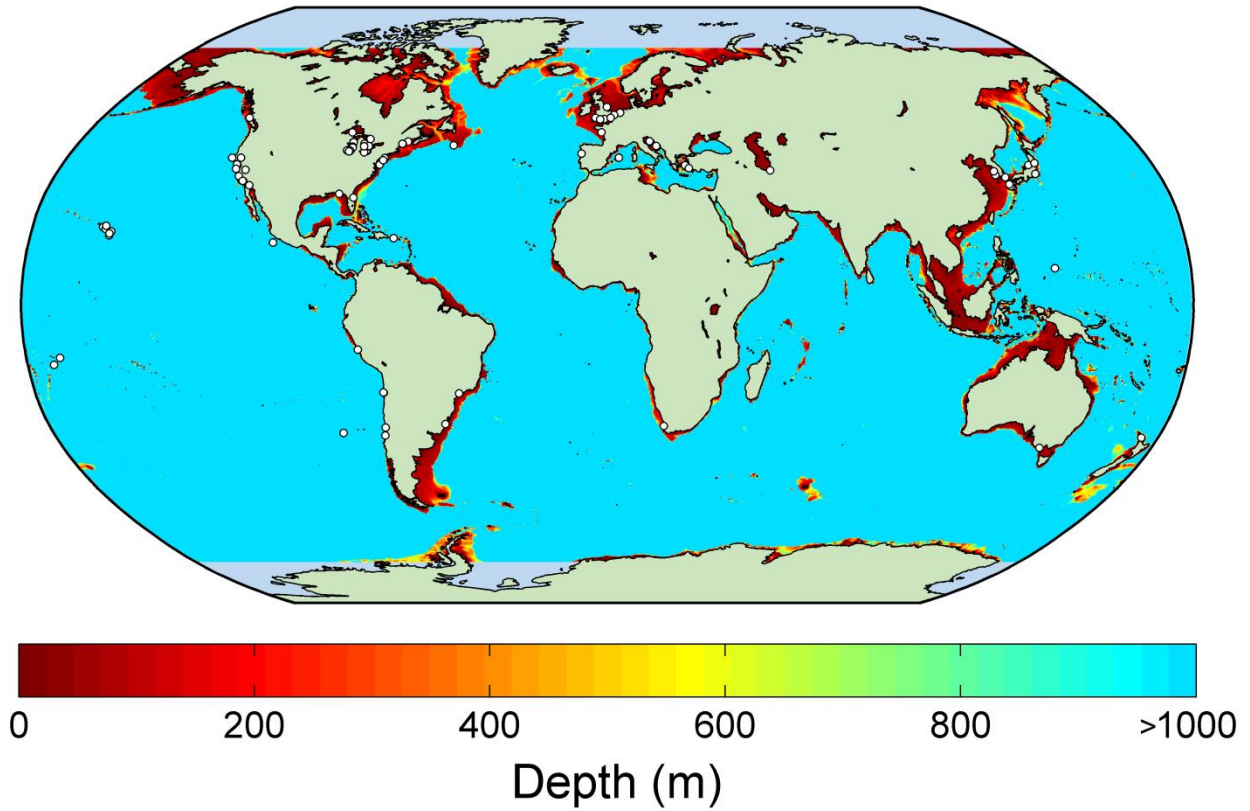


Figure B1: Bathymetry compared with world meteotsunami occurrences, plotted as dots (○).

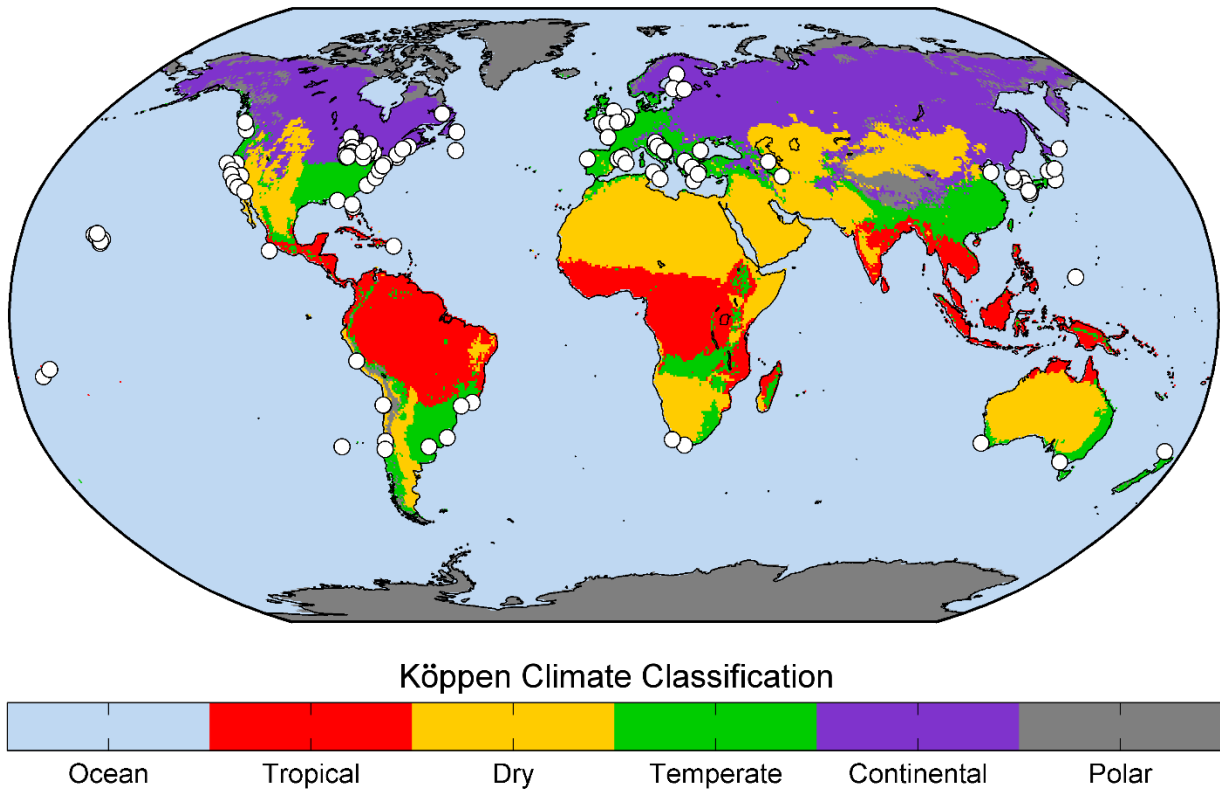


Figure B2: Köppen climate classifications compared with world meteotsunami events, plotted as dots (○)

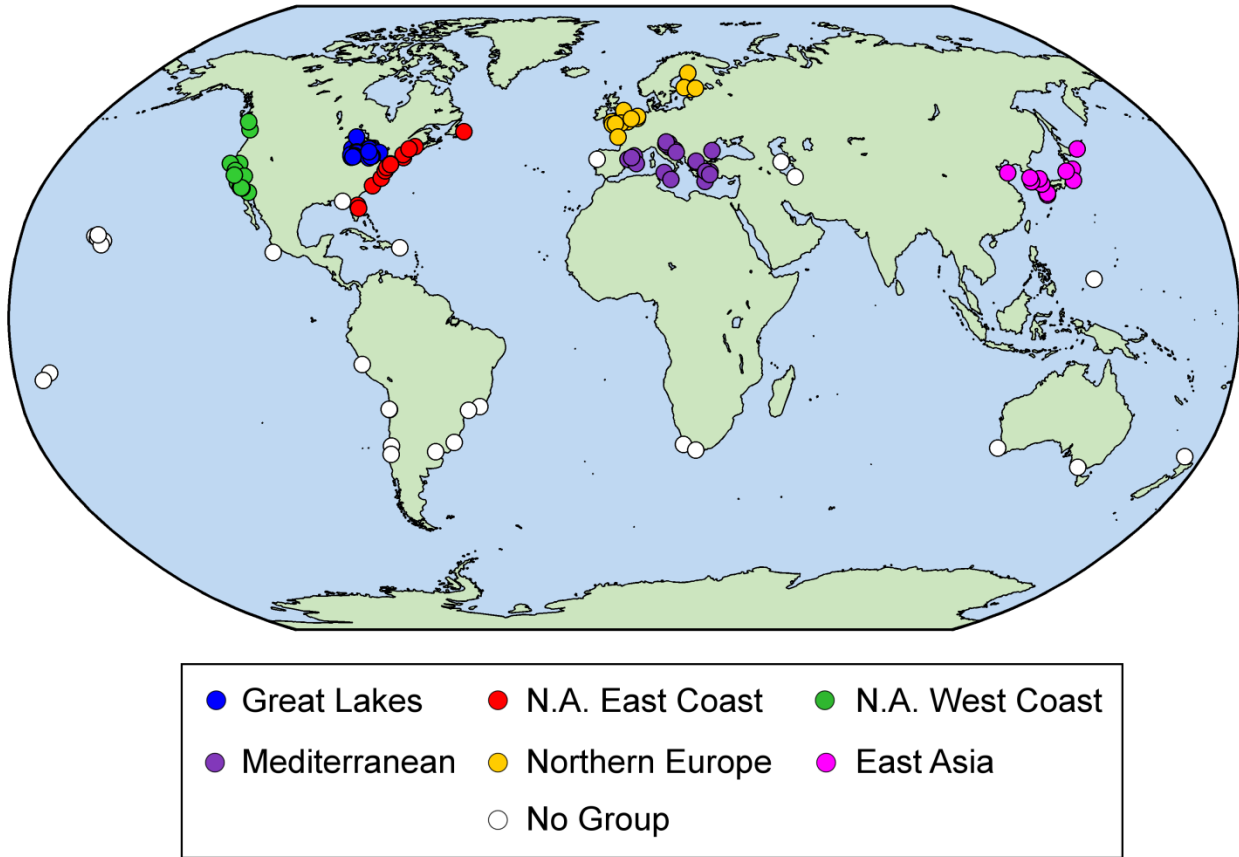


Figure B3: World meteotsunami zones defined based upon geographic proximity and water body.

B.2 Supplemental Tables

Table B1: Worldwide meteotsunami events from the literature

Lat	Lon	Country	Body of Water	Date	Injury	Damage	Death	Source
-34.60	-58.38	Argentina	Atlantic Ocean	1985/10/12				Dragani et al. 2002
-33.65	115.35	Australia	Indian Ocean	2013/06/10				Pattiaratchi and Wijeratne 2014
40.40	49.88	Azerbaijan	Caspian Sea	-				Bondarenko and Bychkov 1983
-22.91	-43.20	Brazil	Atlantic Ocean	2002/09/07				Candella 2009
43.41	28.38	Bulgaria	Black Sea	2007/05/07				Vilibic et al. 2010
48.94	-125.25	Canada	Straits of Juan de Fuca	2005/12/09				Thomson et al. 2009
48.37	-53.38	Canada	Atlantic Ocean	1999/10/25		Y		Mercer et al. 2002
47.49	-52.85	Canada	Atlantic Ocean	2000/09/25		Y		Mercer et al. 2002
43.74	-81.71	Canada	Lake Huron	1971/08/22				Murty and Freeman 1973
37.63	120.33	China	Bohai Bay	1980/09/01				Wang et al. 1987
45.29	14.56	Croatia	Adriatic Sea	2006/08/20				Sepic et al. 2008
44.27	14.77	Croatia	Adriatic Sea	2007/08/22	Y	Y		Sepic et al. 2009
44.53	14.47	Croatia	Adriatic Sea	2008/08/14		Y		Belusic et al. 2007
42.96	16.72	Croatia	Adriatic Sea	1978/06/21	Y	\$25,000,000		Vucetic et al. 2009
43.18	16.58	Croatia	Adriatic Sea	2003/06/27		\$2,000,000		Vilibic et al. 2004
43.18	16.58	Croatia	Adriatic Sea	2003/06/28		\$2,000,000		Vilibic et al. 2004
43.51	16.45	Croatia	Adriatic Sea	2000/08/31				Vilibic and Mihanovic 2003
45.08	13.63	Croatia	Adriatic Sea	1955/06/13				Sepic et al. 2012
45.08	13.63	Croatia	Adriatic Sea	1955/07/04				Sepic et al. 2012
45.08	13.63	Croatia	Adriatic Sea	1955/07/26				Sepic et al. 2012
45.08	13.63	Croatia	Adriatic Sea	1958/08/22				Sepic et al. 2012
45.08	13.63	Croatia	Adriatic Sea	1960/08/12				Sepic et al. 2012
45.08	13.63	Croatia	Adriatic Sea	1965/07/04				Sepic et al. 2012
45.08	13.63	Croatia	Adriatic Sea	1965/07/22				Sepic et al. 2012

45.08	13.63	Croatia	Adriatic Sea	1968/08/02					Sepic et al. 2012
45.08	13.63	Croatia	Adriatic Sea	1974/06/29					Sepic et al. 2012
45.08	13.63	Croatia	Adriatic Sea	1976/07/22					Sepic et al. 2012
45.08	13.63	Croatia	Adriatic Sea	1976/10/30					Sepic et al. 2012
45.08	13.63	Croatia	Adriatic Sea	1992/09/04					Sepic et al. 2012
45.08	13.63	Croatia	Adriatic Sea	1994/08/17					Sepic et al. 2012
45.08	13.63	Croatia	Adriatic Sea	2000/11/06					Sepic et al. 2012
45.08	13.63	Croatia	Adriatic Sea	2005/06/29					Sepic et al. 2012
45.08	13.63	Croatia	Adriatic Sea	2008/08/15					Sepic et al. 2012
60.01	24.53	Finland	Gulf of Finland	2010/07/29					Pellikka et al. 2014
64.62	24.40	Finland	Gulf of Bothnia	2010/08/08					Pellikka et al. 2015
60.47	22.03	Finland	Archipelago Sea	2011/06/04					Pellikka et al. 2016
60.29	26.10	Finland	Gulf of Finland	1924/05/15					Renqvist 1926
35.33	25.13	Greece	Aegean Sea	1928/04/24					Papadopoulos 1993
40.65	22.90	Greece	Aegean Sea	1959/02/23					Papadopoulos 1993
37.83	26.97	Greece	Aegean Sea	1991/05/07					Papadopoulos 1993
45.63	13.80	Italy	Adriatic Sea	-					Defant 1961
37.65	12.58	Italy	Straits of Sicily	1994/05/17					Candella 1999
32.78	129.87	Japan	East China Sea	1979/03/31	Y	Y	3		Hibiya and Kajjura, 1982
32.78	129.87	Japan	East China Sea	1988/03/16					Rabinovich and Monserrat 1998
31.83	129.87	Japan	East China Sea	2009/02/25				Y	Tanaka et al. 2010
32.30	130.02	Japan	East China Sea	2009/02/25				Y	Tanaka et al. 2013
34.65	129.39	Japan	East China Sea	2009/07/15				Y	Tanaka 2012
35.88	14.50	Malta	Mediterranean Sea	-					Airy 1878
51.92	4.50	Netherlands	North Sea	1995/01/01					de Jong 2003
-35.84	174.49	New Zealand	Pacific Ocean	-				Y	Goring 2009
43.80	146.75	Russia	Sea of Okhotsk	1991/05/01					Rabinovich and Monserrat 1996
-32.70	18.23	South Africa	Atlantic Ocean	1969/08/27				Y	Okal et al. 2014
-34.18	22.13	South Africa	Atlantic Ocean	1981/04/16					Shillington 1984

36.03	129.37	South Korea	Sea of Japan						Park et al. 1986
35.28	126.51	South Korea	Yellow Sea	2007/03/31	1	Y	7		Cho et al. 2013
36.33	126.62	South Korea	Yellow Sea	2008/05/04		Y	9		Cho et al. 2013
42.02	3.22	Spain	Mediterranean Sea	1981/07/02					Rabinovich and Monserrat 1996
41.12	1.25	Spain	Mediterranean Sea	1972/07/11					Rabinovich and Monserrat 1996
40.02	3.82	Spain	Mediterranean Sea	1975/09/16		Y			Rabinovich and Monserrat 1996
40.02	3.82	Spain	Mediterranean Sea	1977/07/14					Rabinovich and Monserrat 1996
40.02	3.82	Spain	Mediterranean Sea	1981/07/02					Rabinovich and Monserrat 1996
40.02	3.82	Spain	Mediterranean Sea	1981/07/18					Rabinovich and Monserrat 1996
40.02	3.82	Spain	Mediterranean Sea	1982/07/29					Rabinovich and Monserrat 1996
40.02	3.82	Spain	Mediterranean Sea	1984/06/21		Y			Rabinovich and Monserrat 1996
40.02	3.82	Spain	Mediterranean Sea	1985/06/14					Rabinovich and Monserrat 1996
40.02	3.82	Spain	Mediterranean Sea	1985/06/19					Rabinovich and Monserrat 1996
40.02	3.82	Spain	Mediterranean Sea	1985/07/03					Rabinovich and Monserrat 1996
40.02	3.82	Spain	Mediterranean Sea	1985/07/31					Rabinovich and Monserrat 1996
40.02	3.82	Spain	Mediterranean Sea	1989/07/07		Y			Monserrat et al. 1991
40.02	3.82	Spain	Mediterranean Sea	1989/08/11					Monserrat et al. 1991
40.02	3.82	Spain	Mediterranean Sea	1990/07/28					Monserrat et al. 1992
40.02	3.82	Spain	Mediterranean Sea	1990/09/07					Monserrat et al. 1992
40.02	3.82	Spain	Mediterranean Sea	1990/09/24					Monserrat et al. 1992
40.02	3.82	Spain	Mediterranean Sea	2006/06/15				\$1,000,0000	Vilibic et al. 2008
41.55	2.35	Spain	Mediterranean Sea	1972/07/11					Rabinovich and Monserrat 1996
50.60	-2.52	United Kingdom	English Channel	1824/11/23		Y	60		Haslett and Bryant 2009

50.31	-4.07	United Kingdom	English Channel	1892/08/18		Y		Haslett and Bryant 2009
51.21	-4.12	United Kingdom	Bristol Channel/Celtic Sea	1910/12/16		Y		Haslett and Bryant 2009
51.08	1.17	United Kingdom	English Channel	1929/07/20	Y	Y	2	Haslett and Bryant 2009
51.04	-4.25	United Kingdom	Atlantic Ocean	1966/07/31		Y		Haslett and Bryant 2009
54.08	-0.19	United Kingdom	North Sea	1938/08/05				Haslett et al. 2009
50.69	-1.10	United Kingdom	English Channel	1957/07/06		Y		Haslett et al. 2009
50.35	-4.00	United Kingdom	English Channel	2011/06/27				Tappin et al. 2013
29.20	-81.03	USA	Atlantic Ocean	1992/07/02	75	Y		Churchill et al. 1995 Paxton and Sobien 1998
27.53	-82.75	USA	Gulf of Mexico	1995/03/25				
43.85	-69.62	USA	Atlantic Ocean	2008/10/28		Y		Vilibic et al. 2014
39.75	-74.11	USA	Atlantic Ocean	2013/06/13		Y		Lipa et al. 2014
41.97	-87.66	USA	Lake Michigan	1954/06/26			7	Ewing et al. 1954
41.73	-86.92	USA	Lake Michigan	1954/06/26				Harris 1958
41.62	-87.32	USA	Lake Michigan	1954/06/26				Harris 1958
41.53	-70.66	USA	Long Island Sound	1953/11/23				Donn and Balachandran, 1960
39.38	-74.45	USA	Atlantic Ocean	2008/03/05				Pasquet et al. 2013
36.18	-75.75	USA	Atlantic Ocean	2008/06/17				Pasquet et al. 2013
39.38	-74.45	USA	Atlantic Ocean	2009/01/08				Pasquet et al. 2013
36.18	-75.75	USA	Atlantic Ocean	2009/01/29				Pasquet et al. 2013
34.21	-77.79	USA	Atlantic Ocean	2009/03/29				Pasquet et al. 2013
42.31	-71.06	USA	Atlantic Ocean	2010/02/26				Pasquet et al. 2013
39.38	-74.45	USA	Atlantic Ocean	2010/03/13				Pasquet et al. 2013
28.42	-80.59	USA	Atlantic Ocean	2011/04/05				Pasquet et al. 2013
36.18	-75.75	USA	Atlantic Ocean	2011/10/28				Pasquet et al. 2013
36.18	-75.75	USA	Atlantic Ocean	2010/05/16				Pasquet and Vilibic 2013

36.18	-75.75	USA	Atlantic Ocean	2012/02/20			Pasquet and Vilibic 2013
43.85	-82.65	USA	Lake Huron	1952/05/05		Y	Donn 1959
41.48	-81.67	USA	Lake Erie	1952/05/05			Donn 1959
42.90	-78.85	USA	Lake Erie	1952/05/05			Donn 1959
43.04	-82.41	USA	Lake Huron	1971/08/22			Murty and Freeman 1973
43.92	-88.33	USA	Lake Michigan	1998/05/31			As-Salek and Schwab 2004
43.38	-86.43	USA	Lake Michigan	1998/05/31		Y	As-Salek and Schwab 2004
42.36	-87.82	USA	Lake Michigan	1954/07/06		Y	Donn and Ewing 1956
41.84	-81.05	USA	Lake Erie	2012/05/27	3		Anderson et al. 2015
41.81	-81.14	USA	Lake Erie	2012/05/27		Y	Anderson et al. 2015
42.10	-86.48	USA	Lake Michigan	1893/04/07		Y	Mortimer 2004
43.24	-77.57	USA	Lake Ontario	1979/08/07		Y	Chaston 1979
43.92	-88.33	USA	Lake Michigan	2012/06/29			Sepic and Rabinovich 2014

Table B2: Worldwide meteotsunami events from news and web reports

Lat	Lon	Country	Body of Water	Date	Injury	Damage	Death	Source
-38.65	143.07	Australia	Indian Ocean	2012/07/09				https://www.youtube.com/watch?v=Lyl7hEAD0Pc
-32.19	-52.15	Brazil	Atlantic Ocean	2014/02/09		Y		http://www.telegraph.co.uk/news/worldnews/southamerica/brazil/10632745/Meteorological-tsunami-hits-Brazilian-beach.html
-23.85	-46.63	Brazil	Atlantic Ocean	2009/04/11	Y			https://www.youtube.com/watch?v=F4FGhp2Dk3A
42.96	16.72	Croatia	Adriatic Sea	2009/11/28				https://www.youtube.com/watch?v=X1j54QGoNqQ&list=PL169EB76838AE117F&index=3
52.46	4.62	Netherlands	North Sea	2012/01/03				http://www.weer.nl/weer-in-het-nieuws/weernieuws/ch/d05d0c68d11417a125c0f9343b59c354/article/meteotsunami_aan_nederlandse_kust.html
41.16	-8.62	Portugal	Atlantic Ocean	2014/01/06				https://www.youtube.com/watch?v=McyPxZK6ZXE
30.18	-85.81	USA	Gulf of Mexico	2014/03/29		Y		http://www.extremestorms.com/meteo_tsunami.htm
46.98	-88.43	USA	Lake Superior	2011/05/31				https://www.youtube.com/watch?v=bY11zljJr4g
46.60	-90.89	USA	Lake Superior	1895/09/14				Quebec Saturday Budget 1895
48.84	-87.52	USA	Lake Superior	1933/10/03				Montreal Gazzette, 1933
46.54	-84.41	USA	Lake Superior	2014/09/04				www.sootoday.com 2014
43.06	-86.23	USA	Lake Michigan	1929/07/04			10	Grand Haven Daily Tribune 1929
42.78	-86.10	USA	Lake Michigan	1938/07/13			3	Reynolds 2001
42.10	-86.48	USA	Lake Michigan	1893/04/07		Y		Mortimer 2004
41.92	-86.59	USA	Lake Michigan	2003/07/04			7	Guenther 2003
42.58	-87.85	USA	Lake Michigan	1912/05/12		Y		Sandusky Star Journal 1905
43.96	-86.44	USA	Lake Michigan	1956/07/01		Y		Ludington Daily News 1956
44.75	-85.53	USA	Lake Michigan	2015/06/10		Y		www.mlive.com 2015
45.21	-82.65	USA	Lake Huron	1925/05/23		Y		Ludington Daily News 1925
41.48	-81.67	USA	Lake Erie	1882/06/23	Y	\$700000	Y	Cleveland Plain Dealer 1882
41.88	-80.80	USA	Lake Erie	1912/04/12		Y		New York Times 1912
41.48	-81.67	USA	Lake Erie	1942/05/31			7	Toledo Blade 1942
43.28	-77.57	USA	Lake Ontario	1925/05/23		Y		Montreal Gazzette 1925
43.24	-77.74	USA	Lake Ontario	2012/07/07				13WHAM Rochester, NY 2012

Table B3: Worldwide meteotsunami events from the National Geophysical Data Center (NGDC)/World Data Service Global Historical Tsunami Database

Lat	Lon	Country	Body of Water	Date	Injury	Damage	Death
57.00	-152.00	USA	Pacific Ocean	1792		Y	
38.08	-75.21	USA	Atlantic Ocean	1821/09/03			
35.60	139.70	Japan	Pacific Ocean	1856/09/01			
35.00	-120.00	USA	Pacific Ocean	1877/04/16			
40.00	-122.00	USA	Pacific Ocean	1884/11/12			
38.20	-122.40	USA	Pacific Ocean	1898/03/31			
33.80	-118.50	USA	Pacific Ocean	1899/12/25			
-14.21	-169.58	USA Territory	Pacific Ocean	1915/02/11			3
10.00	138.00	Micronesia	Pacific Ocean	1925/12/22		Y	
32.50	-115.50	USA	Pacific Ocean	1927/01/01		Y	1
17.00	-104.00	Mexico	Pacific Ocean	1927/09/06			
-23.70	-70.40	Chile	Pacific Ocean	1929/08/09			
39.35	-74.42	USA	Atlantic Ocean	1931/08/19			4
33.62	-117.97	USA	Pacific Ocean	1933/03/11			
33.70	-118.20	USA	Pacific Ocean	1934/08/21		Y	
19.50	-155.50	USA	Pacific Ocean	1935/11/21		Y	
39.95	-74.12	USA	Atlantic Ocean	1938/09/21		Y	
38.93	-74.90	USA	Atlantic Ocean	1944/09/14			
43.10	-82.40	USA	Lake Huron	1952/05/06		Y	
41.70	-86.88	USA	Lake Michigan	1954/06/26			8
37.13	26.83	Greece	Aegean Sea	1991/05/07			
44.40	-67.97	USA	Atlantic Ocean	1994/01/04			
43.80	-69.70	USA	Atlantic Ocean	2008/10/28		Y	
50.50	-3.00	United Kingdom	English Channel	2011/06/27			

Table B4: Worldwide meteotsunami events from the Novosibirsk Tsunami Laboratory (NTL) Historical Tsunami Databases for the World Ocean

Lat	Lon	Country	Body of Water	Date	Damage
34.40	138.40	Japan	Pacific Ocean	1406/10/16	
34.50	137.60	Japan	Pacific Ocean	1510/10/10	
34.50	135.30	Japan	Pacific Ocean	1657/10/28	Y
34.50	135.20	Japan	Osaka Bay	1670/08/31	
36.90	140.90	Japan	Pacific Ocean	1696/07/25	
57.50	-154.00	USA	Pacific Ocean	1792/11/30	
38.00	-122.00	USA	Pacific Ocean	1827/01/18	
37.00	-122.00	USA	Pacific Ocean	1840/01/16	
38.00	139.00	Japan	Pacific Ocean	1844/03/08	
35.40	139.80	Japan	Pacific Ocean	1856/08/31	
20.70	-157.00	USA	Pacific Ocean	1872/01/13	
20.70	-157.00	USA	Pacific Ocean	1872/01/22	
35.00	-120.00	USA	Pacific Ocean	1877/04/16	Y
-33.10	-71.70	Chile	Pacific Ocean	1878/11/23	Y
-33.10	-71.70	Chile	Pacific Ocean	1879/08/08	Y
40.00	-122.00	USA	Pacific Ocean	1884/11/12	
20.00	-155.00	USA	Pacific Ocean	1895/01/28	
38.20	-122.40	USA	Pacific Ocean	1898/03/31	
33.50	-116.50	USA	Pacific Ocean	1899/12/25	
19.00	-155.50	USA	Pacific Ocean	1903/10/08	
20.00	-155.00	USA	Pacific Ocean	1903/11/17	
21.50	-157.00	USA	Pacific Ocean	1903/11/29	Y
-35.30	-72.40	Chile	Pacific Ocean	1923/02/17	Y
47.00	-2.00	France	Bay of Biscay	1924/01/09	Y
-16.09	-171.84	Kingdom of Tonga	Pacific Ocean	1926/03/16	
29.00	-115.00	Mexico	Pacific Ocean	1927/01/01	Y

-23.60	-70.40	Chile	Pacific Ocean	1928/03/31	
36.60	53.40	Iran	Caspian Sea	1932/05/07	
33.53	-118.07	USA	Pacific Ocean	1933/03/11	
33.75	-118.23	USA	Pacific Ocean	1934/08/21	Y
19.50	-155.50	USA	Pacific Ocean	1935/11/21	
40.00	-74.00	USA	Atlantic Ocean	1938/09/21	Y
51.80	2.40	Belgium	North Sea	1953/02/01	
-12.05	-77.15	Peru	Pacific Ocean	1958/04/09	
37.10	26.80	Turkey	Aegean Sea	1991/05/07	
51.00	-127.50	Canada	Pacific Ocean	2005/12/09	

B.3 References

- Anderson, E.J., Bechle, A.J., Wu, C.H., Schwab, D.J., Mann, G.E., and Lombardy, K.A. (2015), Reconstruction of a meteotsunami in Lake Erie on 27 May 2012: Roles of atmospheric conditions on hydrodynamic response in enclosed basins. *J. Geophys. Res. Oceans*. Accepted Author Manuscript, doi: 10.1002/2015JC010883.
- As-Salek, J.A., and D.J. Schwab (2004), High-frequency water level fluctuations in Lake Michigan, *Journal of Waterway, Port, Coastal and Ocean Engineering*, 130(1), 45-53. doi: 10.1061/(ASCE)0733-950X.
- Belušić, D. and N. Strelec Mahović (2009) Detecting and following atmospheric disturbances with a potential to generate meteotsunamis in the Adriatic, *Physics and Chemistry of the Earth*, 34, 918-927.
- Belušić, D., B. Grisogono, and Z. B. Klaić (2007), Atmospheric origin of the devastating coupled air-sea event in the east Adriatic, *J. Geophys. Res.*, 112, D17111, doi:10.1029/2006JD008204.
- Bondarenko, A.L., and Bychkov, V.S. (1983), Marine baric waves, *Meteorologia I hidrologia* (in Russian), No. 6, pp. 86-91.
- Candella, R.N. (2009), Meteorologically induced strong seiches observed at Arraial do Cabo, RJ, Brazil. *Physics and Chemistry of the Earth*, 34(17-18), 989-997.
- Candela J, S. Mazzola, C. Sammari, R. Limeburner, C.J. Lozano, B. Patti, and A. Bonnano (1999), The “Mad Sea” phenomenon in the Strait of Sicily. *J Phys Oceanogr*, 29, 2210–2231.

- Chaston, P.R. (1979) An unusual weather phenomenon: The Rochester Seiche, *Weatherwise*, 32(5), 211.
- Cho, K.-H., J.-Y. Choi, K.-S. Park, S.-K. Hyun, Y. Oh, and J.-Y. Park (2013), A synoptic study on tsunami-like sea level oscillations along the west coast of Korea using an unstructured-grid ocean model, *J. Coastal Res.*, 65, 678–683.
- Churchill, D.D., S.H. Houston, and N.A. Bond (1995), The Daytona Beach wave of 3-4 July 1992 – A shallow-water gravity-wave forced by a propagating squall line, *Bull. Amer. Meteor. Soc.*, 76(1), 21-32, doi: 10.1175/1520-0477(1995)076<0021:TDBWOJ>2.0.CO;2.
- Daniels, Joyce, ed. "Rip Currents: Be Aware, Swim with Care." *Upwellings* 27 (June 2004): 4-7. Print.
- Defant A (1961) *Physical oceanography*, vol 2. Pergamon Press, Oxford, p 729.
- de Jong, M. P. C., and J. A. Battjes (2004), Low-frequency sea waves generated by atmospheric convection cells, *J. Geophys. Res.*, 109, C01011, doi:10.1029/2003JC001931.
- de Jong, M. P. C., L. H. Holthuijsen, and J. A. Battjes (2003), Generation of seiches by cold fronts over the southern North Sea, *J. Geophys. Res.*, 108(C4), 3117, doi:10.1029/2002JC001422.
- Donn, W. L. (1959), The Great Lakes storm surge of May 5, 1952, *J. Geophys. Res.*, 64(2), 191–198, doi:10.1029/JZ064i002p00191.
- Donn, W. L. and Balachandran, N. K. (1969) Coupling between a moving air-pressure disturbance and the sea surface, *Tellus*, 21(5), 701–706.
- Donn, W.L., and M. Ewing (1956), Stokes' edge waves in Lake Michigan, *Science*, 124, 1238–1242, doi: 10.1126/science.124.3234.1238.

- Dragani, W.C., Mazio, C.A., and Nunez, M.N., 2002. Sea level in coastal waters of the Buenos Aires province, Argentina. *Continental Shelf Research*, 22(5), 779-790.
- Ewing, M., F. Press, and W. J. Donn (1954), An explanation of the Lake Michigan wave of 26 June 1954, *Science*, 120, 684–686, doi:10.1126/science.120.3122.684.
- Fifth body recovered from lake today. 1929, July 5. *Grand Haven Daily Tribune*.
- Freak Tidal Wave Sweeps Lake Erie Shoreline; Eight Believed Drowned, *Toledo Blade*, May 31, 1942.
- Goring, D.J. (2009), Meteotsunami resulting from the propagation of synoptic-scale weather systems, *Physics and Chemistry of the Earth*, 34, 1009-1015.
- Harris DL (1957), The effect of a moving pressure disturbance on the water level in a lake, *Meteorological Monographs*, 2(10), 46-57.
- Haslett, S.K., and E.A. Bryant (2009) Meteorological tsunamis in southern Britain: an historical review. *The Geographical Review* 99, 146–163.
- Haslett, S.K., H.E. Mellor, and E.A. Bryant (2009), Meteo-tsunami hazard associated with summer thunderstorms in the United Kingdom, *Phys. Chem. Earth*, 34, 1016-1022, doi: 10.1016/j.pce.2009.10.005.
- Hibiya, T., and K. Kajiura (1982), Origin of the Abiki phenomenon (a kind of seiche) in Nagasaki Bay, *J. Oceanogr. Soc. Jpn.*, 38, 172–182, doi:10.1007/BF02110288.
- Homes evacuated after Lake Superior surge, 2014, September 5, *Soo Today*,
www.sootoday.com/content/news/details.asp?c=78052
- Lake Port Damaged – Strange tidal wave carries away fishing docks, *The Montreal Gazette*, October 4, 1933.

- Lipa, B., H. Parikh, D. Barrick, H. Roarty, and S. Glenn (2014), High-frequency radar observations of the June 2013 US East Coast meteotsunami, *Nat. Hazards*, 74, 109-122, doi: 10.1007/s11069-013-0992—4.
- Mercer, D., J. Sheng, R. J. Greatbatch, and J. Bobanović (2002), Barotropic waves generated by storms moving rapidly over shallow water, *J. Geophys. Res.*, 107(C10), 3152, doi:10.1029/2001JC001140.
- Monserrat S., and A.J. Thorpe (1992), Gravity-wave observations using an array of microbarographs in the Balearic Islands, *Q. J. Roy. Meteorol. Soc.*, 118, 259-282.
- Monserrat S., A. Ibberson, and A.J. Thorpe (1991), Atmospheric gravity waves and the “rissaga” phenomenon, *Q. J. Roy. Meteorol. Soc.*, 117, 553–570.
- Monserrat, S., I. Vilibić, and A. B. Rabinovich (2006), Meteotsunamis: Atmospherically induced destructive ocean waves in the tsunami frequency band, *Nat. Hazards Earth Syst. Sci.*, 6, 1035–1051, doi:10.5194/nhess-6-1035-2006.
- Mortimer, C.H. (2004), *Lake Michigan in Motion*, University of Wisconsin Press, Madison, WI, pp 304.
- Murty, T. S., and N.G. Freeman (1973), Applications of the concepts of edge waves and numerical modelling to storm surge studies on Lake Huron, in *Proc., 16th Conf. Great Lakes Research*, pp. 533-548, Intl. Association of Great Lakes Research, Ann Arbor, Michigan.
- Okal, E. A., J. N. J. Visser, and C. H. de Beer (2014), The Dwarskersbos, South Africa local tsunami of August 27, 1969: Field survey and simulation as a meteorological event, *Nat. Hazards*, 74, 251–268, doi:10.1007/s11069-014-1205-5.

- Orlić, M., D. Belušić, I. Janeković, and M. Pasarić (2010), Fresh evidence relating the great Adriatic surge of 21 June 1978 to mesoscale atmospheric forcing, *J. Geophys. Res.*, 115, C06011, doi:10.1029/2009JC005777.
- Orlić, M. (2015), The first attempt at cataloguing tsunami-like waves of meteorological origin in Croatian coastal waters, *Acta Adriatica*, 56(1), 83-96.
- Papadopoulos, G.A. (1993) On some exceptional seismic(?) sea waves in the Greek archipelago, *International Journal of the Tsunami Society*, 11(1), 25-34.
- Park, Y.H. (1986), Water characteristics and movements of the Yellow Sea Warm Current in summer, *Prog. Oceanog.*, 17, 243-254.
- Pasquet, S., and I. Vilibić (2013), Shelf edge reflection of atmospherically generated long ocean waves along the central U.S East Coast, *Cont. Shelf Res.*, 66, 1–8, doi:10.1016/j.csr.2013.06.007.
- Pasquet, S, I. Vilibić, and J. Šepić (2013), A survey of strong high-frequency sea level oscillations along the U.S. East Coast between 2006 and 2011, *Nat. Hazards Earth Syst. Sci.*, 13, 473–482, doi:10.5194/nhess-13-473-2013.
- Pattiaratchi, C., and E. M. S. Wijeratne (2014), Observations of meteorological tsunamis along the south-west Australian coast, *Nat. Hazards*, 74, 281–302, doi:10.1007/s11069-014-1263-8.
- Paxton, C. H., and D. A. Sobien (1998), Resonant interaction between an atmospheric gravity wave and shallow water wave along Florida's west coast, *Bull. Am. Meteorol. Soc.*, 79, 2727–2732, doi:10.1175/1520-0477(1998)079<2727:RIBAAG>2.0.CO;2.

- Pellikka, H., J. Rauhala, K.K. Kahma, T. Stipa, H. Boman, and A. Kangas (2014), Recent observations of meteotsunamis on the Finnish coast, *Nat. Hazards*, 74(1), 197-215, doi: 10.1007/s11069-014-1150-3.
- Rabinovich, A.B. and S. Monserrat (1996), Meteorological tsunamis near the Balearic and Kuril Islands: descriptive and statistical analysis, *Nat. Hazards*, 13, 55-90.
- Rabinovich, A.B., and S. Monserrat (1998), Generation of meteorological tsunamis (large amplitude seiches) near the Balearic and Kuril Islands, *Natural Hazards*, 18, 27-55.
- Renqvist H (1926), Ein Seebar in Finnland. Zur Frage Nach der Entstehung der Seebaren (in German). *Geogr Ann.*, 8, 230–236.
- Reynolds, G.D. (2001), Fata wave: The “Seiche”, *The Joint Archives of Holland*, 10(2), 1-4.
- Šepić, J., and A. B. Rabinovich (2014), Meteotsunami in the Great Lakes, Chesapeake Bay and on the Atlantic coast of the United States generated by the propagating 'derecho' of 29–30 June 2012, *Nat. Hazards*, 74, 75–107, doi:10.1007/s11069-014-1310-5.
- Šepić J, M. Orlić, and I. Vilibić (2008), The Bakar Bay seiches and their relationship with atmospheric processes, *Acta Adriatica*, 49(2), 107-123.
- Šepić, J., I. Vilibić, and S. Monserrat (2009), Teleconnections between the Adriatic and the Balearic meteotsunamis, *Phys. Chem. Earth*, 34, 928-937, doi:10.1016/j.pce.2009.08.007.
- Shilington, F.A. (1984), Long period edge waves off Southern Africa, *Continental Shelf Research*, 3, 343-357.
- Šepić, J., I. Vilibić, and N. Strelec Mahović (2012), Northern Adriatic meteorological tsunamis: Observations, link to the atmosphere, and predictability, *J. Geophys. Res.*, 117, C02002, doi:10.1029/2011JC007608.

- Tanaka, K. (2010), Atmospheric pressure-wave bands around a cold front resulted in a meteotsunami in the East China Sea in February 2009, *Nat. Hazards Earth Syst. Sci.*, 10, 2599–2610, doi:10.5194/nhess-10-2599-2010.
- Tanaka K (2012), On meteotsunami around Tsushima Strait generated by the Baiu front, *Natural Hazards*, 63,805–822.
- Tappin, D. R., A. Sibley, K. Horsburgh, C. Daubord, D. Cox, and D. Long (2013), The English Channel ‘tsunami’ of 27 June 2011 – a probable meteorological source, *Weather*, 68, 144–152, doi: 10.1002/wea.2061.
- Thomson, R.E., A.B. Rabinovich, I.V. Fine, D.C. Sinnott, A. McCarthy, N.A.S. Sutherland, and L.K. Neil (2009) Meteorological tsunamis on the coasts of British Columbia and Washington, *Physics and Chemistry of the Earth*, 34, 971-988.
- Tidal wave rolled up along shores of Lake Ontario, *The Montreal Gazette*, May 25, 1925.
- A tidal wave sweeps the lake front doing considerable damage – docks four feet under water – hundreds of fish washed ashore, *Cleveland Plain Dealer*, June 24, 1882.
- Tidal wave sweeps Erie, *New York Times*, April 14, 1912.
- A tidal wave swept over Lake Superior, *The Quebec Saturday Budget*, September, 21, 1895.
- Vilibić, I., N. Domijan, M. Orlić, N. Leder, and M. Pasarić (2004), Resonant coupling of a traveling air-pressure disturbance with the east Adriatic coastal waters, *J. Geophys. Res.*, 109, C10001, doi:10.1029/2004JC002279.
- Vilibić, I., S. Monserrat, A. B. Rabinovich, and H. Mihanović (2008), Numerical modelling of the destructive meteotsunami of 15 June, 2006 on the coast of the Balearic Islands, *Pure Appl. Geophys.*, 165, 2169–2195, doi:10.1007/s00024-008-0426-5.

- Vilibić, I., K. Horvath, N. Strelec Mahović, S. Monserrat, M. Marcos, Á. Amores, and I. Fine (2014), Atmospheric processes responsible for generation of the 2008 Boothbay meteotsunami, *Nat. Hazards*, 74, 25–53, doi:10.1007/s11069-013-0811-y.
- Vučetić, T., I. Vilibić, S. Tinti, and A. Maramai (2009), The Great Adriatic flood of 21 June 1978 revisited: An overview of the reports, *Phys. Chem. Earth*, 34, 894-903.
- Wang, X., K. Li, Z. Yu, and J. Wu (1987) Statistical characteristics of seiches in Longkou Harbor, *Journal of Physical Oceanography*, 17, 1063-1065.
- Wind, water on rampage, *Ludington Daily News*, July 2, 1956.
- Weather stages acrobatic stunt, *Ludington Sunday Morning News*, May 24, 1925.